The excited triplet state of azoalkanes: electron spin polarization and magnetic field effects during triplet- sensitized photolysis of trans-azocumene in solution

Milikisiyants, Sergey ; Steiner, Ulrich E ; Paul, Henning

Abstract: The triplet-sensitized photodecomposition of azocumene into nitrogen and cumyl radicals is investigated by time-resolved electron paramagnetic resonance and absorption spectroscopy. The radicals are found to be created spin polarized with a yield depending on the strength of the applied magnetic field. The phenomenon arises because in triplet azocumene, the decay into radicals competes with a fast triplet-sublevel selective intersystem crossing back to the azocumene ground state. The size of the initial spin polarization of the radicals and the magnetic field effect on their yield are determined in solvents of different viscosities. Data analysis yields rate constants for the intersystem crossing and the cleavage reaction of triplet azocumene as well as its zero-field splitting D ZFS. At room temperature in nonpolar solvents, the most probable values are: k x = k y = 1.2 × 1011 s−1 and k z = 1.9 × 1010 s−1 for the intersystem crossing from the energetically lower and upper triplet substates, respectively, k p = 1.6 × 109 s−1 for the cleavage reaction and for the zero-field splitting D ZFS = −3.4 × 1010 s−1 (0.18 cm−1).

DOI: https://doi.org/10.1007/s00723-011-0263-z

Electronic Supplementary Material for

The Excited Triplet State of Azoalkanes. Electron Spin Polarization and Magnetic Field Effects during Triplet Sensitized Photolysis of *trans*- Azocumene in Solution.

by

S. Milikisiyants[1,a], U. Steiner[2,*], and H. Paul[1,b]

Published in **Applied Magnetic Resonance**

[1] Physikalisch-Chemisches Institut, University of Zuerich, CH-8057 Zuerich, Switzerland

[2] Fachbereich Chemie, University of Konstanz, DE-78457 Konstanz, Germany

[a] present address: Rensselaer Polytechnic Institute, Department of Chemistry and Chemical Biology, 110 8th Street, Troy, NY 12180, USA

[b] present address: Ruettebuckstr. 24, DE-79804 Dogern, Germany

[*] corresponding author's address: Prof. Dr. Ulrich Steiner
Fachbereich Chemie
Universitaet Konstanz
DE-78457 Konstanz
Tel: +49 (0)7531 883570
Fax: +49 (0)7531 883014
E: ulrich.steiner@uni-konstanz.de

1 Introduction

The population distribution among the spin states of an ensemble of spin particles in statistical equilibrium is determined by the Boltzmann law:

$$N_i \propto e^{-\frac{E_i}{kT}}$$

where E_i is the energy level of the spin state i. In the case of an electron spin, which interacts with an external static magnetic field B_0, the values of E_i can be expressed in terms of the electron (Bohr) magneton μ_B and the electron g-factor:

$$E_{1,2} = \pm\frac{1}{2} g \cdot \mu_B \cdot B_0$$

where the states 1 and 2 correspond to the two possible orientations of the spin quantized along the magnetic field direction. If the energy gap between the two states, $g \cdot \mu_B \cdot B_0$, is much smaller than kT, the spin polarization caused by the Boltzmann population difference of the states can be well approximated by the equation:

$$p_{eq} = \frac{g \cdot \mu_B \cdot B_0}{2kT}$$

This polarization of a thermally equilibrated ensemble of electron spins is called equilibrium or Boltzmann polarization. In spite of its usually very small value (for B_0 = 0.34 T and room temperature p_{eq} amounts to only $7.8 \cdot 10^{-4}$) the Boltzmann polarization can be successfully detected by Electron Paramagnetic Resonance (EPR) Spectroscopy [1], which is widely used to study paramagnetic particles, e.g. free radicals.

The electron spin system of reactive radicals in liquids is often polarized by chemical reactions, i.e. the populations of the energy levels deviate from the Boltzmann distribution. This so-called Chemically Induced Dynamic Electron Polarization (CIDEP) can result from a spin state selective radical formation or a spin state selective radical reaction. In principal, the polarization can take on any value in the range from –1 to +1. A negative polarization means,

that the EPR spectrum appears in emission, i.e. the radical system then emits microwaves instead of absorbing them. Of course, the CIDEP always disappears by relaxation to thermal equilibrium. Typical relaxation times for free radicals in solution lie in the range from about 100 ns to about 10 μs. Thus, investigations of CIDEP phenomena require Time-Resolved EPR (TREPR) measurements with a time resolution of at least 100 ns.

CIDEP can be induced by a variety of different mechanisms. One of the most prominent ones is the so-called Triplet Mechanism (TM), which is often encountered if radicals are generated by flash photolysis. The principle of this mechanism is sketched in scheme 1.1. Photoexcitation of molecules to an excited singlet state $^1S_1$ is often followed by a rapid Intersystem Crossing (ISC) to the triplet state $^3T_1$, a process which is usually caused by spin-orbit interaction [2]. It is well known [3], that the rates of the ISC process may be different for the three triplet zero-field sublevels T_x, T_y, and T_z. This leads to different populations of these sublevels and, therefore, to a spin polarization in the molecular frame. The relative difference of the ISC rates can reach very large values if one or two of the singlet-triplet sublevel transitions are symmetry forbidden. This situation is present, for example, in benzophenone molecules, where the transitions to two sublevels are symmetry forbidden and, consequently, the third one becomes strongly overpopulated [4].

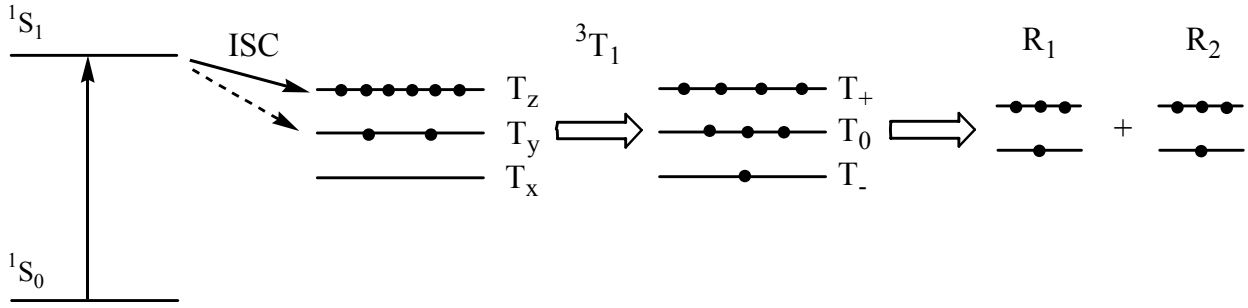

Scheme 1.1

In liquids the orientations of the triplet molecules in the laboratory frame are equally distributed over all possible rotational angles. Therefore, in zero magnetic field the spin polarization in the molecular frame would be invisible in the laboratory frame because of observation of the ensemble average. Nevertheless, under certain conditions the polarization gained in the molecular frame may be partially transferred to the laboratory one. For this to

happen it requires usually two things, namely an applied static magnetic field and a nonzero dipole-dipole interaction which splits the triplet sublevels in the molecular frame. If the triplet molecules obtain an electron spin polarization in the laboratory frame and if they decay into radicals faster than this polarization relaxes to thermal equilibrium, then the radical system will carry an initial spin polarization which can be detected by TREPR spectroscopy. The triplet molecules themselves usually escape the TREPR observation because of their short spin-spin relaxation times (typically a few nanoseconds) and, hence, large EPR linewidths.

The TM was introduced about three decades ago [5,6] and was put on a sound theoretical basis in a variety of publications [7,8,9]. Today it is more precisely named population type (*p*-type) TM in order to distinguish it from the reversed mechanism, the depopulation type (*d*-type) TM. The latter has been proposed by U. Steiner in the early eighties to explain an observed Magnetic Field Effect (MFE) on the radical quantum yield in electron transfer reactions between triplet excited thionine and various halogen substituted anilines [10,11]. Upon collision these molecules form triplet exciplexes which decay rapidly by two competing processes, ISC to the ground state and decomposition by electron transfer into radicals (see scheme 1.2). The

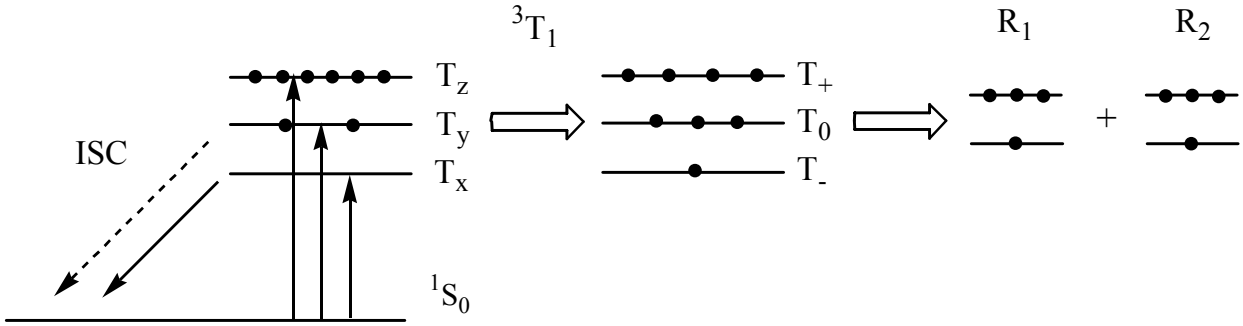

Scheme 1.2

faster the ISC is, the lower will be the radical yield. If the ISC proceeds with different rates from the three sublevels T_x, T_y, and T_z of the exciplex triplet state, the radical yield becomes dependent on the strength of an applied magnetic field, because the field mixes the states T_x, T_y, T_z and, hence, increases the integral ISC rate and, consequently, lowers the radical yield. Of course, this *d*-type TM also leads to an initial spin polarization of the resulting radicals R_1 and

R_2, provided the requirements are fulfilled for the polarization transfer from the zero-field states T_x, T_y, T_z to the radicals. The radical spin polarizations in the thionine/halogen-aniline systems have not been investigated up to now and will be part of this work. However, in rather similar systems consisting of triplet excited dye molecules and halogen substituted anilines the CIDEP of the radicals as well as the MFE upon the radical yield have been observed recently [12].

The conditions for a *d*-type TM to occur are seldom met, especially the required fast ISC of the triplet excited molecule back to its ground state with rates of at least 10^9 s^{-1}. Besides the above mentioned systems, where triplet excited dye molecules form exciplexes with halogen substituted anilines, only one further class of photo-decompositions are known, where a *d*-type TM had to be invoked to explain the initial CIDEP of the radicals generated. Recently, A. Savitsky and H. Paul have observed that alkyl radicals are polarized with an anomalous emission when generated by triplet-sensitized photo-decomposition of acyclic azoalkanes [13]. They have tentatively attributed this polarization to a *d*-type TM, assuming that the radiationless deactivation of the triplet azoalkanes to their singlet ground state occurs faster from the energetically lower triplet sublevels, thus producing an overpopulation of the higher ones. If this assumption holds, the radical yield should depend on the strength of an applied magnetic field, as has been explained above for the thionine/halogen-aniline systems.

In the *d*-type TM the initial CIDEP of the radicals and the MFE upon their yield are two manifestations of one and the same phenomenon. Thus, the magnitudes of both effects should be correctly predictable with one and the same set of parameters, which are essentially the ISC rates of the triplet molecules, their decomposition rates into radicals, their Zero-Field Splitting (ZFS) tensor, as well as the correlation time of their rotational diffusion. The main idea of this work was to check this by measuring under comparable conditions and by analysing quantitatively both the spin polarization of the radicals and the MFE on their yield. Such a unified treatment of both effects has not been tried before, though it is nearly imperative to give conclusive evidence for the *d*-type TM and the soundness and reliability of the theoretical model and its formulation, also in its quantitative details. In addition, the combined analysis of both effects should yield characteristic data of the triplet molecules, which are difficult to obtain with other experimental techniques. This is of particular interest for the triplet state of azoalkanes, as up to now neither kinetic nor spectroscopic data are known for these elusive species.

In the following main chapter 2 of this work the rapidly deactivating triplet state of azocumene (AC) is studied by combination of two experimental methods: TREPR and optical

absorption spectroscopy after laser flash photolysis (LFP). The triplet state of AC is generated by photo-sensitization with 1-nitronaphthalene (1-NN). The cumyl radicals, formed after ^{3}(1-NN) quenching by AC, are investigated in alkane solutions of different viscosity (0.4 cP – 100 cP). A kinetic analysis is developed, which allows an accurate determination of the radical yield from the time profiles of the optical absorption spectrum of the solution. The cumyl radical yield in the various solvents is then determined for different applied magnetic fields ranging from 0.02 T – 3 T. These measurements have been carried through on the LFP set-up of U. Steiner's group at the University of Konstanz.

The second observable, the non-equilibrium initial spin polarizations of the cumyl radicals, are then investigated by TREPR, again for various viscosities ranging from 0.2 cP - 100 cP, but at only one magnetic field strength (350 mT, the field of our X-band TREPR spectrometer). The initial CIDEP of the radicals is determined by fitting the experimental time profiles with Bloch equations, which are modified to account properly for the chemical reaction dynamics of the1-NN/AC system.

It is then shown that all parameters (the different rates for the ISC, the cleavage rate into radicals, and the zero-field splitting parameter D which measures the dipole-dipole interaction between the two unpaired triplet electrons) can be obtained from a combined analysis of the CIDEP and MFE data. Finally, these parameters will be validated by using them in a numerical integration of the relevant Stochastic Liouville Equation (SLE). A short introduction into the photochemistry of acyclic azoalkane is given at the beginning of the chapter in order to facilitate for the reader the further understanding.

The third chapter deals with an experimental TREPR study of the CIDEP of semi-reduced thionine radicals produced by reacting thionine triplets with aniline and some of its halogenated derivatives. These are the chemical systems for which, two decades ago, U. Steiner measured the MFE on the radical yield and first formulated the *d*-type TM. Until now the lack of information on the size of the radical spin polarization created in these systems did not allow a unified theoretical treatment of all relevant observables of the TM.

The quantitative determination of the CIDEP in these systems is somewhat intricate, as there are two polarization mechanisms, a *d*-type and a *p*-type TM. After photo-excitation of thionine the ISC yields a spin polarized triplet thionine because of a *p*-type TM. This polarization is transferred to the thionine/aniline exciplex, in which then a *d*-type TM becomes

operative. It will be shown that both polarizations are separable by measuring the CIDEP at different aniline concentrations. A second obstacle in the analysis of the TREPR results from the structure of the EPR spectrum of the semi-reduced thionine radicals, which consists of many overlapping lines. In cases like that the time profiles can no longer be analysed by just fitting modified Bloch equations to them, as these are valid only for single, fully resolved resonance lines. Therefore, a new signal processing technique is developed based on Laplace trasformation of the Bloch equations and analysis of the total magnetization, i.e. the EPR intensity integrated over the magnetic field. The combined analysis of the CIDEP data with the previously measured MEF data has been carried out by U. Steiner [14] and, therefore, is not discussed in this thesis. Only the final results will be briefly discussed in the last section of chapter 3.

Parts of the PhD work of the author have already been published [14,15,16].

2 The triplet state of *trans*-azocumene: experimental study and theoretical analysis in terms of the *d*-type TM of CIDEP.

2.1 Literature review on relevant aspects of the photochemistry of acyclic azoalkanes.

Azoalkanes have been known since 1909 [17] and represent a very wide class of compounds which have the general formula:

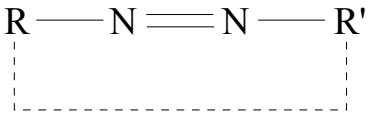

The dotted line in the formula indicates that the compound may be cyclic or acyclic. The distinguishing feature of azoalkanes is, that the nitrogen is bound to saturated carbon. Unsaturation may be present elsewhere in the molecule, but such compounds are also classified as azoalkanes [18].

Azoalkanes have a variety of applications in chemistry, which are mainly based on the fact that azoalkanes are probably the cleanest and most convenient sources of radicals and biradicals of nearly any desired structure. The production of radicals or biradicals may occur thermally or photochemically under a wide variety of conditions according to the general scheme:

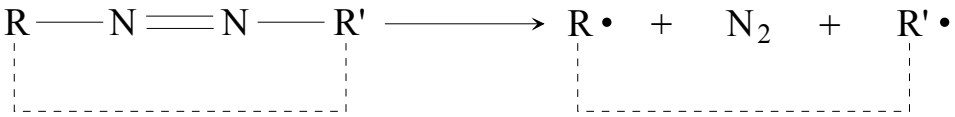

Acyclic azoalkanes are obtained on usual synthetic routes only as *trans*-isomers. The *cis*-azoalkanes are thermally less stable and often effectively decompose at room temperature with elimination of nitrogen [19] . The decomposition activation energies are usually much higher for the *trans*-isomers than for the *cis*-ones. Therefore, the *trans*-isomers are usually stable at room temperature and may be studied directly. The easiest and most effective way to *cis*-isomers is the photochemical isomerization if, of course, some necessary conditions are met.

The photochemical properties of azoalkanes are determined by the azo-group, in which the two nitrogen atoms are sp_2-hybridized and bound with each other by means of one σ- and one π- bond. The azo-group of *trans*-isomers has C_{2h} –symmetry and the azo-group of the *cis*-ones has C_{2v} –symmetry. In the intermediate state, when the rotation angle between the two C-N bonds differs from 0 and 180 degree, the symmetry is lowered to just C_2 .

2.1.1 Direct excitation photochemistry

The dominant electron configurations of the lowest seven states (four singlet and three triplet states) of *trans*-azoalkanes are given below [20]:

S_0 : $(n_-)^2(\pi)^2(n_+)^2$

$S_1\&T_1$: $(n_-)^2(\pi)^2(n_+)(\pi^*)$

$S_2\&T_3$: $(n_-)(\pi)^2(n_+)^2(\pi^*)$

$S_3\&T_2$: $(n_-)^2(\pi)(n_+)^2(\pi^*)$

The orbitals n_-, π, n_+, π* are schematically shown in figure 2.1

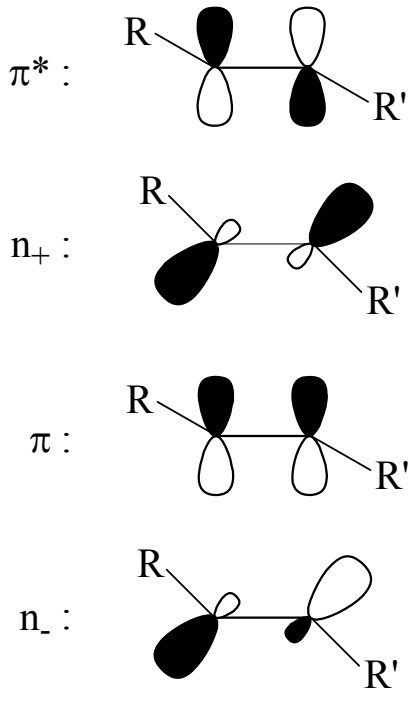

Figure 2.1: Schematic orbitals of trans-azoalkanes.

Azoalkanes exhibit a typical weak absorbtion band in the 300-400 nm region [21,22]. It has been commonly accepted, that this band corresponds to the $S_0 \rightarrow S_1$ transition . As one can see, in the $S_0 \rightarrow S_1$ transition one electron changes its orbital from n_+ to π^*. Under C_{2h}-symmetry this transition is forbidden, what explains the usually very low absorption coefficient of *trans*-isomers. For *cis*-azoalkanes the absorption is caused by a $n_- \rightarrow \pi^*$ transition, which is allowed under C_{2v}-symmetry. Therefore, the absorption coefficients of cis-isomers are considerably larger (typically about ten times) than those of the *trans*-isomers.

Being in their first excited singlet state, acyclic *trans*-azoalkanes undergo three main chemical processes: 1) dissociation into two radicals with elimination of nitrogen, 2) *trans*-*cis* isomerization with formation of the *cis*-isomers, which in turn may decompose thermally, and 3) return to the starting material, i.e. to the ground state of the *trans*-isomer.

At low pressures in the gas phase the photodissociation to N_2 and alkyl radicals is clearly dominating over the other two processes, and the dissociation quantum yield approaches unity. At higher pressures and in liquid solutions the isomerization and return to the ground state successfully compete with the dissociation and for most of azoalkanes even become the major reaction channels. The general reaction scheme of the direct photolysis of acyclic azoalkanes in solution is shown in scheme 2.1 [18].

Up to now there seems to be no clear understanding of all primary processes and mechanisms of the photophysics following direct excitation of acyclic azoalkanes. The situation is somewhat complicated because of the large variety of different azoalkanes possessing various properties and showing different behavior under the same or similar experimental conditions. This also explains, that a variety of contradictory conclusions have been drawn about some mechanisms in the photophysics of azoalkanes [18].

Below we will try to summarize those data available in the literature from previous investigations, which concern in some way this work As for the direct photolysis, the main questions of our attention will be: 1) what is the time scale of the primary photochemical steps shown in scheme 2.1 as compared with the time resolution of our experimental set-ups, counting tens of nanoseconds, and 2) what are the typical quantum yields of the radicals produced via photo-dissociation and via thermolysis of the *cis*-isomers.

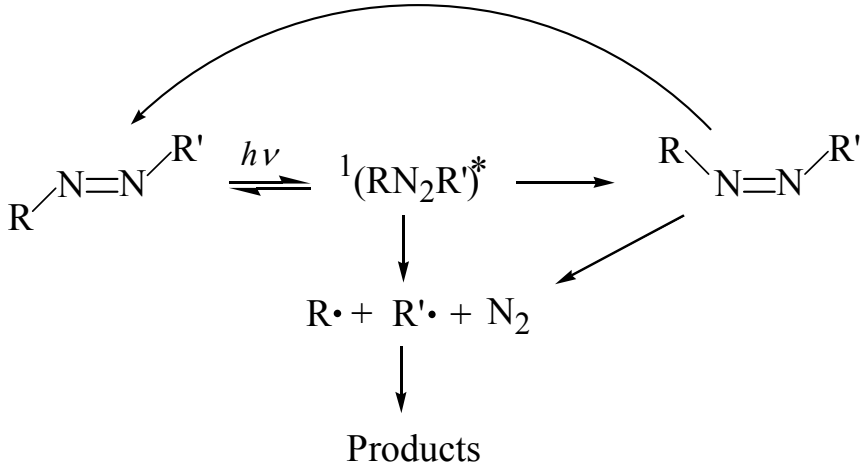

Scheme 2.1

In solution all three processes, dissociation, isomerization and return to the ground state are competing and, therefore, occur on the same time scale determined by the life time of the excited state. Since no fluorescence has ever been seen from any acyclic azoalkane, the return to the starting material seems to be caused by radiationless deactivation of the excited state during collisions with solvent molecules. The collisions should cause the *trans-cis* isomerization as well, as the isomerization occurs only in solution or in the gas phase at high pressures. The literature is very rich with discussions on the mechanisms and time scales of azoalkane decomposition. The failure to observe fluorescence has required the application of numerous indirect methods which have led in many cases to obscure and contradictory results. Nevertheless, one can conclude from the literature, that the dissociation of the S_1-state is a very fast process as compared with our experimental time resolution. It probably occurs on the picosecond or even on the femtosecond time scale. Recently, Zewail and co-workers have studied the photo-decomposition of azomethane in the gas phase and came to the conclusion, that the dissociation proceeds in two steps corresponding to the consecutive breaking of the two C-N bonds within 100 fs [23]. Another evidence for the fastness of the dissociation processes of excited azoalkanes comes from picosecond laser flash photolysis studies of *trans*-AC, where the cumyl radical formation was found to occur faster than the time resolution of the experiment, which was determined by the laser pulse width of about 10 ps [24].

As compared with isomerization, decomposition or radiationless deactivation following the excitation into the $^1(n\pi^*)$ state, the process of thermolysis of the unstable *cis*-isomers is a much

slower process. The life times of the *cis*-isomers are strongly dependent on their chemical structure and may vary from sub-microseconds to practically infinite values for stable *cis*-isomers [18]. Concerning our work we are particularly interested to know the thermolysis rate of *cis*-azocumene (*c*AC). The values 5 μs and 12 μs were reported in cyclopentane [25] and in heptane [26], respectively. This time interferes with time range of our study (10^{-7}-10^{-5} s). Therefore, the thermolysis of the unstable *cis*-isomer of AC has to be considered as a time dependent process.

Finally, the radicals formed via both reaction channels react with each other with a diffusion controlled rate constant, which for radical reactions in solution is typically in the range between about 10^{8} - 10^{10} $M^{-1}s^{-1}$ depending on the viscosity of the solvent [27]. The radical reaction may include both recombination and disproportionation, whose relative yields are of no importance for our study.

The quantum yields of *trans-cis* isomerization and decomposition may take very different values for different azoalkanes. The nitrogen quantum yield Φ_{N_2} varies from almost zero to up to 0.5 [18]. The compounds at the upper limit of this range mainly photo-isomerize to thermally unstable isomers, what causes a higher nitrogen yield. However, some nitrogen may always originate from direct dissociation of the excited state. This is apparent as some azoalkanes exhibit a nonzero Φ_{N_2} even though their *cis*-isomers are absolutely stable at the temperature employed. For example, azoisopropane shows a nitrogen yield of about 0.02 at 25 °C in isooctane [28]. The available literature data clearly show that both channels of azoalkane dissociation, direct cleavage and via isomerization, may have comparable values of quantum yields and must both be considered in any acceptable mechanism of azoalkane photochemistry.

Regarding this work, one may conclude that under light excitation of azoalkanes, one part of the excited molecules either decompose into two radicals and free nitrogen or deactivate to their ground states, and the other part may isomerize and dissociate further on a time scale which may or may not lie in the time range 10^{-7} - 10^{-5} s of our experiments. Both reaction paths may occur with significant quantum yields . The subsequent radical termination occurs with a rate governed by the diffusion-controlled rate constant and by the initial radical concentration, which strongly depends on the experimental conditions (e.g. the absorbed light energy or the irradiated volume).

2.1.2 Triplet-sensitized photochemisty and the triplet state

The triplet energy transfer to azoalkanes is known to be an effective process under the necessary condition, of course, that the triplet state of the donor lies energetically above the triplet state of the azoalkane [18,29,30,31]. The main primary reaction steps after the triplet excitation are generally the same as for direct photolysis [18] (see scheme 2.2).

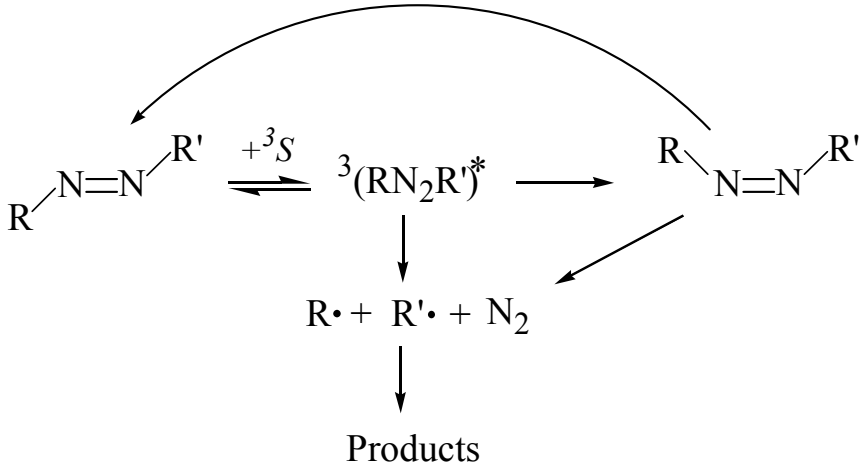

Scheme 2.2

In spite of the fact that the reaction channels are the same, the photochemistry after triplet-sensitization and the direct photolysis via the excited singlet state reveal one essential difference. The total nitrogen quantum yield in solution (composed of both contributions, direct cleavage and thermal decomposition after isomerization) turns out to be much lower for the triplet-sensitized decomposition. It usually does not exceed 0.1-0.15. For example, in the case of R = R' = $EtOOCCMe_2$, the yield of N_2 formation is 0.42 for the direct photolysis in solution and only 0.06 for the triplet-sensitized decomposition [30]. For AIBN the quantum yields are 0.44 and 0.1, respectively [30].

The majority of the triplet excited molecules return to the ground state by radiationless deactivation. This intersystem crossing process is obviously unusually fast for azoalkanes. Quantum chemical calculations of simple azoalkanes suggest as a reason for it, that the potential

surface of the first excited triplet state $^3(n_+\pi)$ crosses that one of the ground state at nuclear configurations, which are located near the potential minimum of the $^3(n_+\pi)$ state [20,32,33]. According to the literature data [18] it seems that the decomposition into radicals can compete with this fast ISC only if the radicals gain some stabilization energy, as it is the case for e.g. the compounds **1**, **2**, **3, 4** (AIBN) [34].

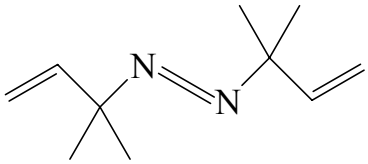

1

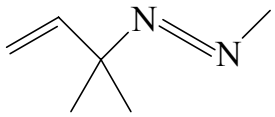

2

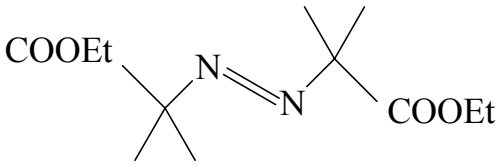

3

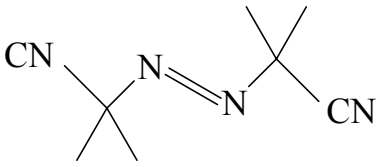

4

Despite the fact that the photochemistry of azoalkanes has been intensively studied, nearly nothing is known about their triplet state. Today's fast spectroscopic techniques are difficult to apply, because the triplet state can be populated only rather slowly via a triplet quenching reaction, and phosphorescence from this state is completely absent. Thus, up to now the only experimental knowledge is: a) azoalkanes possess a triplet state at 218 – 234 kJ/mole above the ground state [31,35] and b) this state is short-lived and, in some cases, decomposes with low quantum yield into radicals and nitrogen. No quantitative data are known concerning the time scales of the primary processes shown in scheme 2.2.

Recently it has been found that the radicals stemming from the decomposition of triplet azoalkanes carry an emissive electron spin polarization, which was tentatively attributed to a *d*-type TM [13]. In the following it will be shown that this interpretation is correct, and that the effect can be exploited to obtain the first quantitative kinetic and spectroscopic data for an azoalkane triplet state. The quenching of the triplet state of 1-nitronaphthalene (1-NN) by azocumene (AC) is used as chemical system.

2.2 The chemical system

1-NN : 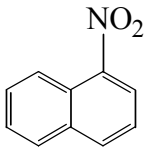

AC: 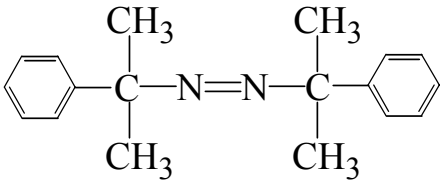

Azocumene (AC) and 1-nitronaphthalene (1-NN) as sensitizer were found to be a very suitable chemical system for an experimental and theoretical study of the *d*-type TM.

1-Nitronaphthalene seems to be an almost ideal triplet sensitizer for our purposes, because:

1) Being excited in its first excited singlet state 1-NN undergoes fast and efficient ISC with a quantum yield of 0.63 [36] and a rate of about 10^{11} s^{-1} in non-polar solvents [37,38]. This ISC rate is much larger than the rate of quenching by AC expected under our experimental conditions (less than 10^{9} s^{-1}). Therefore, any contribution of singlet energy transfer will be negligible (azoalkanes are also efficient singlet quenchers!). The high quantum yield of triplets may be of critical importance for our investigation, as the triplet decomposition of AC is a rather inefficient process and an only low radical yield has to be expected.

2) The triplet state of 1-NN is rather persistent to photochemical reactions [39,40] and lives sufficiently long to be successfully quenched by AC at reasonable concentrations of AC. In this work we have found that the life time of the triplet state, being dependent on the solvent, was longer than 0.5 μs for the solvents used in our study, whereas the inverse quenching rate could be easily varied in the range 60 ns – 2 μs.

3) Despite some emissive *p*-type TM polarization of the 1-NN triplet is expected from its known zero field tensor components (D_{zfs} = 85.5 mT and E_{zfs} = -5.1 mT) and ISC rates (X:Y:Z = 0:0.55:0.45) [41], no polarization transfer to triplet AC was found (see section 2.4.5). This is in accord with the conclusion drawn previously by Tarassov, who checked an eventual polarization transfer from 1-NN triplets to a persistent nitroxide radical and did not find any perceptible transfer [42].

The UV absorption of 1-NN was found to be slightly dependent on the solvent. It is shown in figure 2.2 for a heptane and benzene solution. Within the different alkane solvents the spectra were practically identical, and very small differences have been neglected.

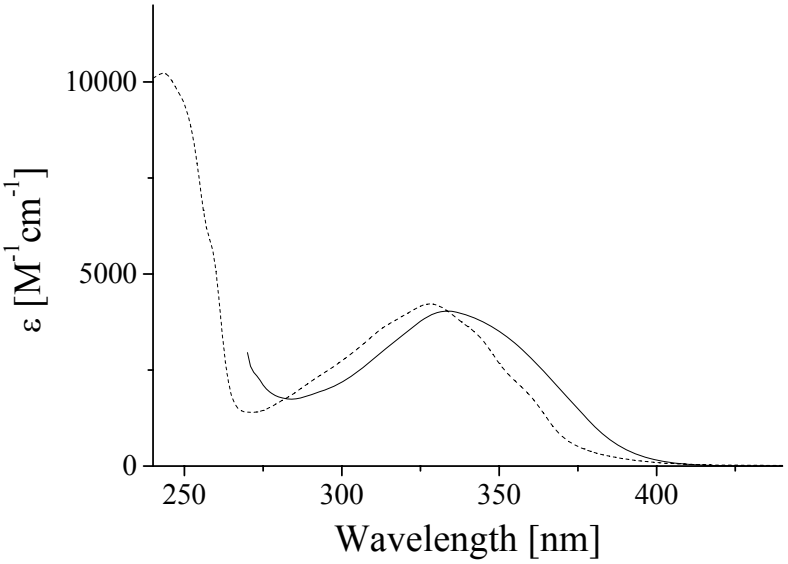

Figure 2.2: UV absorption spectrum of 1-NN ground state in benzene (solid line) and heptane (dotted line).

The main requirements for the azoalkane quencher were:

1) The azoalkane should be symmetric, because decomposition of an asymmetric one would yield two different kinds of radicals, what would complicate appreciably the quantitative analysis of the experimental data..

2) The radicals produced via the azoalkane decomposition should be suitable for both LFP and TREPR experiments.

Azocumene meets these requirements. It is symmetric and decomposes into nitrogene and two cumyl radicals. Because of their narrow resonances cumyl radicals are well detectable by EPR spectroscopy, although the EPR intensity is distributed over many hyperfine lines. They are also well detectable by optical absorption spectroscopy. Due to the conjugation of the unpaired electron into the phenyl ring cumyl radicals possess a strong optical absorption band ($\varepsilon_{max} \approx$ 4500 $M^{-1} \cdot cm^{-1}$) band in the wavelength region 320-330 nm [43,44]. There the absorption

coefficient of the AC ground state is less than 15 M^{-1} cm^{-1} (see figure 2.3), so that there will be no difficulties with an overlap of AC depletion and radical appearance. Other alkyl radicals like *t*.butyl or 2-propyl are much less suitable for our purposes, because they have only weak optical absorption bands at reasonable wavelengths ($\lambda \geq 250$ nm) [45].

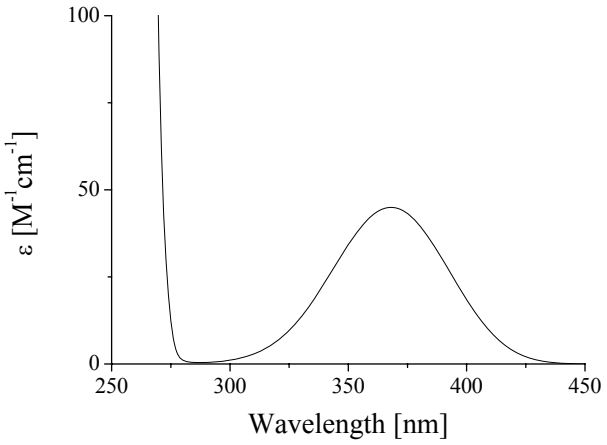

Figure 2.3: UV absorption spectrum of AC ground state in heptane.

Probably as additional advantage of AC may be considered its bulky structure. This slows down the process of rotational diffusion in solution, which tends to destroy the observable effects (MFE and polarization).

Table 2.1: Solvents and their viscosities.

	[1)]η [10^{-3} Pa·s]
Pentane	0.21
Heptane	0.41
Benzene	0.67
Nonane	0.71
Dodecane	1.50
Hexadecane	3.32
Squalane:Heptane (4:1vol.)	8.32
Squalane	32.4
Paraffin oil	106.7

1) Taken from reference [26]

To perform investigations in a wide range of viscosities, we have used as solvents benzene and eight alkanes, which are listed in table 2.1 together with their viscosities at room temperature. *Trans*-azocumene was synthesized from cumylamine using the method described by Stowell for 2,2'-azobisisobutane [46]. Its purity was checked by NMR and HPLC and estimated to be better than 98%. Cumylamine was prepared according to the prescription given in [47]. 1-nitronaphthalene and all solvents were purchased from FLUKA or ALDRICH in their purest commercially available forms and were used without further purification.

2.3 Study with time-resolved optical absorption spectroscopy

2.3.1 Experimental part

The experimental arrangement for time-resolved optical absorption measurements after laser flash photolytic generation of transients has been described in detail previously [48] and is shown in figure 2.4. The set-up is built similarly as others described in the literature [49,50,51], but it possesses one special feature. The quartz cuvette containing the sample solution is placed in the center between two poles of a Varian EM 500 electromagnet, so that measurements can be carried out in static magnetic fields ranging from 0.02 T (residual field) to about 4T. This is practically realized by making the exciting and the probing light beams almost parallel (the angle between the two beams is about 2.5 °), whereas the commonly used geometry for LFP measurements is the perpendicular arrangement of the beams. A frequency-tripled Nd-YAG laser was used as exciting light source, producing 10 ns light pulses at 355 nm with 10 Hz repetition rate.

For the 1-NN concentration we used (1.2 mM). The saturation of the signal was found to start at pulse energies exceeding 6-7 mJ. Therefore, an attenuation to about 6.4 mJ was applied for all measurements. All solutions were deoxygenated by purging with helium for about 1 hour and then pumped in continuous flow (flow rate 10 cm^3/h) through a flat quartz cell (2 mm optical path length). To avoid temperature fluctuation in the irradiated volume (caused by the closeness of the cell to the magnet poles) the cell was blown on by air of room temperature.

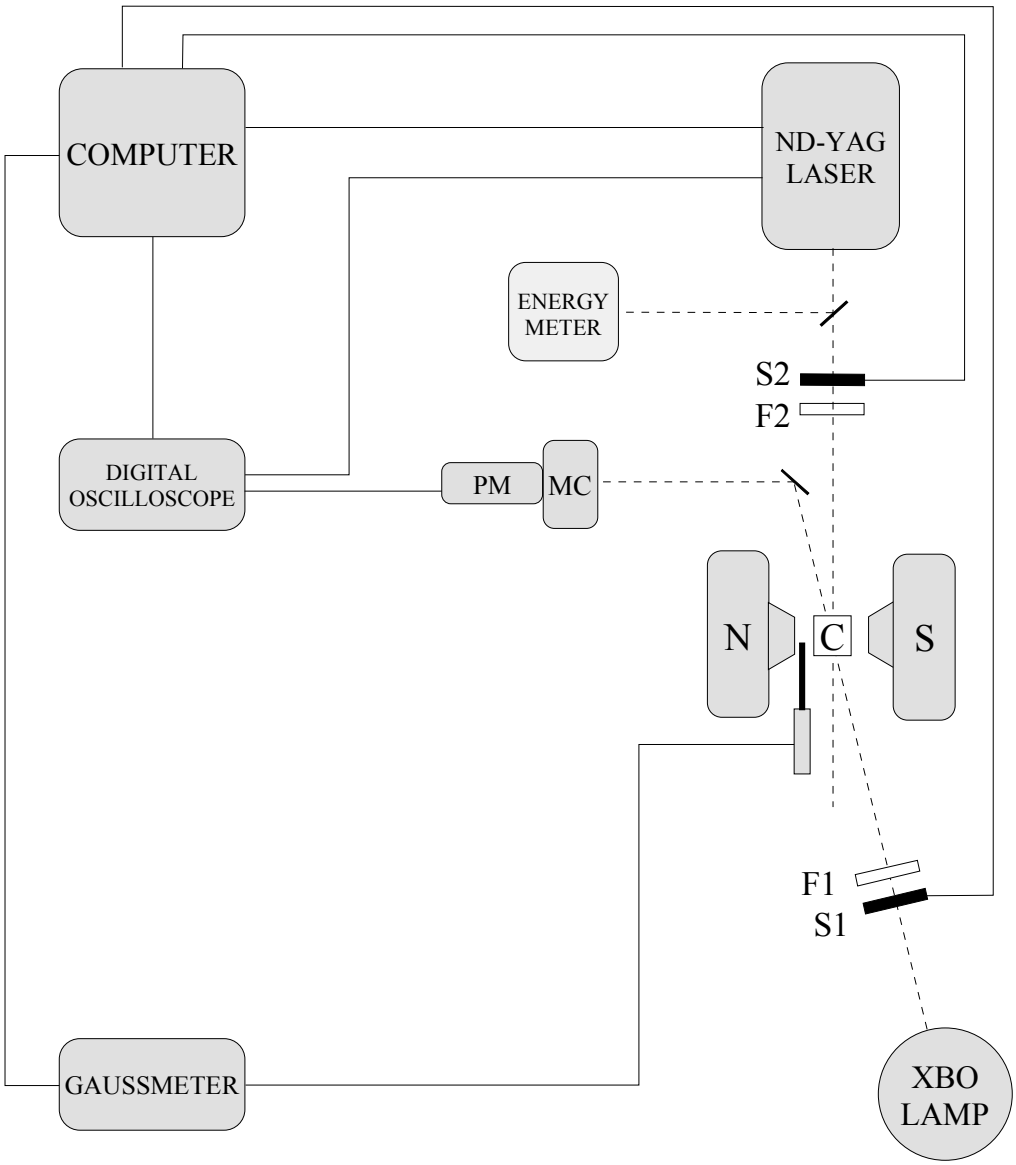

Figure 2.4: Block diagram of the LFP optical spectrometer (C–Cell, PM–photomultiplier, S1,S2 –shutters, F1,F2–optical filters).

2.3.2 Optical spectra of cumyl radical and triplet 1-nitronaphthalene

In order to determine quantitatively the fraction of ^{3}AC which, after formation via quenching of ^{3}(1-NN), cleaves into cumyl radicals, one has to measure the concentration of initially formed ^{3}AC molecules and the concentration of cumyl radicals, which are generated from them. Doing that with optical absorption spectroscopy requires knowledge of the absorption coefficients $\varepsilon(\lambda)$ of the cumyl radicals as well as the ^{3}(1-NN) species (^{3}AC escapes

direct optical observation because of its very short life time). Therefore, the optical absorption spectra of ^{3}(1-NN) and the cumyl radical have been taken after laser irradiation of heptane solutions containing 1-NN (0.4 mM) and AC (100 mM), respectively. The results are given in figure 2.5. Primarily the experiments yielded only the optical densities OD(λ) of the transient species. For the cumyl radicals (figure 2.5 b) OD(λ) was scaled to ε(λ) by adopting the literature value ε ≈ 4500 $M^{-1}cm^{-1}$ for the absorption maximum [43,44], which we found at λ = 329 nm, slightly higher than the literature information (λ ≈ 320-322 nm). For ^{3}(1-NN) (figure 2.5a) the optical density immediately after laser pulse excitation, $OD^T(0)$, was converted to ε via

$$\varepsilon = \frac{OD^T(0) \cdot h\nu \cdot N_A \cdot V}{E_L \cdot \Phi \cdot \left(1 - 10^{-OD}\right)} \quad .$$

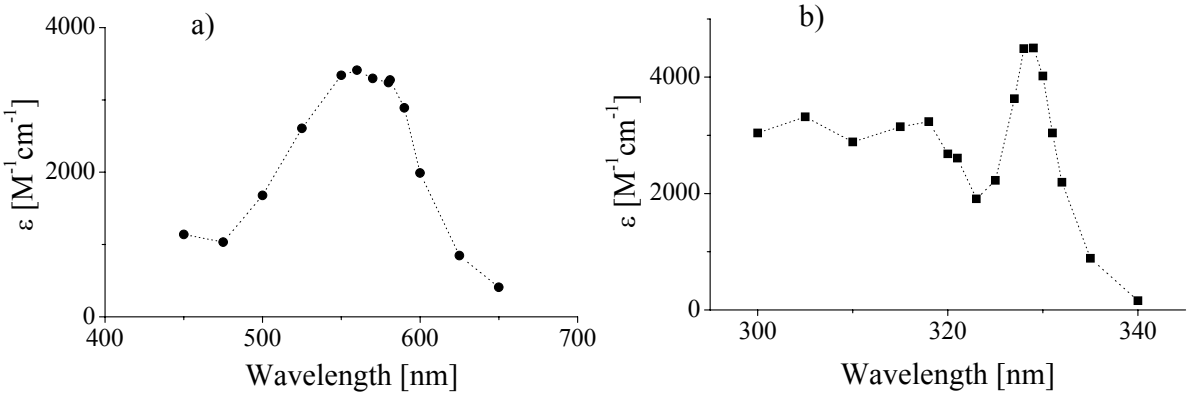

Figure 2.5: Optical spectra of: (a) the triplet-triplet absorption of 1-NN and (b) the absorption of cumyl radicals averaged over the time interval 100-600 ns after the laser flash.

The optical density OD of ground state 1-NN was known and the quantum yield Φ = 0.63 could be taken from the literature [36]. $OD^T(0)$ was extracted by fitting the experimentally measured time-profiles $OD^T(t)$ with a single exponential decay (the triplet concentrations in these experiments, 10^{-5} - 10^{-6} M, were low enough to neglect triplet-triplet annihilation, and at λ > 450 nm there is no overlapping absorption of ground-state 1-NN). The ratio of irradiated volume V to average laser pulse energy E_L was determined by actinometry using as an

actinometer the photolysis of di-*t*.butyl ketone in heptane [49] (the rate constant for *t*.butyl radical self-termination in heptane was taken as $7.9 \cdot 10^9$ $M^{-1}s^{-1}$ [52]).

2.3.3 Quenching of triplet 1-nitronaphthalene by azocumene

For studying the kinetics of the ^{3}(1-NN) decay λ = 580 nm was chosen as wavelength of detection. It is reasonably close to the absorption maximum of ^{3}(1-NN), and neither the cumyl radical nor AC and ground state 1-NN absorb at this wavelength. Thus the time-profiles of the OD at 580 nm (OD_{580}) must reflect the kinetics of ^{3}(1-NN).

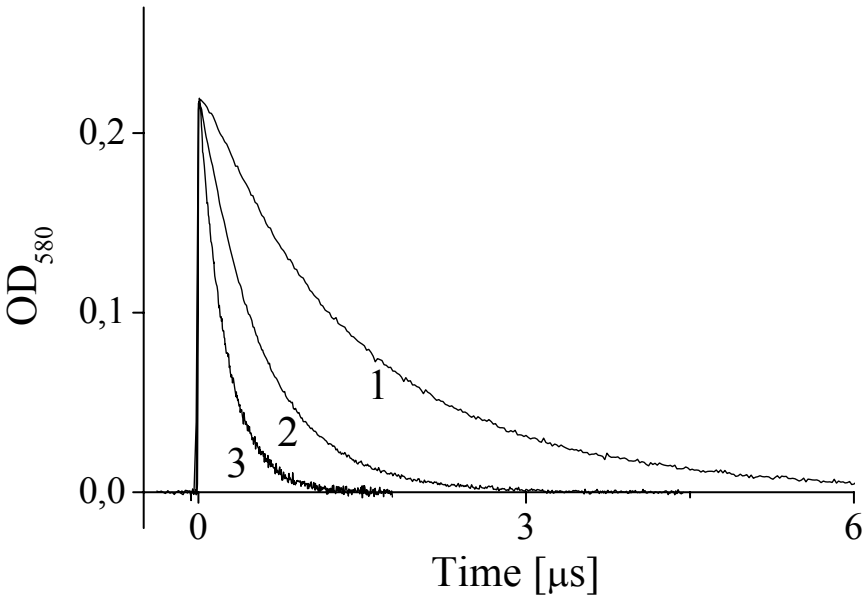

Figure 2.6: Dependence on time of the optical density at 580 nm after LFP of paraffin oil solutions containing 1.2 mM 1-NN (1) and, in addition, 4.5 mM (2), 16.5 mM (3) azocumene.

Figure 2.6 shows as an example the time dependencies of OD_{580} obtained for solutions of 1-NN (1.2 mM) in paraffin oil containing three different AC concentrations. The decay kinetics is determined by three factors: the rate of triplet quenching by azocumene, the rate of triplet-triplet annihilation, and the residual life time of ^{3}(1-NN). Thus, the rate equation for the triplet concentration reads

$$\frac{d}{dt}[T] = -k_{TT}[T]^2 - \left(\frac{1}{\tau_0} + k_Q[AC]\right)[T]$$

with τ_0 being the residual triplet life time and k_Q and k_{TT} the rate constants of quenching and triplet-triplet annihilation, respectively. Integration and multiplication with the absorption coefficient at 580 nm yields

$$OD_{580}(t) = \frac{\varepsilon_{580} \cdot [T]_0 \cdot e^{-\frac{t}{\tau}}}{\tau \cdot k_{TT} \cdot [T]_0 \cdot \left(1 - e^{-\frac{t}{\tau}}\right) + 1} \qquad (2.1)$$

where $[T]_0$ is the initial triplet concentration and $1/\tau = k_Q[AC] + 1/\tau_0$ represents the rate of the first order decay. To avoid many parameter fitting in the analysis of the triplet kinetics, each time-profile was divided into a short- and a long-time part. Triplet-triplet annihilation, being a second order reaction, does not contribute noticeably in the long-time part of the time-profiles, where the triplet concentration is 5-10 times smaller than at the beginning. Thus, this part can be described by a single exponential decay with life time τ, i.e.

$$OD_{580}(t) \approx \frac{\varepsilon_{580} \cdot [T]_0 \cdot e^{-\frac{t}{\tau}}}{1 + \tau \cdot k_{TT} \cdot [T]_0} \qquad (2.2)$$

Fitting the long-time part of the time-profile by equation (2.2) yielded the parameter τ, which was then kept fixed in a subsequent fit of equation (2.1) to the whole curve, with ε_{580} = 3240 $M^{-1}cm^{-1}$ and k_{TT} and $[T]_0$ being two variable parameters. The fitting procedure is illustrated in figure 2.7. For all time-profiles excellent agreements of fitted and experimental curves could be reached.

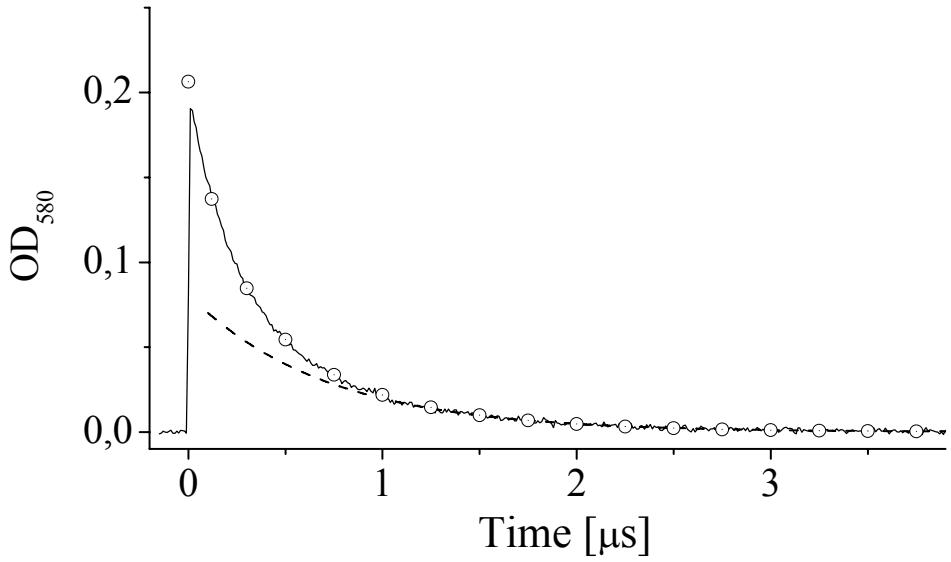

Figure 2.7: Solid noisy line represents the experimental time-profile and the dashed one is its simulation at times over 1μs by equation (2.2) with parameter τ = 709 n. Points are the simulation of the whole time-profile by equation (2.1) with $[T]_0 = 3.2 \cdot 10^{-4}$ *M and* $k_{TT} = 7.6 \cdot 10^9$ $M^{-1}s^{-1}$.

Finally, the quenching rate k_Q and the residual life time of ^{3}(1-NN) were extracted from slope and intercept of linear plots of $1/\tau = 1/\tau_0 + k_Q[AC]$ versus the quencher concentration [AC] as shown in figure 2.8.

The results obtained for the rate constants of the triplet-triplet annihilation and the quenching process are depicted in figure 2.9a and b (for the values of τ_0 see below table 2.3). As expected, the rate constant of triplet-triplet annihilation is in the order of magnitude of 10^9 $M^{-1}s^{-1}$ and varies proportionally to η^{-1}, indicating this reaction to be a diffusion controlled process. The dependence of the quenching rate k_Q on $1/\eta$ is clearly non-linear, approaching diffusion controlled values at high viscosities but staying clearly below that limit at low viscosities. This observation is in full accord with results of previous work, which has also found the rate of quenching by azoalkanes with bulky substituents to be considerably diminished, probably because of steric hindrance [31].

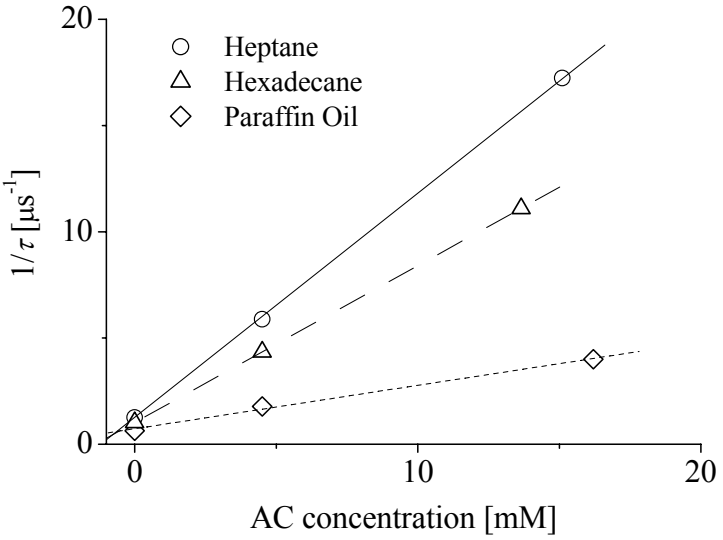

Figure 2.8: Dependencies of the extracted parameter $\frac{1}{\tau}$ *on the AC concentration for three chosen solvents (points) and their linear fits (lines).*

In order to validate this interpretation of the viscosity dependence of the quenching constant we will follow a common scheme for energy transfer processes in solution [53]:

$$S^* + Q \underset{k_{-d}}{\overset{k_d}{\rightleftharpoons}} [S^*Q] \xrightarrow{k_{et}} S^* + Q$$

The result of this model is the following equation for the observed quenching constant:

$$k_q = \frac{k_d k_{et}}{k_{et} + k_{-d}} \tag{2.3}$$

Assuming for estimation as, in [53], that $k_{-d} \approx k_d \cdot 4$ M and $k_d \propto \eta^{-1}$ (i.e. $k_d = \frac{C}{\eta}$), equation (2.3) can be rewritten as:

$$k_q \approx \frac{k_{et}}{4 + \frac{k_{et}\eta}{C}} \tag{2.4}$$

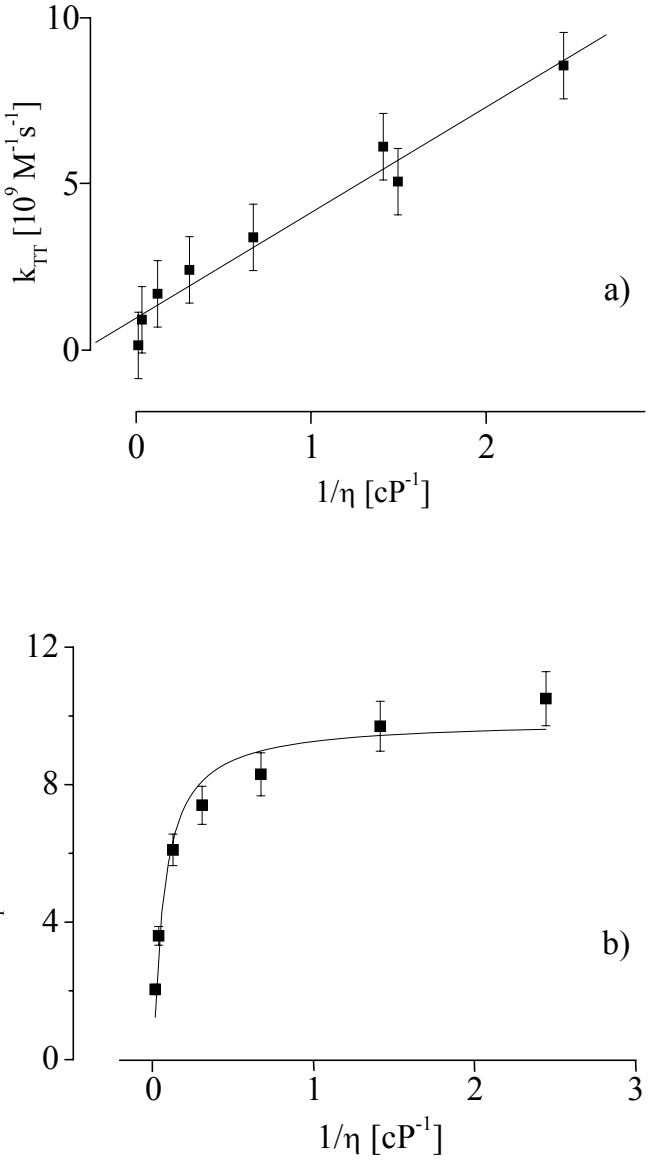

Figure 2.9: Points represent the dependence on viscosity of the calculated rate constants of (a) the triplet-triplet annihilation of ^{3}(1-NN) and (b) the quenching of ^{3}(1-NN) by azocumene. Lines designate (a) a linear fit assuming the triplet-triplet annihilation to be diffusion-controlled, and (b) a two parameter fit by equation (2.4) (see text).

The result of fitting equation (2.4) to the experimental dependence $k_q(\eta)$ (see figure 2.9b) yields for the energy transfer process and the diffusional collision, respectively, the rate constants

$$k_{et} \approx 4 \cdot 10^9 \text{ s}^{-1} \qquad \text{and} \qquad k_d \approx \frac{1.6 \cdot 10^{10} \text{ M}^{-1}\text{s}^{-1}\text{cP}}{\eta}.$$

As expected, the value of k_d is close to the diffusion-controlled limit and of the same order as the k_d value, which with a similar analysis has been determined for the quenching of triplet valerophenone with 2,5-dimethyl-2,4-hexadiene [53]. From this agreement and the fact, that the experimental dependence $k_q(\eta)$ is well described by relation (2.4), we conclude that our k_q values are correctly determined. The rather low value of k_{et} is probably caused, as has already been mentioned, by the bulky structure of AC hindering orbital overlap between donor and acceptor, which is required for the energy transfer to occur.

Finally, it is pointed out that all the measurements of rate constants of quenching and triplet-triplet annihilation were performed at a magnetic field of 0.02 T, caused by the residual magnetization of the magnet poles in the experimental set-up. In order to test a possible influence of magnetic fields on the decay kinetics of ^{3}(1-NN), several control experiments were carried out at high magnetic field strength (2.94 T). No visible changes in the time-profiles were observed, indicating that eventual effects of a magnetic field on the kinetics of ^{3}(1-NN) were small enough to be neglected.

2.3.4 Quantum yield of cumyl radicals and magnetic field effect

In order to obtain quantitative information about the quantum yield of cumyl radicals and its dependence on an external magnetic field, the dependence on time of the optical density at 329 nm was measured for magnetic fields between 0.02 and 2.94 T, using solutions of 1.2 mM 1-NN and 4.5 mM AC in various alkanes and benzene. The time-profiles obtained in paraffin oil at minimum (0.02 T) and maximum (2.94 T) magnetic field are given, as an example, in figure 2.10. λ = 329 nm corresponds to the absorption maximum of the cumyl radicals, but both ground-state 1-NN as well as its excited triplet also have strong absorption bands at this wavelength. At sufficiently high AC concentrations the quenching of 1-NN proceeds much faster than the self-termination of the cumyl radicals. Thus, already during the laser flash the total optical density of the solution is lowered because of depletion of 1-NN and formation of some ^{3}(1-NN).

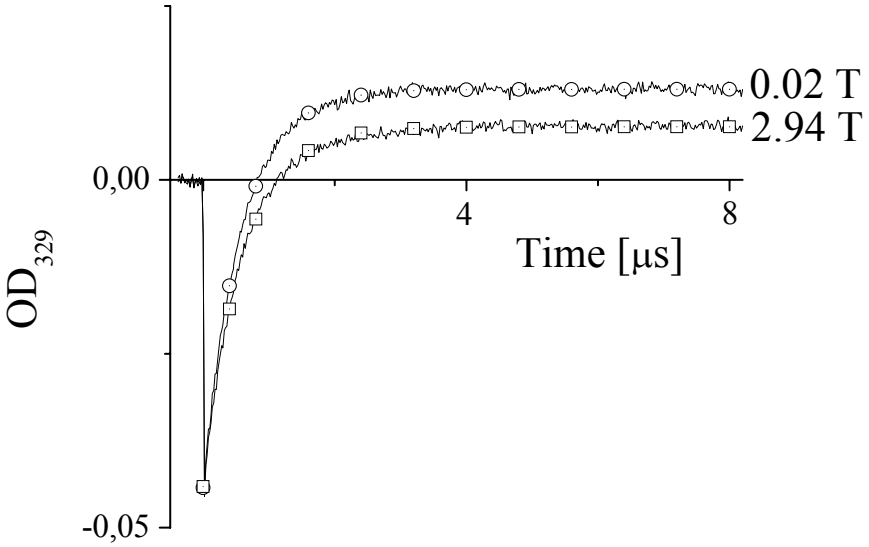

Figure 2.10: Time dependence of the optical density at 329 nm recorded at low and high magnetic field. Points represent their simulations by equation 2.5 with parameters: $[R]_\infty$ = $1.4 \cdot 10^{-5}$ M, τ = 570 ns for B =0.02 T, and $[R]_\infty$ = $8.02 \cdot 10^{-6}$ M, τ = 590 ns for B =2.94 T respectively.

Afterwards, the change of the optical density on the short-time scale is strongly influenced by the ^{3}(1-NN) decay kinetics, and only finally on the long-time scale, where the triplet concentration vanishes, the transient absorption is determined almost exclusively by the absorption of the radicals. Only there, the optical density measures the amount of cumyl radicals, which were generated. However, part of them turned out to have been initiated via direct photolysis of AC. Despite the fact that the optical density of AC at the excitation wavelength ($OD_{355}^{AC} \approx 0.035$) was much lower than that of 1-NN ($OD_{355}^{1-NN} \approx 0.75$), the contribution of direct photolysis of AC to the total quantity of radicals amounted to about 10-15% in low viscous solvents. This noticeable contribution is explainable by the lower quantum yield of radical production from ^{3}(1-NN) as compared with the direct photolysis. For quantitative estimations of the contribution of the direct photolysis, time-profiles obtained for solutions containing the same AC concentration, but no 1-NN, were measured and analysed. The profiles were fitted by a simple constant function and the values extracted were then corrected by multiplying with $\frac{OD_{355}^{AC} \cdot \left(1 - 10^{-OD_{355}^{AC} - OD_{355}^{1-NN}}\right)}{\left(OD_{355}^{AC} + OD_{355}^{1-NN}\right) \cdot \left(1 - 10^{-OD_{355}^{AC}}\right)}$, taking into account the

difference of light absorption by AC in the presence and absence of 1-NN in the solution. The estimated contributions of the direct photolysis OD_{DrPh} are collected in table 2.2. With increasing viscosity the influence of the direct photolysis decreased by a factor of about 3-5 because of the decrease of the radical quantum yield via direct photolysis in more viscous solvents, due to the so called "cage effect" [54]. This decrease is in agreement with literature data concerning the "cage effect" for AC [55].

Table 2.2 Corrections of OD_{329} due to the direct photolysis of azocumene.

	$OD_{DrPh} \cdot 10^3$
Heptane	1.8
Benzene	1.45
Nonane	1.55
Dodecane	1.6
Hexadecane	1.3
Squalane:Heptane (4:1 vol.)	1.1
Squalane	0.6
Paraffin oil	0.4

Taking into account these corrections regarding the direct photolysis, the curves depicted in figure 2.10 were fitted using the equation:

$$OD_{329}(t) = OD_R(t) + \Delta OD_{1-NN}(t) + OD_{DrPh} \tag{2.5}$$

where OD_{DrPh} is the constant contribution of the direct photolysis (see table 2.2), $OD_R(t) = \left(1 - e^{-t/\tau}\right) \cdot [R]_\infty \cdot \varepsilon_{329}^R$ the optical density of the radicals formed by triplet-sensitization, and $\Delta OD_{1-NN}(t) = \Delta OD_{1-NN}(t=0) \cdot e^{-t/\tau}$ the total change of the optical density due to excitation of ground-state 1-NN to its triplet state ^{3}(1-NN). Variable parameters of the fits were $[R]_\infty$, $\Delta OD_{1-NN}(t=0)$ and τ . The parameter $[R]_\infty$ is determined mainly by the level of the plateau, which the experimental curves reach at longer times. It depends only weakly on the values of the two other parameters. For this reason it was possible to extract $[R]_\infty$ by using an approximate simple exponential decay for ^{3}(1-NN). This simplification did not affect the

accuracy of the $[R]_\infty$ analysis. Firstly, $[R]_\infty$ is very insensitive to changes in the short-time part of the curve, and secondly, even in low viscous solvents the contribution of the triplet-triplet annihilation to the decay of ^{3}(1-NN) is only marginal.

It should be noted here, that in equation (2.5) we did not take into account the possible contribution of *trans-cis* isomerization, which may also be a radical source as the produced *cis*-isomer is thermally unstable. The life time of *cis*-AC lies in the range of 5 - 12 μs [25,26], what is much longer than the quenching time of 1-NN (about 0.4 - 0.5 μs). Therefore, *trans-cis* isomerisation, followed by decomposition of the *cis*-isomer would yield a slow rise of the cumyl radical absorption on the time scale 5 - 12 μs. This was not really observed (see figure 2.10). Attempts to simulate the time-profiles on a longer time scale, taking into account isomerization, showed that its contribution is insignificant (less than 10-15 % of the radical yield).

From $[R]_\infty$ the magnetic field effect $MFE(B)$ on the radical production was calculated according to MFE(B) = $\{[R]_\infty(B) - [R]_\infty(0.02\ T)\}$ / $[R]_\infty(0.02\ T)$. In addition, the radical "quantum yield" Φ_R was determined, i.e. the average number of cumyl radicals, which are generated per one ^{3}AC molecule or per one ^{3}(1-NN) molecule quenched by AC. Taking into account all channels of the ^{3}(1-NN) decay (triplet-triplet annihilation, quenching by AC, and residual decay rate) the fraction ξ of triplets quenched by AC is

$$\xi = \frac{k_Q \cdot [AC]}{k_{TT} \cdot [T]_0} \cdot \ln\left\{1 + \frac{\tau_0 \cdot k_{TT} \cdot [T]_0}{1 + \tau_0 \cdot k_Q [AC]}\right\},$$

and, therefore, the yield of radical production per ^{3}AC molecule reads

$$\Phi_R = \frac{[R]_\infty}{[T]_0 \cdot \xi} = \frac{[R]_\infty \cdot k_{TT}}{k_Q \cdot [AC] \cdot \ln\left\{1 + \frac{\tau_0 \cdot k_{TT} \cdot [T]_0}{1 + \tau_0 \cdot k_Q [AC]}\right\}} \qquad (2.6)$$

The magnetic field effect on the radical formation in various solvents is plotted in figure 2.11 versus the external field B. Characteristic feature of the MFE(B) is a pronounced change in the low-field region only, approaching a plateau with a maximum absolute MFE at magnetic

fields B > 1 T. The maximum value, MFE_{max}, obviously depends on the viscosity of the solution.

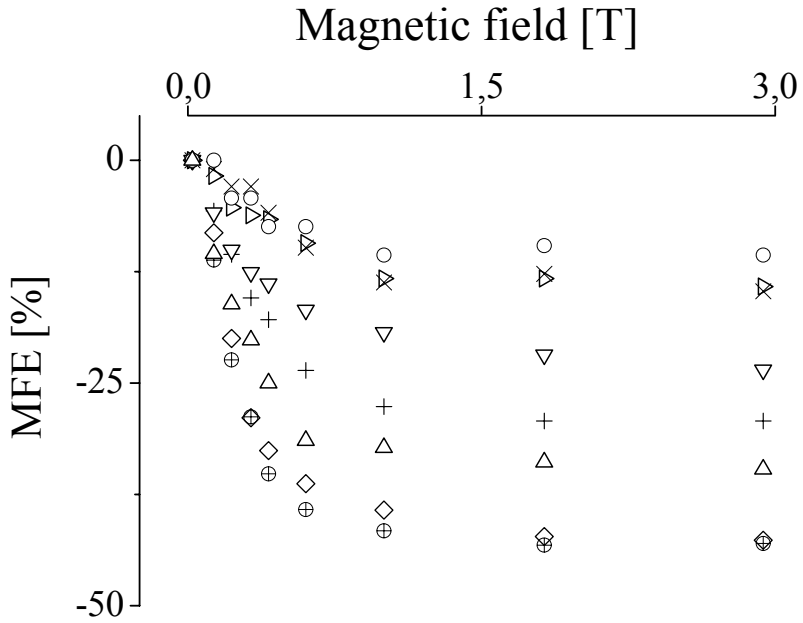

Figure 2.11: Magnetic field dependencies of the magnetic field effect measured in: heptane (○), nonane (▷) , benzene (×), dodecane (▽), hexadecane (+), squalane:heptane (4:1 vol.) mixture (△), squalane (◊) and paraffin oil (⊕).

This dependence is given in figure 2.12a (for MFE_{max} we have taken the average of the high-field values at 1.82 and 2.94 T). MFE_{max} sharply decreases with viscosity until $\eta \approx 30$ cP and then levels off at a value MFE_{max} = -43% in squalane and parrafin oil. Figure 2.12b shows the dependence on viscosity of the radical quantum yield Φ_R, calculated according to equation (2.6) for the minimum magnetic field 0.02 T. Φ_R also levels off at high viscosities and shows a sharp decrease at low ones.

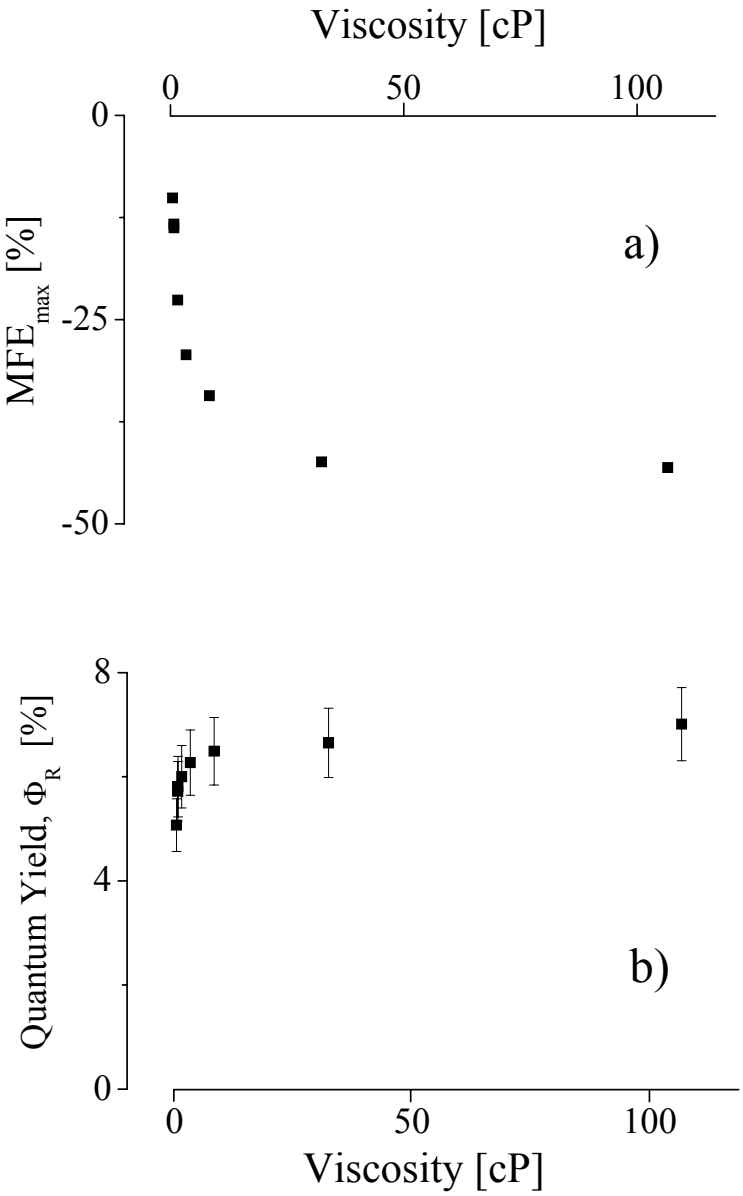

Figure 2.12: Dependence on viscosity of: (a) the maximum magnetic field effect and (b) the cumyl radical yield per quenched triplet 1-NN.

2.4 Study with time-resolved EPR spectroscopy

2.4.1 Experimental part

Cumyl radicals were generated by laser flash photolysis (Nd-YAG laser, λ = 355 nm, 10 ns pulse width, or XeCl excimer laser, λ = 308 nm, 15 ns pulse width) of benzene or alkane solutions containing different concentrations of 1-NN and AC. They were detected at

microwave powers in the range 0.3 - 20 mW using a cw-EPR spectrometer without field modulation (response time about 100 ns). The details of the set-up shown in figure 2.13 have

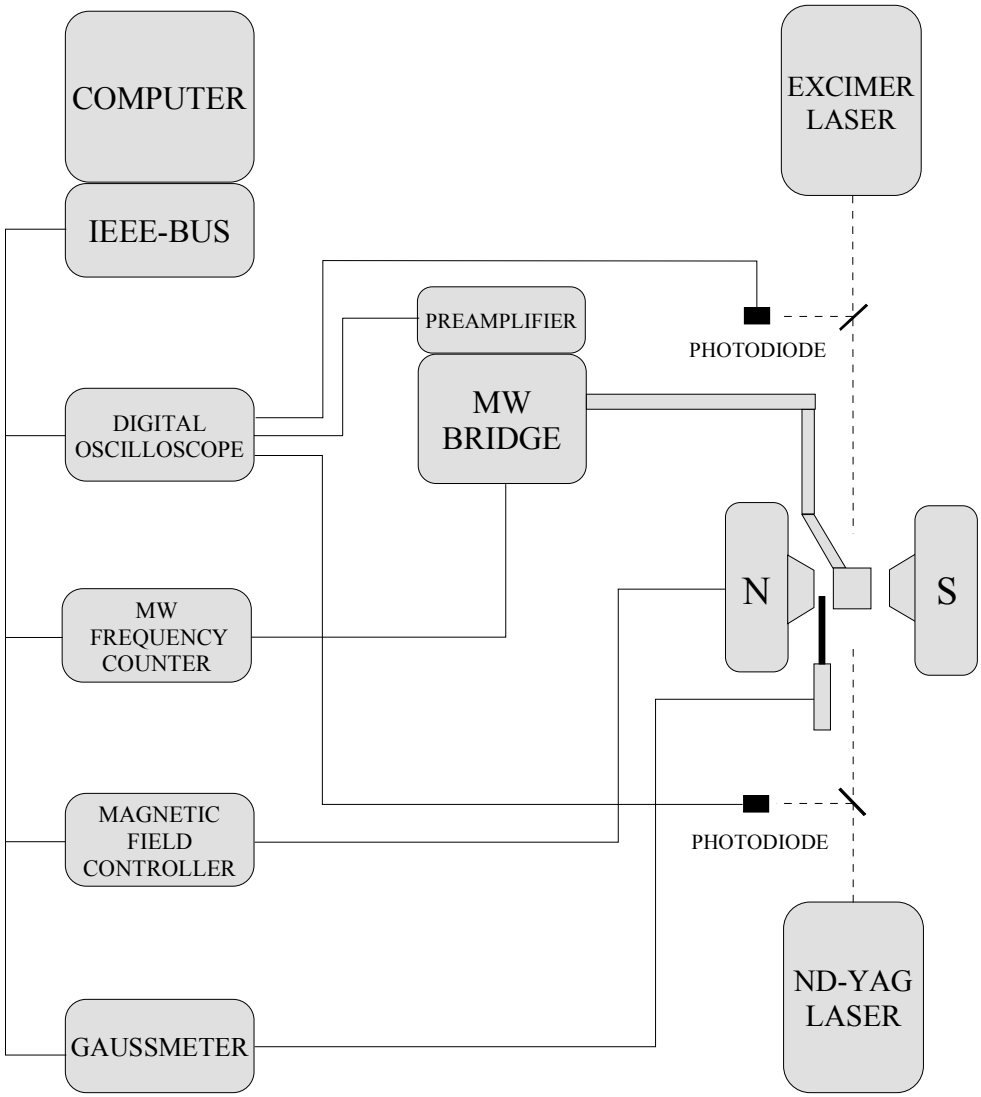

Figure 2.13: Block diagram of the TREPR spectrometer.

been described previously [56]. All solutions were deoxygenated in the same way as it was done in the case of the optical absorption experiments. The flat cell in the EPR cavity had an optical path length of 0.7 mm, a flow rate of 10 cm^3/h was chosen. The laser pulse energy was kept below 5 mJ, so that the depletion of the solutions (all contained about the same 1-NN concentration of 2.1 mM) due to irradiation was negligibly small (checked by UV absorption

spectroscopy before and after irradiation). The sensitivity factor of the spectrometer (which is just the proportionality coefficient between the v-magnetization, measured in units of Boltzmann polarized spins, and the observed TREPR signal measured in volts) was estimated from previous work [26] to be about $1.2 \cdot 10^9$ V/mole. All measurements were performed at room temperature.

2.4.2 TREPR spectrum of cumyl radicals after triplet-sensitized photolysis of azocumene

Figure 2.14 shows the EPR spectrum which is observed about 3 μs after laser flash irradiation at λ = 355 nm of a benzene solution containing 1-NN (2.1 mM) and AC (7.5 mM). According to its hyperfine pattern and phase it has to be attributed unequivocally to an ensemble of cumyl radicals, which is spin polarized in emission. Under the conditions of the

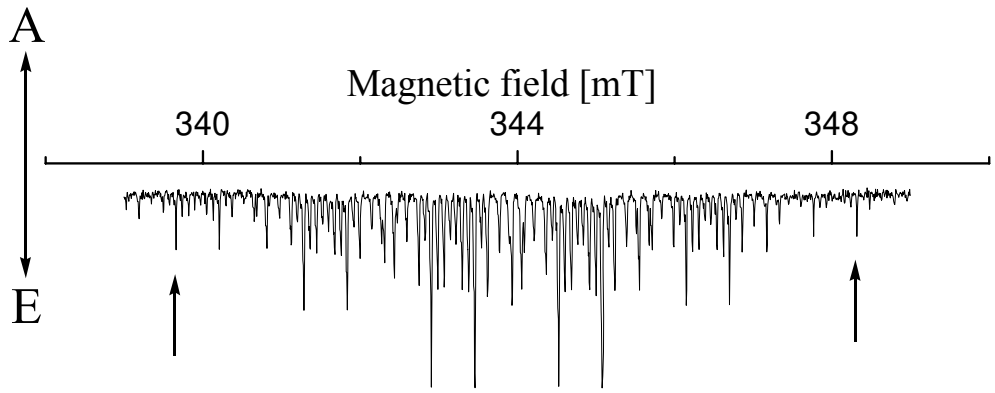

Figure 2.14: TREPR spectrum of cumyl radicals recorded 3 μs after triplet-sensitized photolysis of azocumene in benzene. The high- and low-field resonance lines under study are marked by arrows. A/E designate absorption and emission, respectively.

experiment, the species can not stem from a direct photolysis of AC. Firstly, the direct photolysis of azoalkanes occurs from their excited singlet state and, therefore, leads to TREPR spectra, which initially exhibit a spin polarization with enhanced absorption on the low-field and emission on the high-field site [57]. Secondly, at 355 nm the absorption coefficients of 1-NN and AC are 3200 $M^{-1}cm^{-1}$ and 40 $M^{-1}cm^{-1}$, respectively. Thus, nearly all the light is absorbed primarily by 1-NN, which is known to undergo fast ISC within about 10 ps to its

triplet state ^{3}(1-NN) [37,38]. Quenching of ^{3}(1-NN) by AC then leads to ^{3}AC, which partially cleaves into cumyl radicals and N_2.

Regarding the observed emissive CIDEP of the cumyl radical ensemble three sources are conceivable. Firstly, ^{3}(1-NN) might be spin polarized by the p-type TM and transfer this polarization via ^{3}AC to the radicals. However, this source can be excluded, as the radical polarization turns out to be independent of the AC concentration, i.e. the rate of quenching (vide infra). Moreover, previous quenching experiments of ^{3}(1-NN) with TEMPO radicals have given no indication of any p-type TM polarization of ^{3}(1-NN) [42]. Secondly, the CIDEP might be due to the radical-triplet pair mechanism (RTPM) [58,59], i.e. it might be generated in diffusional collisions of the cumyl radicals with ^{3}(1-NN) or ^{3}AC. This is also very unlikely, because the life times of both triplets are rather short in comparison with the time needed for diffusional radical-triplet collisions at the low concentrations of both species. Thus, all experimental features point to the third possibility, namely the existence of a d-type TM in ^{3}AC, i.e. a cleavage into radicals competing with a fast state selective ISC $^3\text{AC}\rightarrow\text{AC}$ to the ground state, as it has been observed previously also for the triplet state of AIBN [13,26,60]. If this interpretation is correct, then the cumyl radical yield must depend on the magnetic field strength and that is what we have been observing above using LFP with optical absorption spectroscopy.

In order to obtain quantitative information about the electron spin polarization in the 1-NN/AC system one has to measure the magnetization of the cumyl radicals in dependence on time. These time-profiles of the EPR signals may then be analysed with Bloch equations, which describe the evolution of the magnetization vector with time. To do so, the usual Bloch equations have to be modified to account for all processes influencing the dynamics of the magnetization, like e.g. generation of CIDEP, chemical reactions, and spin exchange [61,62]. In addition it has to be kept in mind, that the usual Bloch equations are valid only for single resonance lines, well separated from neighboring lines.

In the spectrum given in figure 2.14 two resonance lines are marked with arrows. They have been used to measure and analyse quantitatively the magnetization in dependence on time. These two lines are separated well enough from neighboring resonances to allow an analysis via Bloch equations. In addition, these two lines are positioned symmetrical to the center of the spectrum. This will be of importance for the separation of the net emissive polarization of the radical ensemble from a superimposed weak emission/absorption multiplet type polarization (note that from the two marked resonance lines the low-field one carries a little bit more

emission than the high-field one because of the superimposed multiplet polarization). The additional emission/absorption type polarization is generated by the well known Radical Pair Mechanism (RPM) [63,64] in pairs consisting of two cumyl radicals, which are formed at the radical initiation stage (geminate pairs) and later on in free diffusional encounters (F-pairs).

2.4.3 The Bloch equations

The most important processes which determine the time behavior of the magnetization vector originating from an ensemble of polarized cumyl radicals are: 1) generation of the magnetization due to production of non-thermally polarized radicals during the triplet decomposition of AC, 2) interaction of the magnetization with the external static and microwave magnetic fields, 3) longitudinal and transversal relaxations of the polarization, 4) spin exchange between the radicals of the ensemble, and 5) formation of F-pair polarization resulting from the RPM in free diffusional encounter pairs of two cumyl radicals. The second and third process is described by the well known Bloch equations [65]. In order to account for the last two processes (4 and 5) we will supplement the Bloch equations with the same additional terms as it was done in [66]. And finally, the rate of the generation of magnetization is determined by the quenching rate of ^{3}(1-NN) by AC as well as by the decomposition rate of ^{3}AC. The decay of ^{3}AC into two radicals occurs on the sub-nanosecond time scale. This is orders of magnitude faster than all other processes. Therefore, for simplicity the decay of ^{3}AC will be considered as instantaneous. The quenching rate depends directly on the quencher concentration. For the concentrations used in our experiments quenching occurred within times ranging from tens of nanoseconds to about one microsecond, i.e. the quenching rate was in the order of magnitude of the rates of the other processes. Thus, the process of generation of magnetization we will have to describe by including in the equation for the z-magnetization of the line i an additional term: $\frac{d}{dt}M_z^i = x_i P^i P_{eq} \Phi_R k_Q [AC][T]$. Here, x_i is the statistical weight of the line under study, P^i is the polarization of the generated radicals, measured in units of the Boltzmann polarization P_{eq}, Φ_R is the quantum yield of the radicals per one excited triplet of AC, k_Q is the rate constant of triplet quenching by AC molecules in their ground state, [AC] is the quencher concentration, and [T] is the concentration of ^{3}(1-NN).

Summarizing all the above discussion and using the same notation as in [66] we can write the modified Bloch equations for the on-resonance case (i.e. the microwave frequency coincides with the resonant frequency of the transition i) :

$$\frac{d}{dt}v^i = -\frac{v^i}{T_2} + \omega_1 M_z^i - k_{ex}[R]v^i$$

$$\frac{d}{dt}M_z^i = -\omega_1 v - \frac{M_z^i}{T_1} + x_i P^i P_{eq} \Phi_R k_Q [AC][T] + \frac{P_{eq}[R]}{T_1} - k_{ex}[R]M_z^i + k_{ex}[R]M_z^{tot} + x_i P_F^i P_{eq} 2k_t [R]^2$$

with initial conditions: $v^i(t=0) = 0$, $M_z^i(t=0) = 0$

and the additional equations for $[R]$ and M_z^{tot} :

$$\frac{d}{dt}[R] = -2k_t[R]^2 \quad , \quad \frac{d}{dt}M_z^{tot} = -\frac{1}{T_1}\cdot\left(M_z^{tot} - P_{eq}[R]\right)$$

These equations are pretty complicated and contain a large amount of unknown parameters, what makes the analysis very difficult and aggravates the quality with which the unknown parameters can be determined. Thus, it turned out to be very convenient to choose such experimental conditions for which the influence of some of the unknown values becomes negligible. The terms in the equations which describe the generation of magnetization in F-pairs and the spin exchange are proportional to the square of the radical concentration in solution. At sufficiently small laser pulse energies these terms become negligibly small. If in addition the initial radical polarization is much larger than P_{eq} (what is the case in our chemical system), the exclusion of the term $\frac{P_{eq}[R]}{T_1}$, which contains the equilibrium polarization, from the equations does not practically influence the quality of the analysis. In this case the equations can be written in the much simpler form:

$$\begin{aligned} \frac{d}{dt}v^i &= -\frac{v^i}{T_2} + \omega_1 M_z^i \\ \frac{d}{dt}M_z^i &= -\omega_1 v^i - \frac{M_z^i}{T_1} + x_i P^i P_{eq} \Phi_R k_Q [AC][T] \end{aligned} \qquad (2.7)$$

The magnitude of the concentration [AC] remains almost constant, because only a small portion of the AC molecules are excited in comparison with the initial concentration. Therefore, we need only one additional rate law for the ^{3}(1-NN) concentration [T], which reads

$$\frac{d}{dt}[T] = -k_{TT}[T]^2 - \left(\frac{1}{\tau_0} + k_Q[AC]\right)[T] \tag{2.8}$$

where k_{TT} is the rate constant of triplet-triplet annihilation and τ_0 the residual life time of ^{3}(1-NN) in the absence of the quencher. The solution of the equation (2.8) with initial condition $[T](t=0) = [T]_0$ is the expression:

$$[T] = \frac{[T]_0 \cdot e^{-\frac{t}{\tau}}}{\tau \cdot k_{TT} \cdot [T]_0 \cdot \left(1 - e^{-\frac{t}{\tau}}\right) + 1} \tag{2.9}$$

where $\frac{1}{\tau} = \frac{1}{\tau_0} + k_Q[AC]$ represents the effective first order decay rate constant. The time-profile of the function (2.9) depends on the unknown parameter $[T]_0$, the accurate estimation of which is very difficult. Additionally, due to the fact that we do not know the profile of the intensity distribution across the laser beam, which is more or less inhomogeneous, the Bloch equations written for different places of the irradiated volume have to contain different time functions [T](t), what makes any correct analysis practically impossible. Thus, it is very convenient to choose experimental conditions for which the influence of the second order kinetics becomes negligible, i.e. $k_{TT}[T]_0 << \frac{1}{\tau}$. In this case the expression (2.9) can be simplified and the time-profile of [T] becomes independent of the parameter $[T]_0$:

$$[T] = [T]_0 \cdot e^{-\frac{t}{\tau}} \tag{2.10}$$

Since we have to separate quantitatively the multiplet and the net polarizations, it is very suitable to analyse the sum and the difference of the two symmetrically placed lines in the spectrum (see the marked lines in figure 2.14). Let i and j to be such lines. Then, introducing the

assignments: $v^{\pm} = v^i \pm v^j$, $M_z^{\pm} = M_z^i \pm M_z^j$, $x = x^i + x^j = 2x^i$, $P^{\pm} = \frac{P^i \pm P^j}{2}$, and also putting (2.10) into (2.7) it is easy to obtain the equations for the sum and difference of the magnetizations of the lines:

$$\begin{aligned} \frac{d}{dt} v^{\pm} &= -\frac{v^{\pm}}{T_2} + \omega_1 M_z^{\pm} \\ \frac{d}{dt} M_z^{\pm} &= -\omega_1 v^{\pm} - \frac{M_z^{\pm}}{T_1} + x P^{\pm} P_{eq} \Phi_R k_Q [AC] \cdot [T]_0 \cdot e^{-\frac{t}{\tau}} \end{aligned} \qquad (2.11)$$

with the initial conditions: $v^{\pm}(t=0)$, $M_z^{\pm}(t=0) = 0$

Here P^+ and P^- have the meaning of the net and multiplet constituents of the total polarization P^i, respectively.

2.4.4 Analytical solutions of the Bloch equations

The equation (2.11) is a first order linear differential equation. Its solution can be easily obtained by a standard procedure and reads:

$$v^{\pm}(t) = \frac{x P^{\pm} P_{eq} \Phi_R k_Q [AC] \cdot [T]_0 \omega_1}{(\tau^{-1} + \lambda_1)(\tau^{-1} + \lambda_2)(\lambda_1 - \lambda_2)} \left\{ (\lambda_1 - \lambda_2) e^{-\frac{t}{\tau}} + (\tau^{-1} + \lambda_2) e^{\lambda_1 t} - (\tau^{-1} + \lambda_1) e^{\lambda_2 t} \right\} \qquad (2.12)$$

where $\lambda_{1,2} = -\frac{1}{2}\left(\frac{1}{T_1} + \frac{1}{T_2}\right) \pm i \cdot \sqrt{\omega_1^2 - \frac{1}{4}\left(\frac{1}{T_1} - \frac{1}{T_2}\right)^2}$.

Introducing the assignments $\sigma = \frac{1}{2}\left(\frac{1}{T_1} + \frac{1}{T_2}\right)$ and $\omega_T = \sqrt{\omega_1^2 - \frac{1}{4}\left(\frac{1}{T_1} - \frac{1}{T_2}\right)^2}$ the expression (2.12) can be rewritten as:

$$v^{\pm}(t) = \frac{x P^{\pm} P_{eq} \Phi_R k_Q [AC] \cdot [T]_0 \omega_1}{\left[(\tau^{-1})^2 + \omega_T^2 - 2\tau^{-1}\sigma\right] \cdot \omega_T} \left\{ \omega_T \left(e^{-\frac{t}{\tau}} - e^{-\sigma t} \cos(\omega_T t) \right) + (\tau^{-1} - \sigma) e^{-\sigma t} \sin(\omega_T t) \right\} \qquad (2.13)$$

If the rate of magnetization generation is much larger than the relaxation parameter σ (i.e. $\tau^{-1} >> \sigma$), than at the times much longer than τ, equation (2.13) can be approximated as:

$$v^{\pm}(t) \xrightarrow{t>>\tau} \frac{xP^{\pm}P_{eq}\Phi_R k_Q [AC]\cdot[T]_0 \omega_1}{\omega_T \sqrt{\left(\tau^{-1}\right)^2 + {\omega_T}^2}} e^{-\sigma t} \sin(\omega_T t - \varphi) \qquad (2.14)$$

with $\mathrm{tg}\varphi = \dfrac{\omega_T}{\tau^{-1} - \sigma} \approx \omega_T \tau$.

As one can see, at longer times the function turns into a simple damped sinusoid known as Torrey oscillations [67,68]. Here, the oscillation has a shifted phase, and its amplitude is reduced due to a dephasing effect. If in addition the quenching rate becomes much larger than the frequency of the oscillations ($\tau^{-1} >> \omega_T$), then the process of generation of magnetization can be described as instantaneous and equation (2.14) gets its simplest and well known [69] form:

$$v^{\pm}(t) \approx \frac{\omega_1}{\omega_T} M_z^{\pm}(0) \cdot e^{-\sigma t} \sin(\omega_T t) \qquad (2.15)$$

where $M_z^{\pm}(0) = xP^{\pm}P_{eq}\Phi_R \tau k_Q [AC]\cdot[T]_0 = xP^{\pm}P_{eq}[R]_0$ is the initial radical magnetization.

The signal that is measured with the TRESR spectrometer represents the v-component of the magnetization vector, integrated over the irradiated volume, convoluted with the response function, and multiplied with the sensitivity factor of the spectrometer C (choosing the dimension of C equal V/mole we put $P_{eq} = 1$) :

$$S(t) = C \cdot f(t) \otimes \int v(t) dV_{irrad} \qquad (2.16)$$

Here, f(t) is the response function determined by the expression:

$$\begin{cases} t \le 0 : f(t) = 0 \\ t > 0 : f(t) = \dfrac{1}{\tau_{exp}} e^{-\frac{t}{\tau_{exp}}} \end{cases} \tag{2.17}$$

When integrating over the irradiated volume the only one parameter $[T]_0$ can noticeably depend on the integration coordinates. Therefore, the integration of the magnetization comes down to just a replacement of the parameter $[T]_0$ in expression (2.13) by its integrated value, which can be estimated from the known quantum yield Φ_T of ^{3}(1-NN) and the amount of light energy absorbed by the 1-NN molecules (LE_{NN}):

$$\int [T]_0 \, dV_{irrad} = \frac{LE_{NN}\Phi_T}{h\nu N_A} \tag{2.18}$$

Putting (2.13), (2.17), (2.18) in (2.16) it is easy to get the analytical expression for $S^{\pm}(t)$:

$$S^{\pm}(t) = \frac{CxP^{\pm}\Phi_R k_Q [AC] LE_{NN}\Phi_T \omega_1}{h\nu N_A \left[\left(\tau^{-1}\right)^2 + {\omega_T}^2 - 2\tau^{-1}\sigma\right]\cdot\omega_T} \left\{ \frac{\omega_T\left(e^{-\frac{t}{\tau}} - e^{-\frac{t}{\tau_{exp}}}\right)}{1 - \frac{\tau_{exp}}{\tau}} + \right.$$

$$+ \frac{e^{-\sigma t}\sin(\omega_T t)\left[\left(\tau^{-1} - \sigma\right)\left(1 - \sigma\tau_{exp}\right) - {\omega_T}^2\tau_R\right]}{\left[\left(1 - \tau_{exp}\sigma\right)^2 + \left(\omega_T\tau_{exp}\right)^2\right]} -$$

$$\left. - e^{-\sigma t}\omega_T \cos(\omega_T t)\left(1 + \frac{\tau_{exp}}{\tau} - 2\sigma\tau_{exp}\right) + e^{-\frac{t}{\tau_{exp}}}\omega_T\left(1 + \frac{\tau_{exp}}{\tau} - 2\sigma\tau_{exp}\right)\right\} \tag{2.19}$$

Despite the majority of the parameters in expression (2.19) are known or were determined earlier, there still remain the unknown parameters $P^{\pm}$, σ, ω_T, and ω_1. The quenching rate constants (k_Q), the residual life times of ^{3}(1-NN) (τ_0), as well as the radical quantum yields (Φ_R) for all solvents under study have been obtained in the optical absorption experiments (see section 2.3) and are collected in table 2.3.

The radical quantum yield after triplet decomposition of AC depends on the magnitude of the external magnetic field. The values Φ_R which are listed in table 2.3 are those which have been measured by optical absorption spectroscopy at a magnetic field strength of 320 mT. The resonant fields of the two EPR lines, which are analysed here, are only slightly larger at about 339 and 349 mT (see figure 2.14). Having analysed the rate of change of the quantum yield with the magnetic field we came to the conclusion, that the magnetic field variation by about 20-30 mT changes the magnitude of the quantum yield not more than by 2-3%. Therefore, the value of Φ_R at 320 mT should be correct with good accuracy. Φ_T is also known and equals 0.63 for unpolar solvents [36]. Finally, the amount of absorbed light energy was calculated according to the equation: $\frac{LE \cdot OD_{355}^{NN}}{OD_{355}^{NN} + OD_{355}^{AC}} \left\{1 - 10^{-\left(OD_{355}^{NN} + OD_{355}^{AC}\right)}\right\}$ from the laser pulse energy per shot (LE) and the optical densities of 1-nitronaphthalene (OD_{355}^{NN}) and azocumene (OD_{355}^{AC}) in the solution. The statistical weight of the lines under study (i.e. the number of radicals in that particular hyperfine state, divided by the total number of radicals) was x_i = 20/2048.

Table 2.3 Kinetic parameters of the quenching of ^{3}(1-NN) by AC, obtained in LFP experiments

	k_Q [10^9 $M^{-1}s^{-1}$]	τ_0 [μs]	1) Φ_R
Paraffin Oil	2.0	1.4	0.050
Squalane	3.6	1.2	0.047
Squalane:Heptane	6.1	1.1	0.052
Hexadecane	7.4	1.0	0.053
Dodecane	8.3	0.6	0.052
Nonane	9.7	0.5	0.054
Benzene	3.1	1.0	0.055
Heptane	10.5	0.8	0.049

1)Obtained for an external magnetic field of 320 mT

As has been mentioned above (section 2.4.1) the sensitivity factor C = $1.2 \cdot 10^9$ V/mole was known from previous work [26]. The microwave amplitude ω_1 could be extracted from the slope of linear plots of ω_T^2 versus the microwave power, because ω_1^2 is proportional to the

microwave power and $\omega_T = \sqrt{{\omega_1}^2 - \frac{1}{4}\left(\frac{1}{T_1} - \frac{1}{T_2}\right)^2}$. Thus, the only really unknown parameters which have to be determined by fitting (2.19) to the experimental time-profiles, are $P^{\pm}$, ω_T, and σ, which correspond to amplitude, frequency, and damping rate of the oscillations, respectively.

In order to carry out the fitting procedure with better quality it turned out to be suitable to compare the function (2.19) with the spectral power of the Fourier transform of the signal, as in this case all three parameters are clearly separated, and the influence of the high and low frequency noise, distorting the real signal, becomes minimal. The additional advantage of fitting the spectral power is a very accurate (within 2-3 % error) determination of the parameter ω_T, what in turn facilitates an accurate determination of the two remaining parameters $P^{\pm}$ and σ.

2.4.5 Paraffin oil solutions

Due to its very high viscosity paraffin oil turns out to be very suitable solvent, because all above made approximations and approaches hold with very good accuracy for a wide range of quencher concentrations and absorbed light energies. The processes of triplet-triplet annihilation, spin exchange and radical self-termination are limited by the slow diffusion and on a time scale, which is long enough to e.g. replace (2.9) by its approximation (2.10) and to use the simplified form of the Bloch equations (2.11). In order to make this sure, we will make some simple estimations:

1) Having estimated the irradiated volume as about 7µl and the absorbed light energy as not more than 5 mJ, it is clear that the initial triplet concentration did not exceed the value 1-1.5 mM. This means that the parameter $k_{TT}[T]_0$ in equation (2.9) is less than $2.7 \cdot 10^5$ s^{-1}, as k_{TT} in paraffin oil was found to be $k_{TT} \approx 1.8 \cdot 10^8 M^{-1}s^{-1}$. On the other hand, the value of the parameter τ^{-1} for the lowest quencher concentration was about 10^6 s^{-1}, what is nearly four times larger than the estimated upper limit for $k_{TT}[T]_0$. Thus, neglect of the second order kinetics in (2.9) is certainly justified.

2) We do not know what the exact value is for the self-termination rate constant of cumyl radicals in paraffin oil, but its magnitude can be estimated by extrapolating an earlier measured value of $2k_t = 1.2 \cdot 10^9\ M^{-1}s^{-1}$ in *t.*butylbenzene as solvent [43]. Taking into account that the ratio of the solvent viscosities is about 1:100 (η(*t.*butylbenzene) ≈1 cP), we obtain an estimation for the self-termination rate in paraffin oil as $2k_t \approx 1.2 \cdot 10^7\ M^{-1}s^{-1}$. For diffusion controlled reactions one expects, that the ratio between the rates of radical spin exchange and self-termination $k_{ex}/2k_t$ does not exceed 3 [70,71]. Therefore, the upper limit of k_{ex} is about $k_{ex} \approx 3.6 \cdot 10^7\ M^{-1}s^{-1}$. Using the above estimated maximum triplet concentration of 1-1.5 mM and the radical quantum yield of about 5%, it is easy to calculate the upper limit of the radical concentration, which is about 50-75 μM. Therefore, it turns out that $k_{ex}[R]_0 \leq 2.7 \cdot 10^3\ s^{-1}$ and $2k_t[R]_0 \leq 9 \cdot 10^2\ s^{-1}$, what is two - three orders of magnitude less than the inverse values of the relaxation times, which amount to several microseconds. Thus, it is also justified to neglect in the modified Bloch equations the exchange term and the second-order term for CIDEP production in the cumyl radical F-pairs.

Figure 2.15 shows, in a plot versus the microwave power, the values of $\omega_T^{\ 2}$ which were obtained by fitting relation (2.19) to the sum of the time-profiles of the two resonance lines under study. The free parameters of the fitting procedure were σ, ω_T, and the product $\left(P^+\omega_1\right)$.

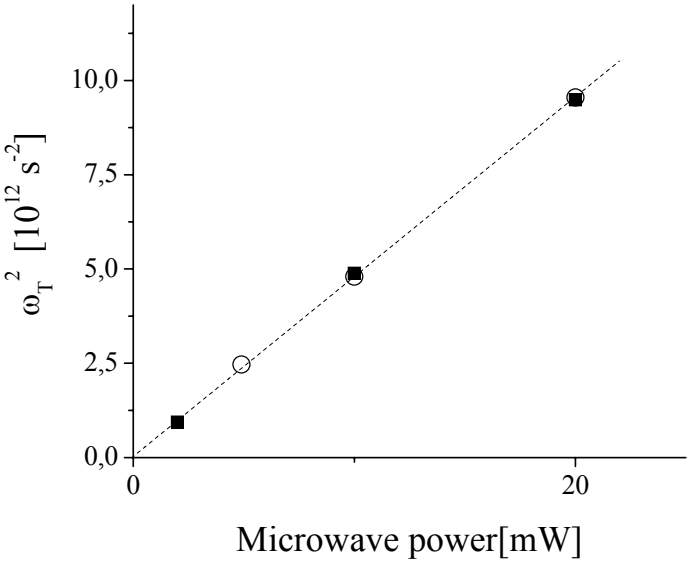

Figure 2.15: Dependence of the parameter ω_T on the microwave power, obtained by fitting of EPR time-profiles recorded for solutions containing 2.1 mM of 1-NN and 15 mM of AC (black squares) and 47 mM AC (open circles). Dotted line represents the linear fit to both data.

The differences between the $\omega_T{}^2$ values obtained for different quencher concentrations did not exceed 2-3 %. Figure 2.15 contains only the results for $\omega_T{}^2$ obtained for two quencher concentrations (15 mM and 47 mM). As expected, the dependence of $\omega_T{}^2$ on the microwave power is linear with very good accuracy. The slope of the line is the magnitude of $\omega_1{}^2$ at 1 mW microwave power incident at the EPR cavity. The intercept should be the value of the parameter $\frac{1}{4}\left(\frac{1}{T_1}-\frac{1}{T_2}\right)^2$. Apparently it is so small in comparison with $\omega_1{}^2$, that the number obtained from the linear fit turned out to be even smaller than the tiny statistical error. Therefore, in the further treatment we will just consider the case when $\frac{1}{4}\left(\frac{1}{T_1}-\frac{1}{T_2}\right)^2$ is equal to zero and put $\omega_1 = \omega_T$. This will allow to determine directly the size of the polarization while fitting the signals by function (2.19).

Figure 2.16a presents experimental and with equation (2.19) simulated time-profiles of $S^+(t)$ for two quencher concentrations: 4.6 mM and 47 mM. The curves were calculated with the parameters, which were obtained by fitting the numerically calculated Fourier transforms of the experimental time-profiles, as it is shown in figure 2.16b. The fitting procedure was implemented only in the frequency range lying relatively near to the maximum peak in the Fourier space, which corresponds to the Torrey oscillation frequency. This seems to be quite reasonable, because the ratio of useful information to noise is maximal in this frequency range, what in turn leads to a more accurate determination of the unknown parameters.

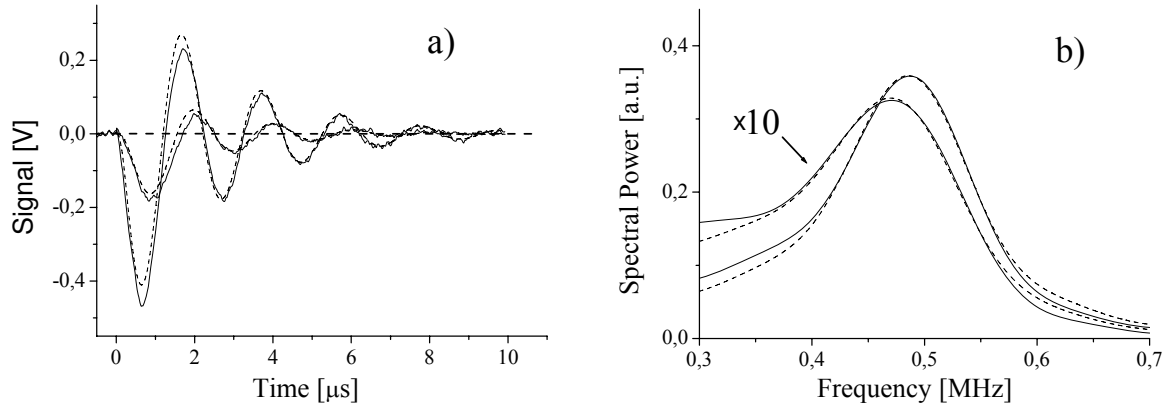

Figure 2.16: Comparison of the time profiles $S^{+}(t)$ recorded at 20 mW microwave power for two paraffin oil solutions containing 1-NN (2.1 mM) and AC (4.6 mM and 47 mM respectively) with their simulations by equation (2.19) calculated for the optimal set of fit parameters: (a) time representation (b) spectral (frequency) representation.

For the smaller concentration of AC (4.6 mM) in paraffin oil the parameter τ is found to be about 610 ns, whereas it is about 60 ns for the larger one (47 mM). According to equation (2.14) this should lead to a phase shift between the two oscillations in figure 2.16a of about $\varphi \approx \mathrm{arctg}(\omega_T \Delta\tau) \approx 55°$ (ω_T = $3.06 \cdot 10^6$ s^{-1}) and that is indeed observed (one can see, that the curve corresponding to the smaller quencher concentration crosses the zero line with a time delay of about $\delta T \approx 300$ ns, while the oscillation period is approximately $T \approx 2$ μ. This means that the observed phase shift is $\varphi \approx 360° \frac{\delta T}{T} \approx 55°$).

An additional manifestation of the slower quenching at smaller AC concentrations is the noticeable drop in the oscillation amplitude. It is due to a dephasing effect and also due to the fact, that at slow quenching rates the processes determining the residual life time τ_0 of ^{3}(1-NN) begin to compete with the quenching process. In spite of the fact, that the values of the absorbed light energies and also the parameters P^+ are rather similar in the experiments with both AC concentrations (LE_{NN} = 2.8 mJ and 2.6 mJ, P^+= -95.2 P_{eq} and -100.1 P_{eq} for 4.6 mM and 47 mM respectively), the oscillation amplitudes differ from each other about three - four times at times longer than about 2μs. This corresponds well with an estimation of the amplitude decrease for a quencher concentration of 4.6 mM from equation (2.14): $\frac{k_Q[AC]}{\sqrt{\omega_T{}^2 + \left(\tau^{-1}\right)^2}} \left([AC] = 4.6\mathrm{mM}\right) \approx \frac{1}{4}$.

Figure 2.17 presents the values of the parameters P^+ and σ, obtained as result of fitting equation (2.19) to experimental time profiles $S^+(t)$ for a set of different microwave powers and AC concentrations in the range 2.5 - 82 mM. As one can see from the figure the average values of the parameters are -106 P_{eq} and $4.2 \cdot 10^5$ s^{-1} for P^+ and σ, respectively. Within the limits of their statistical scattering (about 10-15 %) they are independent of the quencher concentration. It is evident that the parameter σ must be independent of the quenching rate, as its value is determined only by the rates of spin relaxation in the cumyl radicals, which remain unchanged when varying the AC concentration. It is more interesting that the net polarization P^+ does not depend on the quencher concentration. In principle the observed net emissive polarization could be a superposition of a) a *d*-type TM polarization induced in the ^{3}AC molecules and b) a *p*-type TM polarization induced in the ^{3}(1-NN) molecules and transferred via quenching with AC to

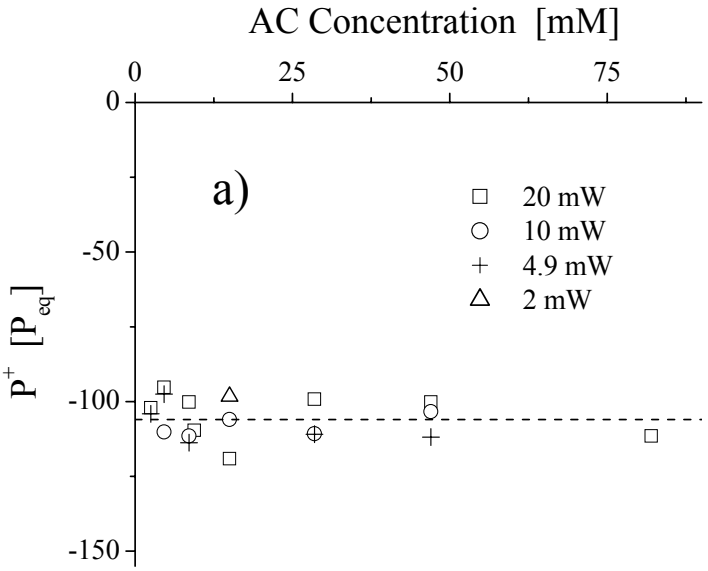

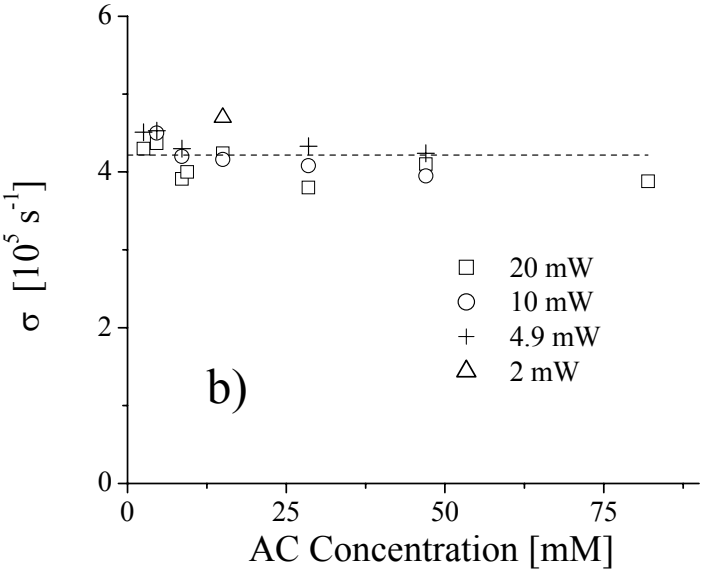

Figure 2.17: Dependence on the quencher concentration of (a) the absolute value of the net polarization and (b) the relaxation parameter σ, both given for several different microwave powers.

the cumyl radicals. However, in the latter case the quenching reaction would compete with the decay of the spin polarization in the ^{3}(1-NN) molecules because of spin relaxation. Therefore, the amount of polarization transferred to the radicals would depend on the rate of quenching i.e. the AC concentration. In our quenching experiments the life time of ^{3}(1-NN) is varied from about 60 ns to 1 μs without observing any change of the emissive cumyl radical polarization. Therefore, we conclude that this polarization is exclusively due to a *d*-type TM in triplet azocumene.

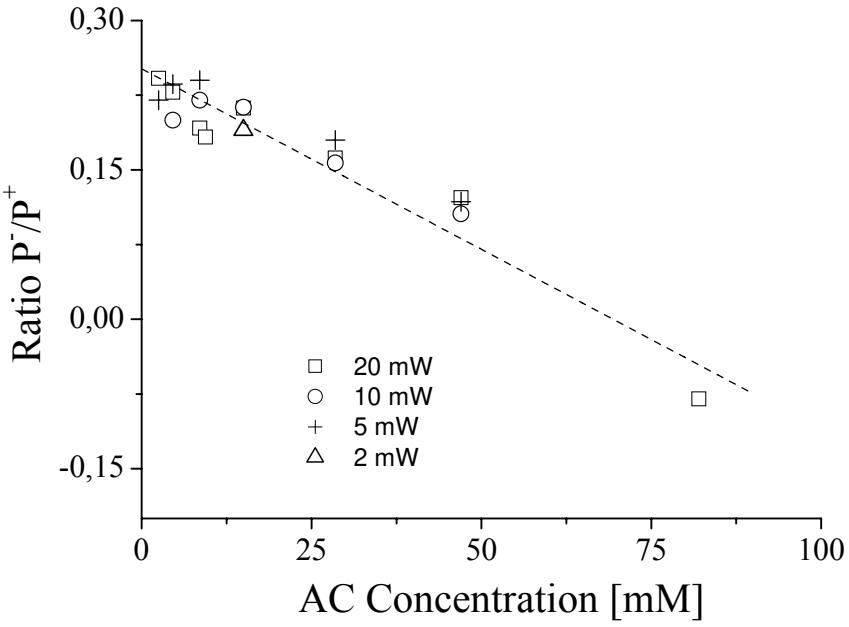

Figure 2.18: Dependence of the ratio of multiplet to net polarizations on the quencher concentration, obtained at different microwave powers.

The ratio $\frac{P^-}{P^+}$ between the multiplet and net polarization may be used for an independent check, if our value $P^+ \approx -106 \cdot P_{eq}$ makes sense. This ratio is not affected by a variety of possible systematic errors, which might be contained in the determination of P^+ (inaccuracy of quantum yield , the value of absorbed light energy, …). As visible in figure 2.18 the ratio $\frac{P^-}{P^+}$ decreases with increasing AC concentration and even changes sign at high AC concentrations. This behavior is caused by the direct photolysis of AC, which for higher quencher concentrations becomes more and more prominent ($OD_{355}^{AC}(82\ mM) \approx 0.23$). A linear fit of the ratio $\frac{P^-}{P^+}$ versus the AC concentration yields an intercept at $\approx \frac{1}{4}$, i.e. the multiplet polarization amounts to $P^- \approx -26.5 \cdot P_{eq}$. Assuming that the ratio between the multiplet polarizations stemming from radical pairs with singlet and triplet precursors should be about 3:1, it is easy to obtain an estimation of about $-80 \cdot P_{eq}$ for the multiplet polarization in the case of direct singlet photolysis of AC. This value is not far away from the previously measured multiplet polarization $(-111 \pm 25) \cdot P_{eq}$ for the direct photolysis of AC in paraffin oil solution [26].

2.4.6 Other alkane solvents

When the viscosity of the solvent decreases the triplet-triplet annihilation rate increases much faster than the rate of triplet quenching by AC (see figure 2.9), and for small concentrations of the quencher both rates can become comparable. The method which we have developed for the analysis of the time-profiles is based on the condition $k_{TT}[T]_0 << \frac{1}{\tau}$. At low viscosity and small quencher concentration it would become incorrect. Therefore, all measurements at lower viscosity and their analysis were carried out only for AC concentrations larger than 30 mM. At this high quencher concentration the contribution of the triplet-triplet annihilation to the kinetics of the ^{3}(1-NN) decay becomes negligibly small and the quenching rate is fast enough to consider the process of generation of magnetization to be instantaneous. In this case $v^{\pm}(t)$ is determined by equation (2.15) and the analytical expression for the measured signal (equation (2.19)) takes the form

$$S^{\pm}(t) = \frac{C \cdot M_z^{\pm}(0)}{\tau_{exp}\left[\omega_1{}^2 + \left(\frac{1}{\tau_{exp}} - \sigma\right)^2\right]}\left\{\omega_1\left(e^{-\frac{t}{\tau_{exp}}} - e^{-\sigma t}\cos\omega_1 t\right) + \left(\frac{1}{\tau_{exp}} - \sigma\right)e^{-\sigma t}\sin\omega_1 t\right\} \qquad (2.20)$$

with $M_z^{\pm}(0) = xP^{\pm}P_{eq}\Phi_R[T]_0$ (the rate of ^{3}AC decay was taken equal to the quenching rate, i.e. $\frac{1}{\tau} = k_Q[AC]$). The magnitude of the initial magnetization $M_z^{\pm}(0)$ were obtained by Fourier spectral power fitting of relation (2.20) to the experimental curves measured at low laser light intensity (see figure 2.19). It should be noted here, that this procedure is very similar to the method which has been used previously [66] for the analysis of the TREPR spectra recorded after direct photolysis of 2,2'-azobisisobutyronitrile.

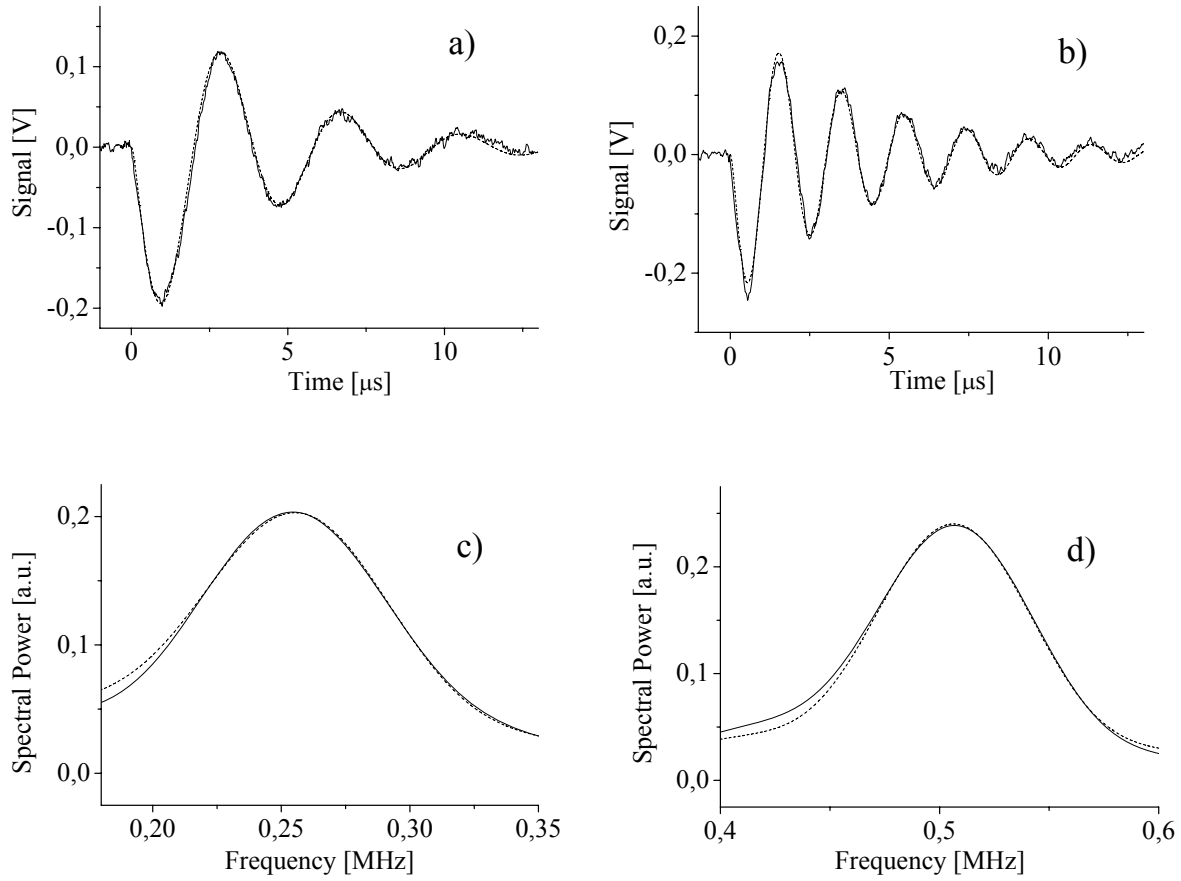

Figure 2.19: Solid lines are the time profiles $S^+(t)$ measured in dodecane solution containing 2.1 mM of 1-NN and 35 mM of AC at 1.3 mJ absorbed light energy for two microwave powers: 20 mW (a),(c) and 5 mW (b),(d). The dashed lines represent the simulations with relation (2.20) with the following parameters: $C \cdot M_z^+(0) = -0.250$ V, $\sigma = 2.35 \cdot 10^5\ s^{-1}$, $\omega_1 = 3.2 \cdot 10^6\ s^{-1}$ for (a) and (c), and $C \cdot M_z^+(0) = -0.256$ V, $\sigma = 2.75 \cdot 10^5\ s^{-1}$, $\omega_1 = 1.64 \cdot 10^6\ s^{-1}$ for (b) and (d), respectively.

Since in the data analysis of the measurements in paraffin oil solutions we have not found any evidence for a noticeable contribution of a polarization transfer from ^{3}(1-NN), the obtained magnitudes of the parameter P^+ can be directly ascribed to the polarizations induced by the *d*-type TM in ^{3}AC. All results for P^+ and the solution viscosities at which they were measured are listed in table 2.3.

Finally, we have to note here, that we did not take into account any possible influence of a *trans-cis* isomerization process on the polarization. This should be absolutely correct because of the following reasons: 1) We did not observe any significant contribution of a *trans-cis*

isomerization to the radical yield, 2) the radicals produced by thermolysis of the unstable *cis*-isomer are only polarized by the radical pair mechanism, which for two identical radicals in the

Table 2.3 Dependence of the d-type TM polarization induced in ^{3}AC on solvent viscosity

	[1] η [cP]	P^+ [P_{eq}]
Paraffin Oil	106.7	-106
Squalane	32.4	-104
Squalane:Heptane (4:1 vol.)	8.32	-104
Hexadecane	3.32	-100
Dodecane	1.50	-82
Nonane	0.71	-63
Benzene	0.67	-61
Heptane	0.41	-51
Pentane	0.24	[2]-36

1) at room temperature

2) obtained under assumption that the radical quantum yield at 3 T equals 0.05

pair can induce only a multiplet type polarization, 3) the magnetization of the radicals produced via an eventual slow thermolysis would not be seen at the high microwave powers which we used in order to observe the Torrey oscillations, because the formation of the magnetization would occur on the time scale of the life time of the *cis*-isomer (5 – 12 μs).

2.5 Theoretical analysis

The observation of a magnetic field effect on the formation of cumyl radicals from triplet azocumene as well as a net spin polarization of the radicals manifests the occurrence of a *d*-type triplet mechanism in ^{3}AC. For a quantitative analysis of our experimental data we follow the model used by Steiner to explain the MFE on the decay of certain exciplexes [11,72]. We assume that ^{3}AC undergoes simultaneously spin state selective ISC to the ground state and spin state independent decay into radicals, according to scheme 2.3. The spin selective ISC causes non-thermal populations of the zero-field sub-states T_x, T_y, and T_z, which are partially transferred to the radical products. The quantum yield of cleavage is determined by the ratio of

the decay rate k_p to the rates k_x, k_y, and k_z of the ISC process. An external magnetic field mixes the zero-field sub-states and, combined with the rotational Brownian tumbling of the molecule, induces transitions between them. This affects the total depopulation rate via ISC and, hence, influences the quantum yield of radicals and their polarization. For simplicity we assume for ^{3}AC axial symmetry of the zero field splitting tensor ($D_{xx} = D_{yy}$) and the ISC rate constants ($k_x = k_y = k_\perp$). As we will see later (section 2.5.1.4) this should be a good approximation, because the triplet electrons are localized on the azo-group having a C_2 symmetry axis, which can be reasonably considered as axial symmetric.

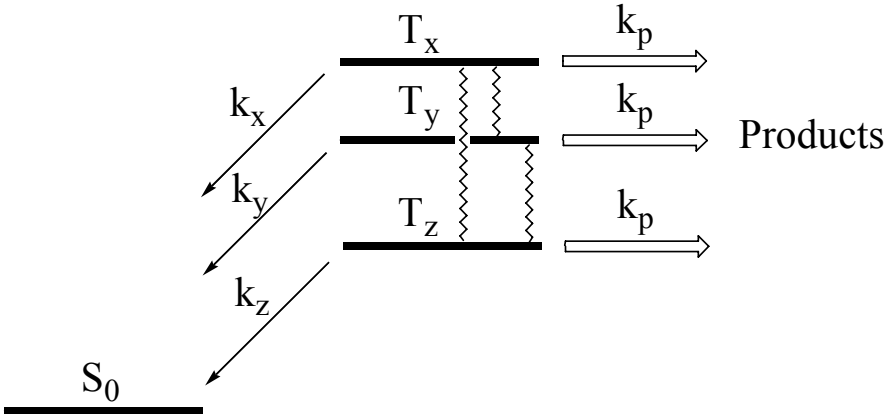

Scheme 2.3

2.5.1 The model of a static triplet

The interactions and processes determining the triplet spin dynamics are: Zeeman and dipole-dipole interaction, rotational diffusion, depopulation via ISC, and decay into radicals. The magnitudes of the Zeeman and dipole-dipole interaction are determined by the magnetic field B and the ZFS parameter D_{ZFS}, respectively, and the rates of the depopulation processes are described by the rate constants $k_\perp$, k_z and k_p. The diffusional tumbling is measured by the correlation time τ_c for reorientational motion. The influence of any of these processes on the spin dynamics is determined by the ratio of the parameter measuring the process to the rate of triplet state depopulation. The value of τ_c increases with increasing viscosity. If the condition $1/\tau_c << \max\{k_p,\min\{k_\perp,k_z\}\}$ is met, the influence of the diffusional motion becomes negligibly small, because the molecule has simply no time to change noticeably its orientation during the life time of the triplet state. Then, the polarization and quantum yield of the radicals become

independent of the viscosity of the solution. We believe that this situation is met for ^{3}AC in the two most viscous solvents, squalane and paraffin oil, as Φ_R and MFE_{max} are nearly the same, although the viscosity differs by more than a factor of three (see figure 2.12). Thus, for these two solvents the experimental data can be analysed with neglect of the rotational diffusion and assumption of a static triplet molecule, what is done in the following. We have to note here, however, that since in both solvents the hyperfine pattern of the TREPR spectra of the cumyl radicals did not differ from those in low-viscous solutions, the diffusional tumbling of the radicals is still fast enough to average the anisotropic part of the radical hyperfine interactions and to yield normal solution EPR spectra.

For analysis we choose a molecular frame {x,y,z} as depicted in scheme 2.4. Let the z-axis be along the axis of symmetry of the ZFS tensor and the ISC rate constants, and the x-axis in the plane formed by the z-axis and the magnetic field vector $\vec{B}$.

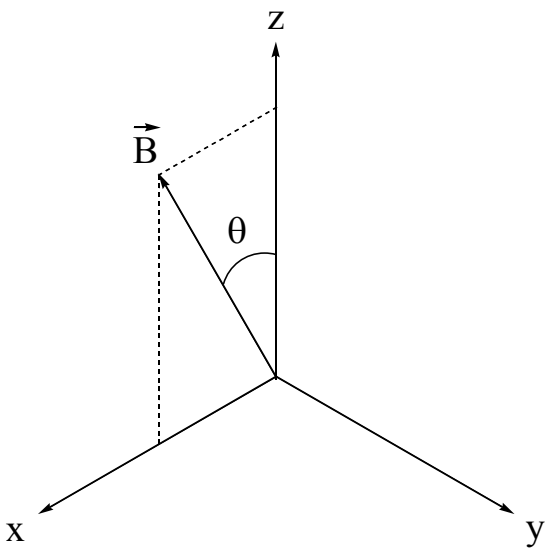

Scheme 2.4

θ is the angle between the z-axis and the field direction. In the general case, the statistical description of the quantum system requires the solution of the appropriate Liouville equation. However, if the influence of diffusion is negligible, the processes can be described in terms of the Schrödinger equation. For our case it reads

$$\frac{\mathrm{d}}{\mathrm{dt}}\Psi = -i\hat{\mathrm{H}}_{\mathrm{EFF}}\Psi = -i\left(\hat{\mathrm{H}}_{\mathrm{Z}} + \hat{\mathrm{H}}_{\mathrm{ZFS}}\right)\Psi - \frac{1}{2}\hat{\mathrm{k}}\Psi \quad . \tag{2.21}$$

In the basis $\{T_+\} = \{-(T_x+iT_y)/\sqrt{2}\}$, $\{T_0\} = \{T_z\}$, and $\{T_-\} = \{(T_x-iT_y)/\sqrt{2}\}$, quantized along the z-direction, the Hamiltonian of the Zeeman interaction, $\hat{\mathrm{H}}_{\mathrm{Z}} = \omega_0\left(\hat{\mathrm{S}}_{\mathrm{z}}\cos(\theta) + \hat{\mathrm{S}}_{\mathrm{x}}\sin(\theta)\right)$, can be expressed in terms of the magnetic field ω_0 and the spin operators

$$\hat{\mathrm{S}}_{\mathrm{z}} = \begin{pmatrix} 1 & 0 & 0 \\ 0 & 0 & 0 \\ 0 & 0 & -1 \end{pmatrix} \text{ and } \hat{\mathrm{S}}_{\mathrm{x}} = \frac{1}{\sqrt{2}}\begin{pmatrix} 0 & 1 & 0 \\ 1 & 0 & 1 \\ 0 & 1 & 0 \end{pmatrix}.$$

The zero-field interaction as well as the operator describing the decay via ISC and cleavage are given by the matrices

$$\hat{\mathrm{H}}_{\mathrm{ZFS}} = \frac{1}{3}\begin{pmatrix} \mathrm{D}_{\mathrm{ZFS}} & 0 & 0 \\ 0 & -2\mathrm{D}_{\mathrm{ZFS}} & 0 \\ 0 & 0 & \mathrm{D}_{\mathrm{ZFS}} \end{pmatrix} \text{ and } \hat{\mathrm{k}} = \begin{pmatrix} \mathrm{k}_{\perp} + \mathrm{k}_{\mathrm{p}} & 0 & 0 \\ 0 & \mathrm{k}_{\mathrm{z}} + \mathrm{k}_{\mathrm{p}} & 0 \\ 0 & 0 & \mathrm{k}_{\perp} + \mathrm{k}_{\mathrm{p}} \end{pmatrix}.$$

H_{EFF} denotes the effective Hamiltonian including all interactions and processes.

The solution of the first order linear differential equation (2.21) has the general form

$$\Psi(\theta,\mathrm{t}) = \mathrm{C}_1 \cdot \mathrm{l}_1 \cdot \mathrm{e}^{\lambda_1 \mathrm{t}} + \mathrm{C}_2 \cdot \mathrm{l}_2 \cdot \mathrm{e}^{\lambda_2 \mathrm{t}} + \mathrm{C}_3 \cdot \mathrm{l}_3 \cdot \mathrm{e}^{\lambda_3 \mathrm{t}} \tag{2.22}$$

with $\mathrm{l}_{1,2,3}$ and $\lambda_{1,2,3}$ being the eigenvectors and corresponding eigenvalues of the matrix $-i\hat{\mathrm{H}}_{\mathrm{EFF}}$ and $C_{1,2,3}$ the set of arbitrary constants, which are determined by the initial conditions. For comparison with the experimental data for the quantum yield and spin polarization, the integrations

$$\Phi_{\mathrm{C}} = \frac{1}{3}\sum_{+,0,-}\mathrm{k}_{\mathrm{p}}\frac{1}{2}\int_0^{\pi}\sin(\theta)\mathrm{d}\theta\int_0^{\infty}\left|\Psi(\theta,\mathrm{t})\right|^2\mathrm{dt} \tag{2.23a}$$

$$\mathrm{P} = \Phi_{\mathrm{C}}{}^{-1}\frac{1}{3}\sum_{+,0,-}\mathrm{k}_{\mathrm{p}}\frac{1}{2}\int_0^{\pi}\sin(\theta)\mathrm{d}\theta\int_0^{\infty}\left\langle\Psi^{+}(\theta,\mathrm{t})\middle|\hat{\mathrm{S}}'_{\mathrm{Z}}(\theta)\middle|\Psi(\theta,\mathrm{t})\right\rangle\mathrm{dt} \tag{2.23b}$$

are required, because the measured quantum yield and polarization are a statistical average over all initial polarizations and orientation angles of the triplet molecule (note, that Φ_C in equation (2.23) now is the quantum yield for cleavage, i.e. $\Phi_C = \Phi_R/2$). Unfortunately, for the general case the dependence of Ψ on θ is too complicated to obtain analytical expressions for Φ_C and P. Therefore, we will consider separately two limiting cases, in which the calculations can be much simplified.

2.5.1.1 Zero magnetic field case

In the absence of a magnetic field, the matrix $\hat{H}_{EFF}$ is diagonal and $\{T_+\}$, $\{T_0\}$, and $\{T_-\}$ are the quasi-stationary eigenstates of the triplet. The population density of the states $\{T_+\}$ and $\{T_-\}$ decays exponentially with a time constant $\tau_\perp = (k_\perp+k_p)^{-1}$, while that of the state $\{T_0\}$ vanishes with $\tau_z = (k_z+k_p)^{-1}$. In the absence of any noticeable polarization transfer from triplet 1-NN the initial population of all three states is the same (1/3), so that an easy calculation delivers Φ_C, i.e. the product yield per ^{3}AC,

$$\Phi_C = k_p \cdot \frac{1}{3}\int_0^\infty \left(2e^{-\frac{t}{\tau_\perp}} + e^{-\frac{t}{\tau_z}} \right) dt = \frac{k_p}{3}\left(\frac{2}{k_\perp + k_p} + \frac{1}{k_z + k_p} \right) \qquad (2.24)$$

Putting $k_\perp+k_p = \alpha k_p$ and $k_z+k_p = \beta k_p$, equation (2.24) can be rewritten in a form which contains only the two unknown parameters α and β,

$$\Phi_C = \frac{1}{3}\left(\frac{2}{\alpha} + \frac{1}{\beta} \right) \ .$$

According to figure 2.12(b) the radical yield amounts essentially to about 7%, i.e. $\Phi_R \approx 0.07$. Therefore $\Phi_C = \Phi_R/2 \approx 0.035$. It is worth mentioning that, strictly speaking, the equality $\Phi_C = \Phi_R/2$ is only an approximation, because Φ_C is calculated for zero magnetic field, while Φ_R was measured at 0.02 T. However, a careful examination of the data given in figure 2.11 shows, that the MFE at 0.02 T can not exceed 2%. Therefore,

$$\Phi_C = \frac{1}{3}\left(\frac{2}{\alpha}+\frac{1}{\beta}\right) \approx 0.035 \qquad (2.25)$$

is a very good approximation. In order to get a second equation for the two unknown parameters α and β, the high-field case is now considered.

2.5.1.2 High magnetic field case

If the magnetic field is large, the effective Hamiltonian becomes dominated by the Zeeman interaction. ZFS tensor and reaction operator can then be treated as weak perturbations. Without perturbation the eigenvectors $l_{1,2,3}$ of the Zeeman Hamiltonian are the triplet states $\{T_+'\}$, $\{T_0'\}$, and $\{T_-'\}$, quantized in field direction, and the corresponding eigenvalues of $-i\hat{H}_{EFF}$ become $\lambda_{1,2,3} = -i\omega_0$, 0, and $+i\omega_0$, respectively. In order to account for the ZFS and reaction operator as a weak perturbation, $\lambda_{1,2,3}$ may written as power series $\lambda_{1,2,3} = \sum_{j=0}^{\infty} \lambda_{1,2,3}^{(j)} \omega_0^{1-j}$ with $\lambda_{1,2,3}^{(0)} = -i$, 0, $+i$, respectively. The first correction terms then become

$$\lambda_{1,3}^{(1)} = \frac{iD_{ZFS}}{6}\left(1-3\cos(\theta)^2\right) - \frac{1}{4}\left[\left(k_\perp + k_p\right)\cdot\left(1+\cos(\theta)^2\right) + \left(k_z + k_p\right)\sin(\theta)^2\right],$$

$$\lambda_2^{(1)} = -\frac{iD_{ZFS}}{3}\left(1-3\cos(\theta)^2\right) - \frac{1}{2}\left[\left(k_\perp + k_p\right)\cdot\sin(\theta)^2 + \left(k_z + k_p\right)\cos(\theta)^2\right].$$

The imaginary parts of $\lambda_{1,2,3}^{(1)}$ correct the energy levels of the quasi-stationary eigenstates $\{T_+'\}$, $\{T_0'\}$, and $\{T_-'\}$, and the real parts determine their life time. Averaging over all initial polarizations gives for the cleavage yield

$$\Phi_{C,\infty}(\theta) = \frac{k_p}{3}\left\{\frac{1}{\left(k_\perp + k_p\right)\sin(\theta)^2 + \left(k_z + k_p\right)\cos(\theta)^2} + \frac{4}{\left(k_\perp + k_p\right)\left(1+\cos(\theta)^2\right) + \left(k_z + k_p\right)\sin(\theta)^2}\right\}$$

Integrating over the orientations according to equation (2.23) and rewriting in terms of the parameters α and β finally yields

$$\Phi_{C,\infty} =$$

$$\frac{1}{3}\left\{\frac{1}{2\sqrt{\alpha(\alpha-\beta)}}\ln\frac{\alpha+\sqrt{\alpha(\alpha-\beta)}}{\alpha-\sqrt{\alpha(\alpha-\beta)}}+\frac{4}{\sqrt{\alpha^2-\beta^2}}\operatorname{arctg}\sqrt{\frac{\alpha-\beta}{\alpha+\beta}}\right\} \quad \text{if} \quad \alpha>\beta \ , \qquad (2.26a)$$

$$\frac{1}{3}\left\{\frac{1}{\sqrt{\alpha(\beta-\alpha)}}\operatorname{arctg}\sqrt{\frac{\beta-\alpha}{\alpha}}+\frac{2}{\sqrt{\beta^2-\alpha^2}}\ln\frac{\beta+\alpha+\sqrt{\beta^2-\alpha^2}}{\beta+\alpha-\sqrt{\beta^2-\alpha^2}}\right\} \quad \text{if} \quad \alpha<\beta \ . \qquad (2.26b)$$

At high magnetic fields the MFE measured in squalane and paraffin oil (see figure 2.12(a)) levels off at about -43 %. Therefore,

$$\mathrm{MFE}_{\max} = \frac{\Phi_{C,\infty} - \Phi_{C,0}}{\Phi_{C,0}} \approx -0.43 \qquad (2.27)$$

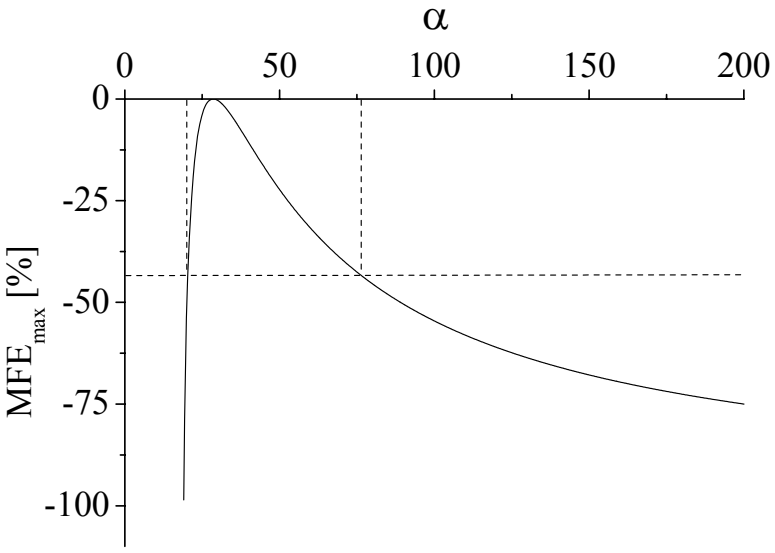

Figure 2.20: Dependence of MFE_{max} on the parameter α as calculated numerically from the equations (2.25), (2.26), and the definition of MFE_{max}. The dashed lines represent the two solutions resulting from the experimental value MFE_{max} = -43%.

Expressing in equation (2.26) β in terms of α via equation (2.25), the numerical calculation of MFE_{max} in dependence on α (see figure 2.20) gives two possible solutions for α. Equation (2.25) and the definition of α and β, then finally yield the following two possible parameter sets, which satisfy all conditions pointed out above:

$$1)\begin{cases}\alpha = 20.36\\ \beta = 147.75\\ k_\perp = 19.36k_p\\ k_z = 146.75k_p\end{cases}\qquad\text{and}\qquad 2)\begin{cases}\alpha = 75.5\\ \beta = 12.72\\ k_\perp = 74.5k_p\\ k_z = 11.72k_p\end{cases} \tag{2.28}$$

2.5.1.3 Intermediate magnetic field case

Although in the two limiting cases of zero and infinite large field the expressions (2.23a,b) can be presented analytically (in both cases P is simply zero), a numerical integration is required for the general case. In order to avoid an additional numerical integration over the time, we put (2.22) into (2.23) and, after having integrated analytically the exponential terms, we obtain:

$$\Phi_C = k_p \frac{1}{2}\int_0^\pi \left\{\frac{1}{3}\sum_{k=+,0,-}\left(\sum_{i,j=1}^{3}\frac{1}{\lambda_j^*(\theta)+\lambda_i(\theta)} C_j^{k*}(\theta)C^k(\theta)\left\langle l_j(\theta)\middle| l_i(\theta)\right\rangle\right)\right\}\sin(\theta)d\theta \tag{2.29a}$$

$$P = \Phi_C^{-1} k_p \frac{1}{2}\int_0^\pi \left\{\frac{1}{3}\sum_{k=+,0,-}\left(\sum_{i,j=1}^{3}\frac{1}{\lambda_j^*(\theta)+\lambda_i(\theta)} C_j^{k*}(\theta)C_i^k(\theta)\left\langle l_j(\theta)\middle|\hat{S}_Z(\theta)\middle| l_i(\theta)\right\rangle\right)\right\}\sin(\theta)d\theta \tag{2.29b}$$

Here, $C^k(\theta)(k = +,0,-)$ are now no arbitrary constants but vectors, each of which is determined by the condition when the triplet has one of the three possible initial polarizations:

$$\left\{C^+(\theta), C^0(\theta), C^-(\theta)\right\} = \left[l_1|\theta|\quad l_2(\theta)\quad l_3(\theta)\right]^{-1}\cdot\left\{\begin{pmatrix}1\\0\\0\end{pmatrix},\begin{pmatrix}0\\1\\0\end{pmatrix},\begin{pmatrix}0\\0\\1\end{pmatrix}\right\},$$

where $[l_1(\theta)\quad l_2(\theta)\quad l_3(\theta)]$ is a matrix composed of the eigenvectors $l_i(\theta)(i = 1,2,3)$.

Note, since H_{EFF} is no hermitian matrix (because of the reaction operator) the condition of orthogonality of the l_i may not be fulfilled, i.e. $\langle l_j(\theta)|l_i(\theta)\rangle \neq \delta_{ij}$.

From equation (2.29b) we have calculated the polarizations in dependence on the parameter D_{ZFS} for different values of k_p, the rate of cleavage into two cumyl radicals. In these calculations the ISC rates were introduced as multiples of k_p according to $\alpha - 1 = \frac{k_p}{k_\perp} = 19.36$ and $\beta - 1 = \frac{k_p}{k_z} = 146.75$ for solution 1) in (2.28), as well as $\alpha - 1 = \frac{k_p}{k_\perp} = 74.5$ and $\beta - 1 = \frac{k_p}{k_z} = 11.72$ for the second possible solution in (2.28). The results for the parameter sets 1) and 2) are given in the figures 2.21a and 2.21b, respectively.

Comparison of the numerically calculated polarizations P with the experimentally measured value $P^+ = -106 \cdot P_{eq} = -0.082$ allows to find a correlation between the two unknown parameters D_{ZFS} and k_p for each of the two possible sets $\{\alpha,\beta\}$ in (2.28). Figure 2.21 illustrates the procedure of determining D_{ZFS} for each given value of k_p. In fact, there are two values of D_{ZFS},

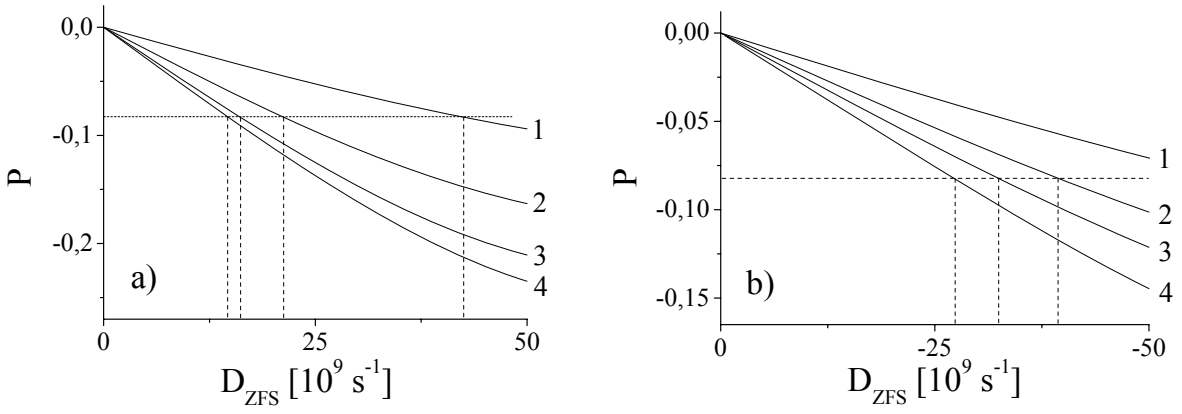

Figure 2.21: Dependence of the calculated polarization value on parameter D_{ZFS} under following conditions: (a) α = 20.36, β = 147.75, $k_p = 10^9\ s^{-1}$ (1), $5 \cdot 10^8\ s^{-1}$ (2), $2.5 \cdot 10^8\ s^{-1}$ (3), $10^8\ s^{-1}$(4); (b) α =75.5, β = 12.72, $k_p = 3 \cdot 10^9\ s^{-1}$ (1) ,$2 \cdot 10^9\ s^{-1}$ (2), $1.5 \cdot 10^9\ s^{-1}$ (3), $10^9\ s^{-1}$(4). Dashed lines illustrate obtaining of the parameter D_{ZFS} for every given k_p from comparing of a calculated curve with experimental value -0.082.

at which the curve $P(D_{ZFS})$ crosses the horizontal line determined by the condition P = -0.082, because $P(D_{ZFS})$ must vanish when D_{ZFS} approaches either zero or infinity and reaches the maximum of its absolute value when D_{ZFS} becomes comparable with the external magnetic field. However, the D_{ZFS} values corresponding to the second crossing turned out to be well above 1 T and were simply rejected as physically unrealistic.

k_p was varied in sufficiently small steps (we took $5\cdot10^7$ s^{-1}) over the range from 10^8 s^{-1} to 10^{10} s^{-1}, and for each k_p the matching zero-field splitting D_{ZFS} was determined as described above. Doing that for both parameter pairs $\{\alpha,\beta\}$ in (2.28) resulted in two vectors, each of them containing as elements 200 number pairs $\{k_p, D_{ZFS}\}$, for which the set of all four values $\{\alpha,\beta,k_p,D_{ZFS}\}$ satisfied the requirement: $\{\Phi_C = 0.035, MFE_{max} = -0.43, P = -0.082\}$.

Equation (2.29a) was then used to calculate the magnetic field effect MFE(B) for all 2×200 number pairs $\{k_p, D_{ZFS}\}$. Using a least squares procedure the results were compared with the experimentally obtained MFE(B) in paraffin oil solution (see figure 2.11). Two best parameter sets 1) and 2) were found, which are listed in (2.30).

$$1)\begin{cases} \alpha = 20.36 \\ \beta = 147.75 \\ k_p = 8\cdot10^8\,s^{-1} \\ k_\perp = 19.36k_p \approx 15.5\cdot10^9\,s^{-1} \\ k_z = 146.75k_p \approx 11.7\cdot10^{10}\,s^{-1} \\ D_{ZFS} = 30.7\cdot10^9\,s^{-1} \approx 174\,mT \end{cases} \qquad 2)\begin{cases} \alpha = 75.5 \\ \beta = 12.72 \\ k_p = 1.65\cdot10^9\,s^{-1} \\ k_\perp = 74.5k_p \approx 12.3\cdot10^{10}\,s^{-1} \\ k_z = 11.72k_p \approx 19.34\cdot10^9\,s^{-1} \\ D_{ZFS} = -34.2\cdot10^9\,s^{-1} \approx -194\,mT \end{cases} \tag{2.30}$$

Figure 2.22 illustrates the quality of the agreement between the experimental and calculated curves as well as the sensitivity of the calculated MFE(B) to changes of the parameter pairs $\{k_p, D_{ZFS}\}$. In fact MFE(B) is rather sensitive to the parameters, because the dependence of the radical yield on the magnetic field is mainly determined by the ratio between on one hand k_p and on the other hand the ISC rates and, therefore, the size of D_{ZFS}. The larger the values are for D_{ZFS} and k_p the stronger must be the magnetic field to produce a similar magnetic effect. In view of the good sensitivity to the parameters we estimate the accuracy of the determination of k_p and D_{ZFS} from MFE(B) to be not worse than 20%.

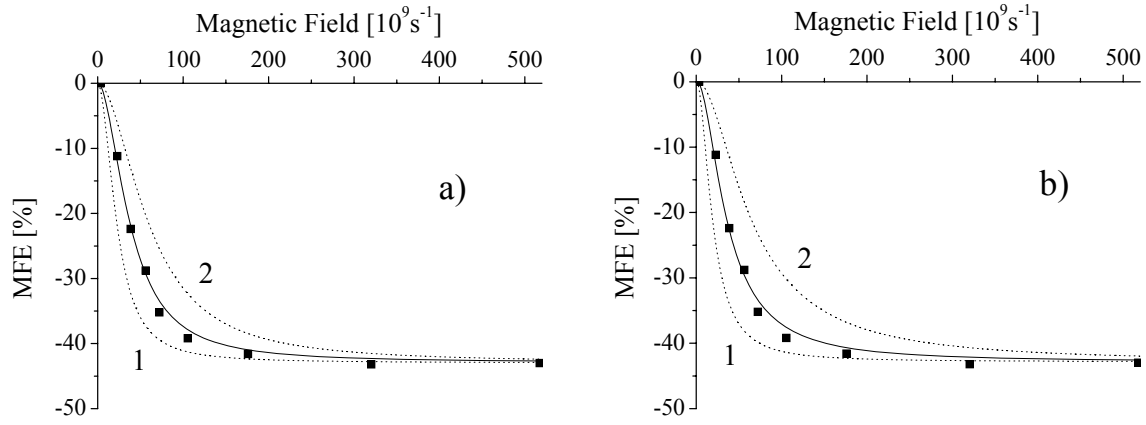

Figure 2.22: Dependence of the calculated MFE on the magnetic field for the following parameter sets: (a) $\alpha = 20.36$, $\beta = 147.75$, $\{k_p, D_{ZFS}\} = \{8\cdot10^8\ s^{-1}\ ,\ 30.7\cdot10^9\ s^{-1}\}$*-solid line,* $\{4\cdot10^8\ s^{-1}\ ,\ 18.5\cdot10^9\ s^{-1}\}$*-dashed line (1),* $\{12\cdot10^8\ s^{-1}\ ,\ 54.8\cdot10^9\ s^{-1}\}$*-dashed line (2); (b)* $\alpha = 75.5$, $\beta = 12.72$, $\{k_p, D_{ZFS}\} = \{1.65\cdot10^9\ s^{-1}\ ,\ 34.2\cdot10^9\ s^{-1}\}$*-solid line,* $\{8\cdot10^8\ s^{-1}\ ,\ 25.6\cdot10^9\ s^{-1}\}$*-dashed line (1),* $\{3\cdot10^9\ s^{-1}\ ,\ 59.5\cdot10^9\ s^{-1}\}$*-dashed line (2). Points represent experimental values for paraffin oil solutions, given for comparison.*

The agreement between experiment and numerical calculation turns out to be equally good for both parameter sets given in (2.30), so that it is impossible to make a choice in favor of one of them.

2.5.1.4. Selection rules for the ISC in triplet azocumene

A possibility to find arguments in favor of either the first or the second parameter set in (2.30) is, to consider the symmetry properties of the ^{3}AC molecule. It is well known that excitation of *trans*-azoalkanes from their ground state to the first singlet or state is a ($n_+\pi^*$) transition [20,73]. Quantum mechanical calculations made for azomethane [20,32] predict that the equilibrium structure of the first triplet state should be non-planar, the potential minimum corresponding to a tetrahedral angle close to 90°. It is expected that the intersystem crossing proceeds mainly at the nuclei configuration where the potential surfaces of triplet and singlet states cross each other. The position of the crossing point can appreciably depend on the substituents of the azo-group, but theoretical results for azomethane [20,32] allow to draw the analogy conclusion, that the crossing point for AC corresponds also to a non-planar structure, probably with tetrahedral angle also close to 90° . Becoming non-planar, the CNNC group

changes its symmetry from C_{2h} to C_2 . The only symmetry operation of C_2 is rotation by 180° around the symmetry axis (except the identity transformation), which in the case of the CNNC-group is perpendicular to the NN bond and forms two equal angles with both CN as shown in scheme 2.5.

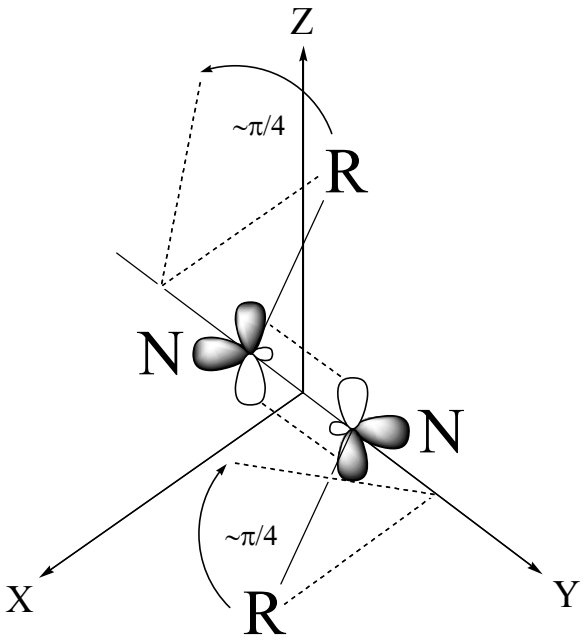

Scheme 2.5

Let this symmetry axis be the z-axis of a molecular frame. It is easy to see that the axis is one of the three main axes of the ZFS tensor. To prove it, we just need to show that both zx and zy non-diagonal elements of the tensor are zero. The zx- nondiagonal element is defined as [74,75]

$$-\frac{1}{2}g^2\mu_B{}^2\int\frac{3(x_1-x_2)(z_1-z_2)}{|\vec{r}_1-\vec{r}_2|^5}|\Psi_T(\vec{r}_1,\vec{r}_2)|^2\,d\vec{r}_1 d\vec{r}_2 \qquad (2.31)$$

where $\vec{r}_{1,2}$ denote the coordinate vectors of two (1 and 2) unpaired electrons, $x_{1,2}$ and $z_{1,2}$ are their projections on x and z axes respectively, Ψ_T is the orbital part of the triplet wave function. The integral (2.31) can be presented as the summation of two integrations: the first one over half-space $x > 0$ and the second one over $x < 0$. It is clear that these two contributions are

equal in absolute value but have opposite signs, so that the whole integral (2.31) is equal to zero. This can be understood if one realizes, that the C_2 operation (rotation around z by 180°) transforms the first half-space to the second one and vice versa. Being symmetry element of the system the rotation does not affect the value of $|\Psi_T(\vec{r}_1,\vec{r}_2)|^2$, but only changes the sign of the factor $\frac{3(x_1-x_2)(z_1-z_2)}{|\vec{r}_1-\vec{r}_2|^5}$, what results in a sign change of the integral over a half-space. The same, of course, is valid for the yz-element of the ZFS tensor.

Let now the other two main axes of the ZFS tensor be the x and y axes of the molecular frame. We want to show, that simple group theory considerations predict the ISC from the T_z state to be symmetry forbidden, whereas it is allowed from both T_x and T_y. In order to do this we have to use the following basic theorem [76]: for a quantum-mechanical system under a certain symmetry group a matrix element of an operator is nonzero only if it contains the unit representation.

Table 2.4 Characters of irreducible representations of the C_2 symmetry group

C_2	A	B
1)E	1	1
2)C_2	1	-1

1)Identity transformation

2)Rotation around symmetry axis by 180°

The only irreducible representations of C_2 are two one-dimensional representations A an B. Under the C_2 rotation operation the first one (A) does not change its sign, whereas the second one (B) does (table 2.4).

As commonly accepted the ISC is induced by spin-orbit interaction, which according to [2] is determined by a Hamilton operator of the following form:

$$\hat{H}_{so} = \frac{e}{m_e c}\sum_i \hat{\vec{\mathbf{B}}}_\mathbf{i}\cdot\vec{\mathbf{s}}_\mathbf{i}$$

where $\vec{\hat{\mathbf{s}}}_\mathbf{i}$ is the spin vector operator of the electron i and $\vec{\hat{\mathbf{B}}}_\mathbf{i}$ is the vector operator representing the local magnetic field at the electron i, interacting with its spin and induced by the orbital motions of all electrons in the molecule. The summation is extended over all electrons in the molecule. The ISC rate constant from a triplet sub-state T_j is determined by the non-diagonal matrix element between this state and the singlet ground state S,

$$\left\langle \Psi_S S \left| \hat{H}_{so} \right| \Psi_T T_j \right\rangle = \left\langle \Psi_S S \left| \frac{e}{m_e c} \sum_i \vec{\hat{\mathbf{B}}}_\mathbf{i} \cdot \vec{\hat{\mathbf{s}}}_\mathbf{i} \right| \Psi_T T_j \right\rangle \tag{2.32}$$

(Ψ_S, Ψ_T - denote the corresponding orbital wave functions). Since under ISC one electron undergoes a $\pi^* \rightarrow n_+$ transition (note, in spite of the orbital wave functions may differ from π^* and n_+ at tetrahedral angels different from 180°, their symmetry properties must be kept according to the orbital symmetry conservation [77,78]), the matrix element (2.32) is direct proportional to:

$$\propto \left\langle n_+ S \left| \frac{e}{m_e c} \sum_i \vec{\hat{\mathbf{B}}}_\mathbf{i} \cdot \vec{\hat{\mathbf{s}}}_\mathbf{i} \right| \pi^* T_j \right\rangle \tag{2.33}$$

To determine whether the matrix element (2.32) is nonzero, we have to check the symmetry properties of (2.33), which in turn are determined by the transformation rules of each element contained in the expression. Concerning the spin-orbit operator, one can conclude that it is simply scalar i.e. unit representation A, since it is proportional to the scalar product of two vectors: local magnetic field and spin moment. In order to find out the symmetry properties of the spin states, we should note, that in the frame of the main axes of the ZFS tensor S and T_j are defined as [74]:

$$S = \frac{1}{\sqrt{2}}(\alpha\beta - \beta\alpha),\ T_x = \frac{1}{\sqrt{2}}(\beta\beta - \alpha\alpha),\ T_y = \frac{i}{\sqrt{2}}(\alpha\alpha + \beta\beta),\ T_z = \frac{1}{\sqrt{2}}(\alpha\beta + \beta\alpha)$$

Under rotation around the z-axis by a certain angle θ, single electron spin functions undergo the transformation operation [79]

$$\begin{pmatrix}\alpha'\\ \beta'\end{pmatrix} = e^{i\sigma_z\theta}\begin{pmatrix}\alpha\\ \beta\end{pmatrix} = (\theta=\pi) = \begin{pmatrix} i\alpha\\ -i\beta\end{pmatrix} \qquad \text{with} \quad \sigma_z = \frac{1}{2}\begin{pmatrix}1 & 0\\ 0 & -1\end{pmatrix} \text{- Pauli matrix}$$

what in turn directly determines the symmetry properties of the singlet and the three triplet sub-states. The transformation rules of all elements included in equation (2.33) under the symmetry group C_2 are collected in table 2.5.

Table 2.5: Symmetry properties of the elements contained in equation (2.33).

	n_+	$\pi*$	S	T_x	T_y	T_z	$\vec{\hat{\mathbf{B}}}_\mathbf{i}\cdot\vec{\hat{\mathbf{s}}}_\mathbf{i}$
E	n_+	$\pi*$	S	T_x	T_y	T_z	$\vec{\hat{\mathbf{B}}}_\mathbf{i}\cdot\vec{\hat{\mathbf{s}}}_\mathbf{i}$
C_2	n_+	$-\pi*$	S	$-T_x$	$-T_y$	T_z	$\vec{\hat{\mathbf{B}}}_\mathbf{i}\cdot\vec{\hat{\mathbf{s}}}_\mathbf{i}$

Putting the data from table 2.5 into equation (2.33) it is easy to see, that each of the two matrix elements $\left\langle S\left|\hat{H}_{so}\right|T_x\right\rangle$ and $\left\langle S\left|\hat{H}_{so}\right|T_y\right\rangle$ is A representation of the group C_2 and, therefore, should be non-zero. By contrast, the matrix element $\left\langle S\left|\hat{H}_{so}\right|T_z\right\rangle$ changes its sign under rotation transformation (representation B) and can not include representation A and, hence, has to be equal to zero, i.e. forbidden.

Thus, we can conclude, that the second parameter set of (2.30), where there are two fast and one slow ISC rates, is expected to be met in reality (although a quantum chemical calculation of the sign of the parameter D_{ZFS} is required to confirm this assumption). The difference between the ISC rates from T_x and T_y should be much smaller than that one between T_z and each one of these two states. Thus, the reaction operator $\hat{k}$ in the Schrödinger equation (2.21) can be reasonably considered as axial symmetric. The same approximation should be valid for the ZFS tensor as well, since the influence of its two parts D_{ZFS} and E_{ZFS} on the observable polarization should be determined by the multiplications $D_{ZFS}\left(k_z - \frac{k_x + k_y}{2}\right)$ and $E_{ZFS}(k_x - k_y)$, respectively (this situation is met for the *p*-type TM [8,9], and it is unlikely to expect a big difference between the cases of both types of TM). Therefore, the influence of E_{ZFS} is expected to be insignificant.

2.5.2. The case of rotational diffusion

As seen from the experimental results the values of the polarizations and the magnetic field effect noticeably decrease with decreasing solvent viscosity. This effect is associated with the increase of the influence of the rotational diffusion on the spin dynamics in triplet AC. In fact, the stochastic tumbling of the triplet molecule induces transitions between different triplet states, equalizing thereby their populations and, therefore, reducing any magnetic field dependent effect. The diffusional rotation of the molecule may be a very anisotropic and complex process, but in order to check qualitatively the dependence on viscosity in the frame of our model of a *d*-type TM and to also check the estimated values of the parameters $k_p, k_\perp, k_z$ and D_{ZFS}, we will limit ourselves to the case of isotropic continuous diffusion. In this case the spin evolution of the system has to be described by the stochastic Liouville equation (SLE) proposed by Pedersen and Freed for the *p*-type TM [9] and modified later by Steiner [80,72] for the case of a *d*-type TM,

$$\frac{d}{dt}\rho(\Omega,t) = -i\left[\hat{H}_Z + \hat{H}_{ZFS}(\Omega), \rho(\Omega,t)\right] - \frac{1}{2}\left\{\hat{k}(\Omega), \rho(\Omega,t)\right\} + D_r\nabla^2\rho(\Omega,t) \qquad (2.34)$$

with $D_r\nabla^2\rho(\Omega,t)$ being the diffusional operator describing the action of the rotational diffusion on the evolution of the spin density matrix. The important parameter of the SLE is the rotational diffusion coefficient D_r, which by means of the Debye-Stokes equation is dependent on the solvent viscosity, $6D_r \approx \frac{3kT}{4\pi\eta a^3}$ (here *a* is the hydrodynamic radius of the triplet AC). The equation is written now in the laboratory frame $\{x', y' z'\}$, where the earlier introduced operators $\hat{H}_Z$, $\hat{H}_{ZFS}$ and $\hat{k}$ are given by the following expressions:

$$\hat{H}_Z = \begin{pmatrix} \omega_0 & 0 & 0 \\ 0 & 0 & 0 \\ 0 & 0 & -\omega_0 \end{pmatrix}, \quad \hat{H}_{ZFS} = D_{ZFS}\cdot\hat{A}, \quad \hat{k} = (k_\perp - k_z)\cdot\hat{A} + \left[\frac{1}{3}(2k_\perp + k_z) + k_p\right]\cdot\hat{I}$$

with $\hat{I} = \begin{pmatrix} 1 & 0 & 0 \\ 0 & 1 & 0 \\ 0 & 0 & 1 \end{pmatrix}$ and $\hat{A} = \begin{pmatrix} \frac{1}{12}(3\cos 2\theta + 1) & \frac{1}{2\sqrt{2}} e^{i\phi}\sin 2\theta & \frac{1}{2} e^{2i\phi}\sin^2\theta \\ \frac{1}{2\sqrt{2}} e^{-i\phi}\sin 2\theta & -\frac{1}{6}(3\cos 2\theta + 1) & -\frac{1}{2\sqrt{2}} e^{i\phi}\sin 2\theta \\ \frac{1}{2} e^{-2i\phi}\sin^2\theta & -\frac{1}{2\sqrt{2}} e^{-i\phi}\sin 2\theta & \frac{1}{12}(3\cos 2\theta + 1) \end{pmatrix}$

The matrix $\hat{A}$ depends on two orientation angles of the triplet, the axial and azimuthal angles ϕ and θ, respectively, as shown in scheme 2.6. We should note here that in the general case the triplet orientation is determined by three Euler angles, but as we supposed axial symmetry in the molecular frame any change of the third angle does not affect the spin dynamics and, therefore, may be ignored in our consideration.

The solution of the SLE is determined by the initial condition $\rho(\Omega,0)=\rho_0(\Omega)$ (in our case the initial condition is $\rho_0(\Omega)=\frac{1}{12\pi}\hat{I}$) and contains all information about the observable values of Φ_C and P, which can be calculated by following formulas:

$$\begin{cases} \Phi_C = \int_0^\infty dt \int_\Omega k_c Sp\{\rho(\Omega,t)\}d\Omega \\ P = \Phi_C^{-1} \int_0^\infty dt \int_\Omega k_c Sp\{\hat{S}_z \rho(\Omega,t)\}d\Omega \end{cases} \qquad (2.35)$$

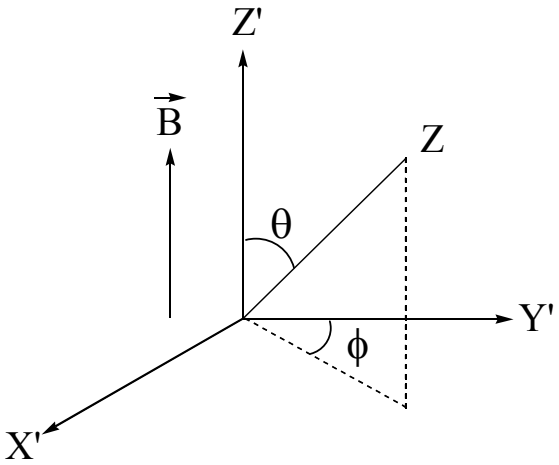

Scheme 2.6

In the general case equation (2.34) can not be solved analytically. Also a numerical solution requires nontrivial methods of calculation, because the direct integration over time is problematic due to the presence of the second order derivatives in the diffusional operator. In order to carry out a numerical integration of equation (2.34), we will follow a method, which has been applied by Tarassov with respect to the *p*-type of TM [42]. The main idea consists in

replacing the stochastic diffusion term in the SLE by a summation over all possible diffusional trajectories, i.e. the time evolutions of the orientation angles:

$$\text{SLE} \Rightarrow \sum_j \frac{d}{dt}\rho_j(t) = \sum_j -i\left[\hat{H}_Z + \hat{H}_{ZFS}(\Omega_j(t)), \rho_j(t)\right] - \frac{1}{2}\left\{\hat{k}(\Omega_j(t)), \rho_j(t)\right\}$$

This can be done, because the diffusion process is not affected by spin interactions and, therefore, can be considered independently. For each given trajectory $\Omega_j(t)$ the evolution of the spin density matrix $\rho_j(t)$ is determined by a simple differential equation of first order,

$$\frac{d}{dt}\rho_j(t) = -i\left[\hat{H}_Z + \hat{H}_{ZFS}(\Omega_j(t)), \rho_j(t)\right] - \frac{1}{2}\left\{\hat{k}(\Omega_j(t)), \rho_j(t)\right\},$$

which can be easily integrated numerically according to the following scheme:

$t = t_0 = 0$: $\rho_j(t_0) = \rho_j(0)$

$t = t_1 = \Delta t$: $\rho_j(t_1) = \exp\left(-i\hat{H}_{eff}(\Omega_j(t_0))\Delta t\right)\rho_j(t_0)\exp\left(i\hat{H}_{eff}{}^*(\Omega_j(t_0))\right)$

.
.
.

$t = t_{k+1} = t_k + \Delta t$: $\rho_j(t_{k+1}) = \exp\left(-i\hat{H}_{eff}(\Omega_j(t_k))\Delta t\right)\rho_j(t_k)\exp\left(i\hat{H}_{eff}{}^*(\Omega_j(t_k))\right)$,

where $\hat{H}_{eff} = \hat{H}_Z + \hat{H}_D(\Omega) - i\hat{k}(\Omega)$,

Scheme 2.7

which considers the diffusion trajectory as a discontinuous process with time increment Δt, which has to be chosen smaller than the rotational correlation time, i.e. $D_r \Delta t << 1$.

A possible diffusional trajectory can be constructed using the so-called Monte-Carlo method generation [81]. The method is commonly used for generation of values x distributed

by a given probability function P(x). If one can generate in two dimensional space points (y,x) uniformly distributed over an area that includes the function P(x), then a number of points for which the condition $y \le P(x)$ is met will be distributed by P(x) (see figure 2.23). A similar procedure may be carried out, of course, in the case of a many-dimensional distribution function $P(x_1, x_2, \ldots)$.

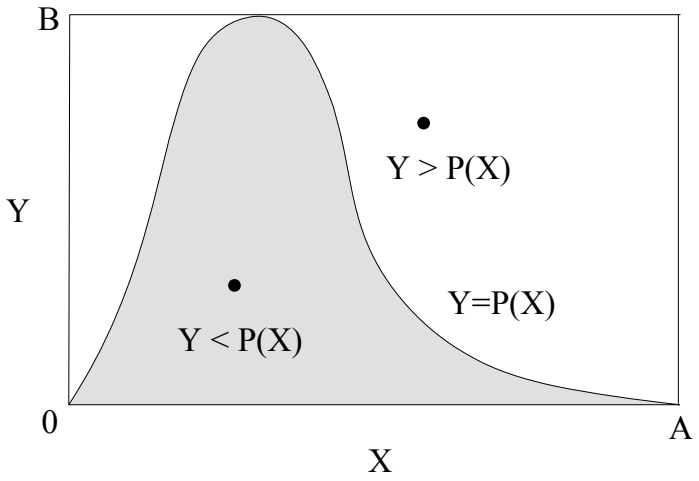

Figure 2.23: Illustration of the Monte-Carlo method applied for generating values with a given distrubution.

If a molecule at time t=0 had both orientation angles equal to zero ($\phi = \theta = 0$), then in the case of isotropic continuous diffusion (i.e. described by equation $\frac{d}{dt}\rho = D_R \nabla^2 \rho$) the probability to find an orientation determined by arbitrary ϕ and θ at any arbitrary time t is given by a sum over an infinite series [74]:

$$P(00|\phi\theta, t) = \sum_l \frac{2l+1}{4\pi} P_l^0(\cos\theta) \exp(-l(l+1) D_R t) \sin\theta$$

As this function does not depend on the axial angel ϕ, this angle is uniformly distributed over the range $[0; 2\pi]$. If however the initial orientation was determined by arbitrary values ϕ_0 and θ_0, then the probability to find the molecule at new angels ϕ , θ is given by the formula:

$$P(\phi_0\theta_0|\phi\theta, t) = \sum_l \frac{2l+1}{4\pi} P_l^0(\cos(\Delta\theta)) \exp(-l(l+1) D_R t) \sin(\Delta\theta) \; . \qquad (2.36)$$

Here $\Delta\phi$ and $\Delta\theta$ are the increments, which are related to the values of ϕ, θ and ϕ_0, θ_0 by means of the geometrical relations (see scheme 2.8):

$$\begin{cases} \cos\theta = \sin\Delta\theta \sin\theta_0 \cos\Delta\phi + \cos\Delta\theta \cos\theta_0 \\ \cos\phi = \dfrac{1}{\sin\theta}\left(\sin\Delta\phi \sin\Delta\theta \sin\phi_0 + \cos\Delta\theta \sin\theta_0 \cos\phi_0 - \sin\Delta\theta \cos\Delta\phi \cos\theta_0 \cos\phi_0\right) \end{cases} \tag{2.37}$$

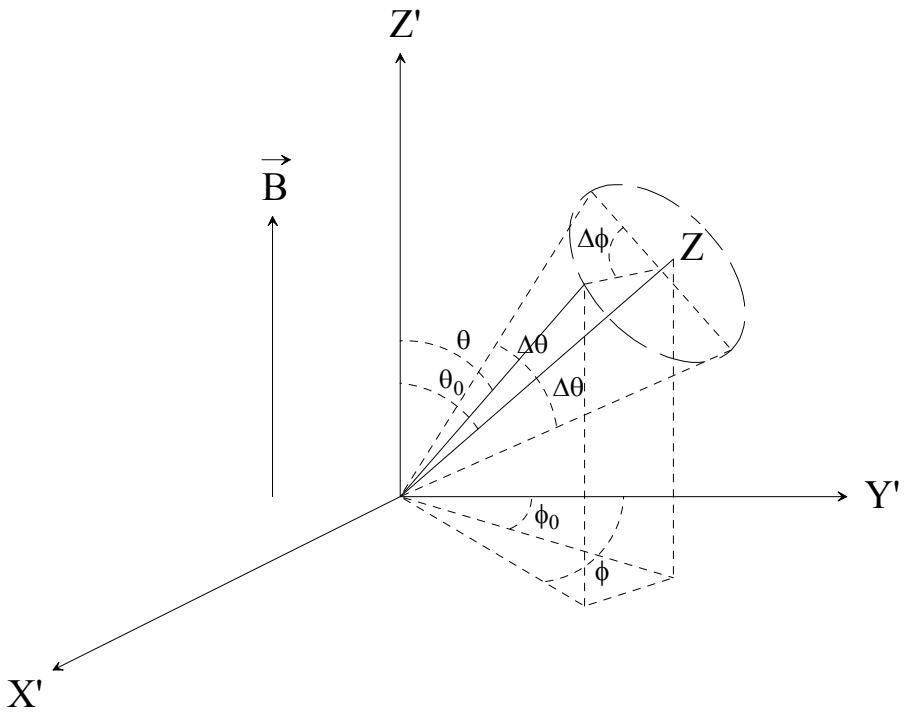

Scheme 2.8

In figure 2.24 is shown an example of a diffusional trajectory simulated according to the above described procedure, i.e. with a given time step Δt a new orientation of the molecule was generated by the Monte-Carlo method with distribution function (2.36), taking into account the initial orientation (in fact one generates increments $\Delta\phi$, $\Delta\theta$ which define in turn a new orientation by means of equation (2.37)). For all calculations which we have done, the diffusion time step was determined by the condition $D_r \Delta t = 0.02$, since a further reduction of the step was found practically not to affect the results of the calculation. For calculation of the probability function (2.36) the first 40 terms were taken into the summation.

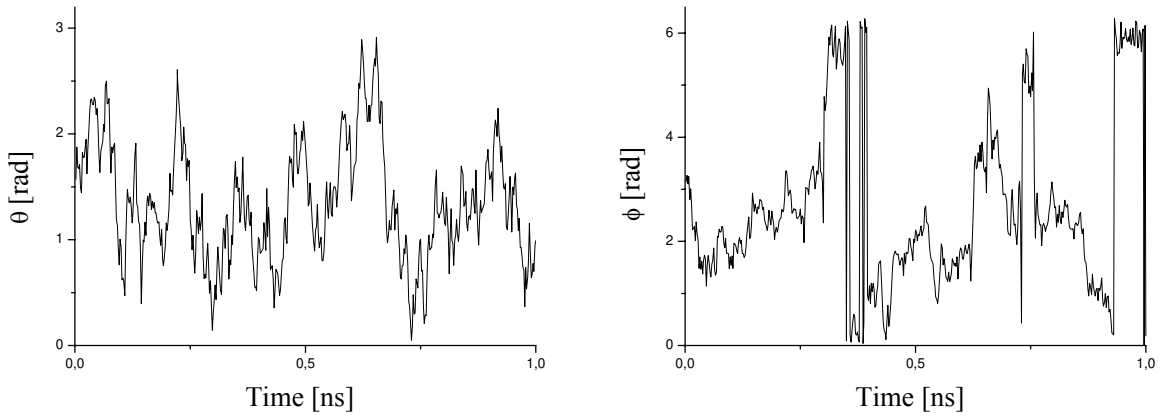

Fig 2.24: Example of a diffusional trajectory determined by means of two orientation angels ϕ and θ. The trajectory was generated with parameters $D_r = 10^{10}\ s^{-1}$ and $\Delta t = 2 \cdot 10^{-12}\ s$.

If we build N diffusional trajectories and for each of them calculate the density matrix according to scheme 2.7, then we can make up a global density matrix $\rho_N(t)$ corresponding to a statistical ensemble of N particles,

$$\rho_N(t) = \frac{1}{N}\sum_j \rho_j(t)$$

If the number of trajectories approaches infinity, i.e. $N \to \infty$, the obtained density matrix $\rho_N(t)$ approaches the solution of the SLE integrated over the orientation angles:

$$N \to \infty,\ \rho_N(t) \to \int_\Omega \rho(\Omega, t) \tag{2.38}$$

The validity of (2.38) also requires to meet the initial conditions, what can be fulfilled if the initial orientations in the ensemble are selected according to the distribution function $P(\Omega) = Sp\{\rho(\Omega,0)\} = Sp\{\rho_0(\Omega)\}$ (in our case $P(\Omega) = \frac{1}{4\pi}$) and for each trajectory j with an initial orientation Ω_0 the density matrix at $t = 0$ is chosen as $\rho_j(0) = \frac{\rho_0(\Omega_0)}{Sp\{\rho_0(\Omega_0)\}}$.

Putting (2.38) in (2.35) we can easily find, that for the infinite ensemble ($N \to \infty$)

$$\begin{cases} \int_0^\infty k_c Sp\{\rho_N(t)\}dt \to \int_0^\infty dt \int_\Omega k_c Sp\{\rho(\Omega,t)\}d\Omega = \Phi_C \\ \left[\int_0^\infty k_c Sp\{\rho_N(t)\}dt\right]^{-1} \int_0^\infty k_c Sp\{\hat{S}_z \rho_N(t)\}dt \to \Phi_C{}^{-1} \int_0^\infty dt \int_\Omega k_c Sp\{\hat{S}_z \rho(\Omega,t)\}d\Omega = P \end{cases}$$

Practically, an infinite number of trajectories is of course unachievable, but in our case we could always find a reasonable number of trajectories, which allowed both rather fast calculation and good accuracy . The error of the calculation caused only by statistical deviations can be estimated, if one compares the result of several calculations with the same number of trajectories $A_1(N)$, $A_2(N)$,…$A_k(N)$. Then, according to standard statistical considerations the error of the result A(N) can be approximated by the relation: $\text{Error}\{A(N)\} \approx \sqrt{\frac{1}{k-1}\sum_i (A_i - \overline{A})^2}$

with $\overline{A} = \frac{1}{k}\sum_i A_i$. All calculations were carried out with an accuracy not worse than 1-2 %.

Figures 2.25 - 2.27 represent the results of the numerical calculations of the SLE for both parameter sets $\{\alpha, \beta, k_p, D_{ZFS}\}$ of (2.30) and three different hydrodynamic radii ($a \cong 2.27\,\mathring{A}$, $2.74\,\mathring{A}$, and $3.45\,\mathring{A}$), in each case in comparison with the experimental results. The calculated and experimental curves show a good qualitative agreement, although some quantitative discrepancy is quite noticeable. This discrepancy can be caused by many different reasons, such as a more complicated nature of the diffusion process than considered in the SLE, or also some possible systematic errors (up to factor of two), either in the experimental determination of the quantum yields and polarizations and/or in the theoretical models, which were used for the analysis of the experimental data. For example, in our analysis of the experimental data we did not include the possible influence of the cage effect on the radical quantum yield, assuming this to be twice of the cleavage one. The cage effect should be rather small as the radicals originate from a triplet precursor and, therefore, any primary cage effect [24] should be absent. However, the secondary cage effect in the very viscous paraffin oil solvent might well reach a value of about 5% and might be one of the reasons for the discrepancy in the experimental and calculated results for Φ_C . Therefore, our quantitative results regarding the triplet state of AC

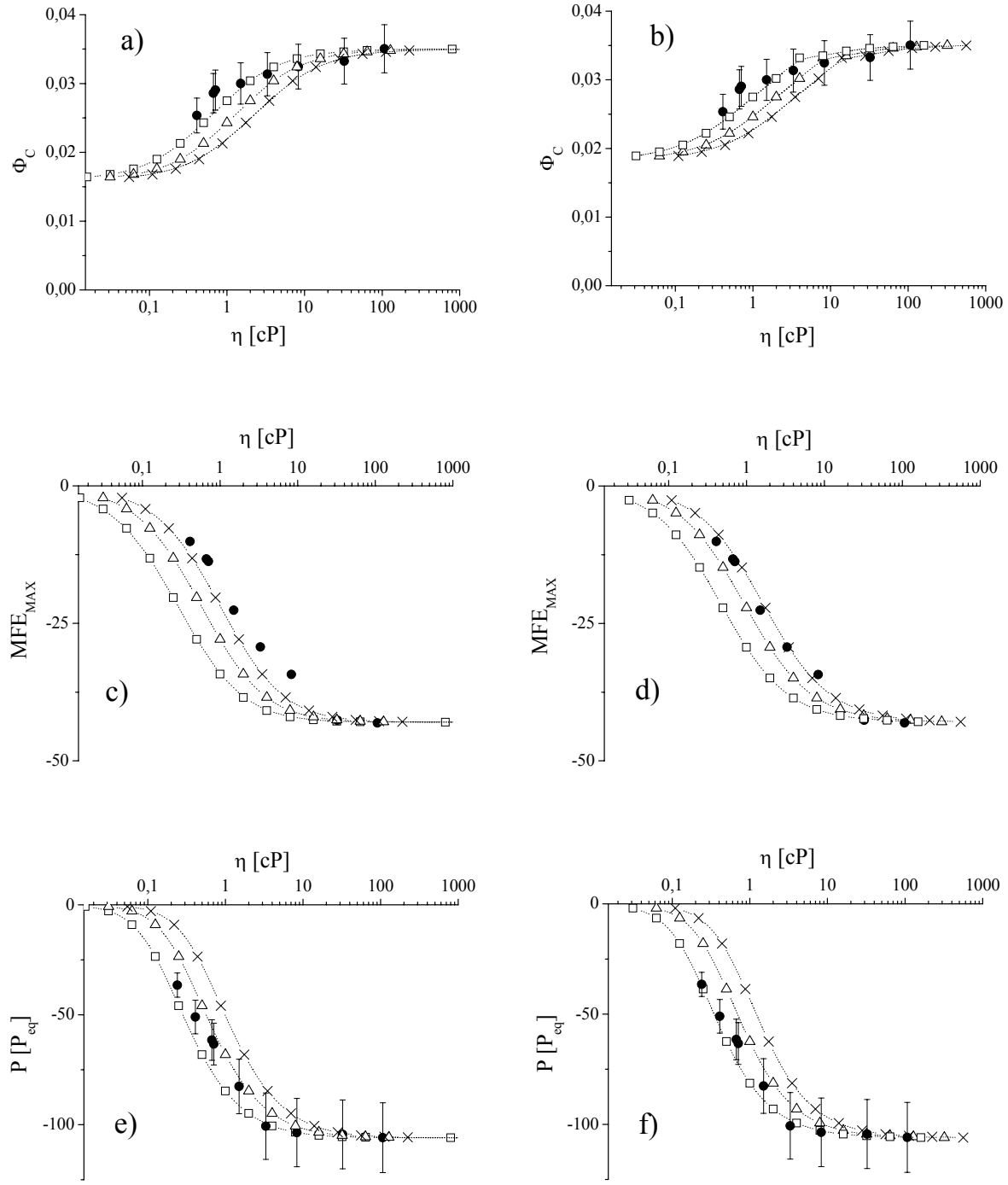

Figure 2.25: Viscosity dependence of the calculated values of: the cleavage quantum yield at zero field-(a,b), the maximum magnetic field effect-(c,d) and the spin polarization-(e,f) obtained with: the first parameter set of (2.30) -(a,c,e), the second parameter set-(b,d,f) for three values of the hydrodynamic radius a: 2.27 Å (squares), 2.74 Å (triangles), 3.45 Å (crosses). Filled circles represent the experimental results.

can not be considered as extremely precise, but they are expected to be good estimations, and they provide a good qualitative description of the intramolecular processes affecting the spin dynamics in the first excited triplet state of AC. Finally, we want to point out, that the obtained values of the diffusional radius ($\approx 3\,\mathring{A}$) seem to be absolutely reasonable, because a sphere with this radius has a volume roughly corresponding to that of the AC molecule.

References

[1] Poole C. P., in: *Electron Spin Resonance,* John Wiley&Sons, New York, **1983**.

[2] Hameka H. F., in *The Triplet State*, A. Zahan, ed.; Cambrige Univ. Press, Cambrige, **1967**.

[3] Van der Waals J. H., de Groot M. S., in: *The triplet state,* A. Zahan, Ed., Cambrige Univ. Press, Cambrige, **1967**.

[4] Yamauchi S., Pratt D. W., *Mol. Phys.* 37 **(1979)** 541.

[5] Wong S. K., Hutchinson D. A., and Wan J. K. S., *J. Chem. Phys*. 58 **(1973)** 985.

[6] Atkins P. W., and McLauchlan K. A., in *Chemically Induced Magnetic Polarization*, Lepley A. R. and Closs G. L., eds.; Wiley Interscience, New York, **1973**.

[7] Adrian F. J., *J. Chem. Phys.* 61 **(1974)** 4875.

[8] Atkins P. W., Evans G. T., *Chem. Phys. Lett.* 25 **(1974)** 108; *Mol. Phys*. 27 **(1974)** 1633.

[9] Pedersen J. B., Freed J. H., *J. Chem. Phys.* 62 **(1974)** 1706.

[10] Steiner U. E., *Chem. Phys. Lett.* 74 **(1980)** 108.

[11] Steiner U. E., *Ber. Bunsenges. Phys. Chem.* 85 **(1981)** 228.

[12] Sasaki S., Kobori Y., Akiyama K., Tero-Kubota S., *J. Phys. Chem. A.* 102 **(1998)** 8078, and references cited therein.

[13] Savitsky A. N., Paul H., *Chem. Phys. Lett.* 319 **(2000)** 403.

[14] Katsuki A., Kobori Y., Tero-Kubota S., Milikisyants S., Paul H., Steiner U. E., *Mol. Phys.* 100 **(2002)** 1245.

[15] Milikisyants S., Katsuki A., Steiner U., Paul H., *Mol. Phys.* 100 **(2002)** 1215.

[16] Bagryanskaya E. G., Ananchenko G. S.,Nagashima T., Maeda K., Milikisyants S., Paul H., *J. Phys. Chem. A* 103 **(1999)** 11271.

[17] Thiele J., *Chem. Ber.* 42 **(1909)** 2575.

[18] Engel P. S., *Chem. Rev.* 80 **(1980)** 99, and references cited therein.

[19] Mill T., Stringham R. S., *Tetrahedron Letters* **(1969)** 1863.

[20] Liu R., Cui Q., Dunn K. M., Morokuma K., *J. Chem. Phys.* 105 **(1996)** 2333.

[21] Rau H., *Angew. Chem. Int. Ed. Engl.* 12 **(1973)** 224.

[22] Robin M. B., in *The Chemistry of the Hydrazo, Azo, and Azoxy Groups*, Patai S., ed.; Wiley, New York **1975**.

[23] Diau E. W. G., Abou-Zied O. K., Scala A. A., Zewail A. H., *J. Am. Chem. Soc.* 120 **(1998)** 3245.

[24] Scott T. W., Doubleday C. J., *Chem. Phys. Lett.* 178 (1) **(1991)** 9.

[25] Boate D. R., Scaciano J. C., *Tetrahedron Letters* 30 **(1989)** 4633-4636.

[26] Savitsky A. N., *PhD thesis*, Universität Zürich, **1998**.

[27] Fischer H., Paul H., *Acc. Chem. Res.* 20 **(1987)** 200.

[28] Fogel L. D., Steel C., *J. Am. Chem. Soc.* 98 **(1976)** 485.

[29] Dürr H., Ruge B., *Top. Curr. Chem.* 66 **(1976)** 53, and references cited therein.

[30] Engel P.S., Steel C., *Acc. Chem. Res.* 6 **(1973)** 275, and references cited therein.

[31] Wamser C. C., Medary R. T., Kochevar I. E., Turro N. J., and Chang P. L., *J. Am. Chem. Soc.* 97 **(1975)** 4864.

[32] Camp R. N., Epstein I. R., and Steel C., *J. Am. Chem. Soc.* 99 **(1977)** 2453.

[33] Monti S., Orlandi G., Palmieru P., *Chem. Phys.* 71 **(1982)** 87-99.

[34] Engel P. s., Bishop D. J., Page M. A., *J. Am. Chem. Soc.* 100 **(1978)** 7009.

[35] Clark W. D., Steel C., *J. Am. Chem. Soc.* 93 **(1971)** 6347.

[36] Hurley R., Testa A. C., *J. Am. Chem. Soc.* 90 **(1969)** 1949.

[37] Anderson R. W. J., Hochstrasser R. M., Lutz M., Scott G. W., *Chem. Phys. Lett.* 28 **(1974)** 153.

[38] Anderson R. W. J., Hochstrasser R. M., Lutz M., Scott G. W., *J. Chem. Phys.* 61 **(1974)** 2500.

[39] Trotter W., Testa A. C., *J. Phys. Chem.* 74 **(1970)** 845.

[40] Capellos C., Porter C., *J. Chem. Soc., Faraday Trans. 2* 70 **(1974)** 1159.

[41] Shioya Y., Yagi M.,Higuchi J., *Chem. Phys. Lett.* 154 **(1989)** 25.

[42] Tarassov V., *PhD thesis*, Universität Zürich, **1999**.

[43] Martschke R., *PhD thesis*, Universität Zürich, **1999**.

[44] Simiyoshi T., Kamachi M., Kuwae Y., Schnabel W., *Bull. Chem. Soc. Jpn.* 60 **(1987)** 77.

[45] Huggenberger C., Fischer H., *Helv. Chim. Acta.* 64 **(1981)** 338-353.

[46] Stowell J. C., *J. Org. Chem.* 32 **(1967)** 2360.

[47] Ritter J. J., Kalish J., *Org. Syntheses* col. Vol. 5 471.

[48] Steiner U., *Z. Naturforsch.* 34a **(1979)** 1093.

[49] Tsentalovich, Y. P., Fischer H., *J. Chem. Soc. Perkin Trans.* 2 **(1994)** 729.

[50] Scaciano J.C., *J. Am. Chem. Soc.* 102 **(1980)** 7747.

[51] Zimmt M. B., Doubleday C., Turro N. J., *J. Am. Chem. Soc.* 108 **(1986)** 3618.

[52] Schuh H., Fischer H., *Helv. Chim. Acta.* 61 **(1978)** 2130.

[53] Wagner P. J., Kochevar I., *J. Am. Chem. Soc.* 90 **(1968)** 2232.

[54] Frank J., Rabinowitch E., *Trans. Faraday Soc.* 30 **(1934)** 120.

[55] Nelsen S. F., Bartlett P. D., *J. Am. Chem. Soc.* 88 **(1966)** 137.

[56] Jent F., Paul H., *Chem. Phys. Lett.* 160 **(1989)** 632.

[57] Savitsky A. N., Paul H., *Appl. Magn. Reson.* 12 **(1997)** 449.

[58] Blätter C., Jent F., Paul H., *Chem. Phys. Lett.* 166 **(1990)** 375.

[59] Blätter C., Paul H., *Res. Chem. Intermed*. 16 **(1991)** 201.

[60] Savitsky A. N., Batchelor S. N., Paul H., *Appl. Magn. Reson*. 13 **(1998)** 285.

[61] Pedersen J. B., *J. Chem. Phys.* 59 **(1973)** 2656-2667.

[62] Verma N. C., Fessenden R. W., *J. Chem. Phys.* 65 **(1976)** 2139-2155.

[63] Freed J. H., Pedersen J. B., *Advan. Magn. Resos.* 8 **(1976)** 1, and references cited therein.

[64] Adrian F. J., *Res. Chem. Intermed.* 16 **(1991)** 99, and references cited therein.

[65] Bloch F., Hansen W., Packard M., *Phys. Rev.* 69 **(1946)** 127.

[66] Savitsky A. N., Paul H., Shushin A. I., *J. Phys. Chem. A* 104 **(2000)** 9091-9100.

[67] Torrey H. C., *Phys. Rev.* 76 **(1949)** 1059.

[68] Verma N. C., Fessenden R. W., *J. Chem. Phys.* 58 **(1973)** 2501.

[69] Hore P. J., Joslin C. G., McLauchlan K. A., in : *Spezialist Period. Report „Electron Spin Resonance",* 5 **(1979)** 1, and references cited therein.

[70] Syage J. A., Lawler R. G., Trifunac A. D., *J. Chem. Phys.* 77 **(1982)** 4774.

[71] Bartels D. M., Trifunac A. D., Lawler R. G., *Chem. Phys. Lett.* 152 **(1988)** 109.

[72] Steiner U. E., Ulrich T., *Chem. Rev.* 89 **(1989)** 51, and references cited therein.

[73] Klessinger M., Michl J., in: *Excited states and photochemistry of organic molecules* , VCH Publishers, New York, **(1995)** , and references cited therein.

[74] Carrington A., McLauchlan A. D., in: *Introduction to magnetic resonance*, Harper International Edition, **(1967)**.

[75] Atherton N. M., in: *Principles of electron spin resonance*, E. Horwood and T. J. Kemp Eds., Ellis Howood PTR Prentice Hall, New York London Toronto Sydney Tokyo Singapore, **(1993)**.

[76] Burns G., in: *Introduction to group theory with applications*, A. M. Alper and A. S. Nowick Eds., Academic Press, New York San Francisco London, **(1977)**.

[77] Woodward R. B., Hoffman R., in: *The conservation of orbital symmetry*, Academic Press, New York, **1970**.

[78] Abrahamson E. W., Longuet-Higgins H. C., *J. Am. Chem. Soc.* 87 **(1965)** 2046.

[79] Landau L. D., Lifshitz E. M., in: *Quantum Mechanics*, Pergamon Press, Oxford-London-Paris, **(1962)**.

[80] Ulrich T., Steiner U. E., Föll R. E., *J. Phys. Chem.* 87 **(1983)** 1873.

[81] Ulam S., Metropolis N., *J. of Am. Statistical Association* 44 **(1949)** 335.

Answers to the comments of reviewer 1

Corrections on pp 1-16 were carried out as suggested.
Page 12: As a response to this remark the following text was added (cf. end of p. 17):

> "..The symmetry arguments suggest that the C_2 symmetry axis as shown in Fig. 11 represents the principal axis of the reaction tensor characterized by the components k_z and $k_\perp$. In our approach (cf. equation 11) identical principal axes were assumed for the ZFS and the reaction tensors. Within a point dipole approximation, i.e. spins localized at the nitrogen nuclei, the principal axis of the ZFS tensor would be expected to coincide with the N-N bond. However, in this triplet, spin-orbit coupling will also strongly contribute to the ZFS. Without a detailed quantum chemical calculation we cannot be sure about the principal axis of the ZFS tensor and the sign of D_{ZFS}. "
>
> The former Figure 9 is now Figure 11, the former Figures 10 and 11 are now Figures 9 and 10.

Figures 1, 2, 8, and 11 (the latter is now Figure 10): all suggestions were taken into account.

Answers to the comments of reviewer 2

General comments:

1. Regarding the contamination of our data analysis by a p-type TM, we note that in the discussion of fig. 3, our paper says: "All other known CIDEP producing mechanisms can be excluded (see ref. [12], p. 34).", and in [12], p. 34 the arguments are given, why a p-type TM can be excluded. In addition, the main argument (the net polarization is independent of the quencher concentration!) is also given in the present paper in the discussion of fig. 6. – We do not see why further arguments in support of this point should be necessary.
2. A thorough discussion of the influence a non-zero E-ZFS might have on our data analysis is beyond the scope of this article. However, at the end of the introduction of our paper we say that it is based on a PhD thesis (ref. [12]), where numerous details, justifications of assumptions, control experiments, etc. can be found, which are omitted in the present paper for space reasons. The possible influence of a non-zero E on our data analysis is briefly discussed in [12], p. 65. – We added this ref. on p. 12, end of last paragraph, of the present manuscript.

Particular comments:

1. The reviewer stated:
   ”The first statement: Despite the fact that the photochemistry of azoalkanes has been studied intensively, information on their triplet state is relatively scarce" **sounds a bit clumsily** because the intensive study of photochemistry of any specie means also obtaining the information on its triplet state as well.”

   In fact, just this latter expectation of the reviewer is not true, as was substantiated with a number of detailed references given in the first paragraph just after the criticized phrase.

2.-5. The reviewer is absolutely right. This paper is the direct continuation of the research outlined in ref. [6]. We studied the decomposition of triplet sensitized azocumene into nitrogen and cumyl radicals by time-resolved EPR and flash photolysis. In [6] we analysed the flash photolysis results and obtained partial information on the triplet state of azocumene. In the present paper we analyse the time-resolved EPR results and gain additional information on that state. From the combined consideration of both, flash photolysis and time-resolved EPR results, we obtain a maximum of information on the triplet state of azocumene.
   The reader of the present paper should be able to understand it without frequent resort to ref. [6]. To achieve this, a certain overlap with [6] is inevitable. We tried to keep this overlap as small as possible. However, in view of the criticism of reviewer 2 we now reduced it even more: the experimental part was considerably shortened, referring to [6]. The conclusive statement was modified, according to reviewer 2’s comment 5 and, in response to reviewer 1, a caveat with regard to the ZFS tensor axes was added.

The Excited Triplet State of Azoalkanes. Electron Spin Polarization and Magnetic Field Effects during Triplet Sensitized Photolysis of *trans*- Azocumene in Solution.

S. Milikisiyants[1,a], U. E. Steiner[2,*], and H. Paul[1,b]

[1] *Physikalisch-Chemisches Institut, University of Zuerich, CH-8057 Zuerich, Switzerland*

[2] *Fachbereich Chemie, University of Konstanz, DE-78457 Konstanz, Germany*

[a] *present address: Rensselaer Polytechnic Institute, Department of Chemistry and Chemical Biology, 110 8th Street, Troy, NY 12180, USA*

[b] *present address: Ruettebuckstr. 24, DE-79804 Dogern, Germany*

[*] *corresponding author's address:*

Prof. Dr. Ulrich Steiner
Fachbereich Chemie
Universitaet Konstanz
DE-78457 Konstanz

Tel: +49 (0)7531 883570

Fax: +49 (0)7531 883014
ulrich.steiner@uni-konstanz.de

Dedicated to Professor Renad Sagdeev on the occasion of his 70th birthday

Abstract

The triplet sensitized photo-decomposition of azocumene into nitrogen and cumyl radicals is investigated by time-resolved EPR and absorption spectroscopy. The radicals are found to be created spin polarized with a yield depending on the strength of an applied magnetic field. The phenomenon arises because in triplet-azocumene the decay into radicals competes with a fast triplet-sublevel selective intersystem crossing back to the azocumene ground-state. The size of the initial spin polarization of the radicals and the magnetic field effect on their yield is determined in solvents of different viscosities. Data analysis yields rate constants for the intersystem crossing and the cleavage reaction of triplet-azocumene as well as its zero-field splitting D_{ZFS}. At room temperature in non-polar solvents, the most probable values are: $k_x = k_y = 1.2\times10^{11}s^{-1}$ and $k_z = 1.9\times10^{10}s^{-1}$ for the intersystem crossing from the energetically lower and upper triplet sub-states, respectively, $k_p = 1.6\times10^{9}s^{-1}$ for the cleavage reaction, and for the zero-field splitting $D_{ZFS} = -3.4\times10^{10}s^{-1}$ (0.18 cm^{-1}).

Keywords:

CIDEP, EPR, photochemistry, energy transfer, triplet mechanism, azo-compounds

1. Introduction

Despite the fact that the photochemistry of azoalkanes has been studied intensively, information on their triplet state is relatively scarce. Only for some cyclic azoalkanes time-resolved spectroscopy found access to the triplet state, and its kinetics could be analyzed [1-2]. For non-cyclic azoalkanes it is only known, that they possess a short-lived triplet state at about $E_T \approx 226$ kJ/mole above their *trans* singlet ground state. When populated via triplet sensitization it deactivates rapidly by two competing processes, radiationless return to the singlet ground state (sometimes accompanied by some *trans-cis* isomerisation) and cleavage into nitrogen and two alkyl radicals, according to Fig. 1, where ^{3}Sens is the triplet sensitizer. No phosphorescence is observed, and the quantum yield for radical formation is usually very small in solution. Thus, the intersystem crossing (ISC) $T_1 \rightarrow S_0$ from triplet to singlet ground state seems to be much faster than the other decay routes, but till today no quantitative data are known concerning the time scales of the primary processes shown in Fig. 1 [3-4].

(Figure 1 about here)

Some years ago we observed by time-resolved EPR (TREPR) spectroscopy, that radicals formed from triplet sensitized non-cyclic azoalkanes carry initially an emissive electron spin polarization [5-6], which we attributed to the occurrence of a depopulation-type triplet mechanism (*d*-type TM [7]) in these compounds. The principle of that mechanism is depicted in Fig. 2. The ISC between triplet and singlet is caused by spin-orbit coupling, which may be quite different for the three zero-field sublevels T_x, T_y, and T_z. If that is the case, then these sublevels decay with different rates to the singlet ground state, causing their populations to become different. In an applied static magnetic field the population difference will be partially transferred, due to the zero-field splitting (ZFS) to the high-field states T_-, T_0, and T_+. Then, radicals stemming from the triplet are formed with an initial net spin polarization, provided the intersystem crossing $T_1 \rightarrow S_0$ can compete both with radical formation and spin relaxation between the triplet sub-states. In addition, the radical yield will become dependent on the strength of the applied static magnetic field, because the field mixes the states T_x, T_y, and T_z, thus increasing

the integral ISC rate and, consequently, diminishing the radical yield. The *d*-type TM was first proposed by Steiner in the early eighties to explain an observed magnetic field effect (MFE) on the radical quantum yield in electron transfer reactions between triplet excited thionine and various halogen substituted anilines [8-9]. The requirements for a *d*-type TM to occur, i.e. especially an intersystem-crossing $T_1 \rightarrow S_0$ with rate $10^9 - 10^{11}$ s^{-1}, are fulfilled only in rare cases. Therefore, until now this mechanism has been observed in only a few systems [5-6, 8-11].

(Figure 2 about here)

In the *d*-type TM the initial chemically induced electron polarization (CIDEP) of the radicals and the magnetic field effect (MFE) upon their yield are two manifestations of one and the same phenomenon. Thus, the magnitudes of both effects should be correctly describable with one and the same set of parameters, which are essentially the ISC rates of the triplet molecules, their decomposition rate into radicals, their zero-field splitting (ZFS) tensor, as well as the correlation time of their rotational diffusion. In order to check this for a non-cyclic azoalkane and to get some information about the elusive triplet state of these compounds, we investigated the decomposition of azocumene (AC) after triplet sensitization with 1-nitronaphthalene (1-NN). The system seemed to be well suited to study the MFE on the cumyl radical yield by laser flash photolysis (LFP) and the CIDEP of the radicals by TREPR spectroscopy.

In the LFP measurements, cumyl radicals formed after ^{3}(1-NN) quenching by AC, were investigated by optical absorption spectroscopy, and their yield was determined in alkane solutions of different viscosities (0.4 cP – 1 P) at various applied magnetic fields (0.02 T – 3 T). The results and a partial discussion of the observed MFEs have already been published [6]. Here, we report on the results of the TREPR experiments, which yielded the initial CIDEP of the cumyl radicals, again at various viscosities (0.2 cP – 1 P) but, of course, at only one magnetic field strength (350 mT, the field of our X-band TREPR spectrometer). We will then show that all parameters (the different ISC rates, the cleavage rate into radicals, and the zero-field splitting parameter D_{ZFS}) can be obtained from a combined analysis of the CIDEP and MFE data, and that this one parameter set allows a sat-

isfactory description of both the CIDEP and the MFEs observed for the decay of triplet azocumene (^{3}AC).

The extensive investigation of the *d*-type TM in triplet sensitized AC has been part of a PhD thesis [12]. We will sometimes refer to it, because it contains numerous details, justifications of assumptions, control experiments, etc., which have to be omitted here for space reasons. Therefore, we give the relevant part of ref. [12] as electronic supplementary material to facilitate access to it.

2. Experimental

Cumyl radicals were generated by laser flash photolysis of benzene or alkane solutions containing different concentrations of 1-NN and AC. They were detected at microwave powers in the range 0.3 - 20 mW using a cw-EPR spectrometer without field modulation. The details of the experimental conditions and the set-up have been described previously [6, 13].The sensitivity factor of the spectrometer (which is just the proportionality coefficient between the transverse magnetization, measured in units of Boltzmann polarized spins, and the observed TREPR signal measured in volts) was estimated from previous work[14] to be about $1.2 \cdot 10^9$ V/mole. All measurements were performed at room temperature. The materials used, their preparation, as well as the viscosities of the solvents have already been given previously [6].

3. Results

Fig. 3 shows an EPR spectrum which is observed about 3 μs after laser flash irradiation at λ = 355 nm of a benzene solution containing 1-NN (2.1 mM) and AC (7.5 mM). According to its hyperfine pattern and phase it has to be attributed unequivocally to an ensemble of cumyl radicals, which is spin polarized in emission. At 355 nm the absorption coefficients of 1-NN and AC are 3200 $M^{-1}cm^{-1}$ and 40 $M^{-1}cm^{-1}$, respectively. Thus, under the conditions of the experiment, nearly all the light is absorbed primarily by 1-NN, which is known to undergo fast ISC within about 10 ps to its triplet state ^{3}(1-NN) [15]. Therefore, the cumyl radicals must originate from ^{3}AC, formed via triplet quenching of ^{3}(1-NN)

by AC. The emissive CIDEP is mainly due to a *d*-type TM occurring during decay of ^{3}AC. All other known CIDEP producing mechanisms can be excluded (see ref. [12], p. 34).

(Figure 3 about here)

In the spectrum given in Fig. 3 two resonance lines are marked with arrows. They have been chosen to measure and analyze quantitatively the magnetization in dependence on time. They are separated well enough from neighboring resonances to allow an analysis via Bloch equations. In addition, these two lines are positioned symmetrically to the center of the spectrum. This will be of importance for the separation of the net emissive polarization of the radical ensemble from a superimposed weak emission/absorption multiplet type polarization (note that from the two marked resonance lines the low-field one carries a little bit more emission than the high-field one because of the superimposed multiplet polarization). The additional emission/absorption (E/A) type polarization is generated by the well known Radical Pair Mechanism (RPM) [16, 17]in pairs consisting of two cumyl radicals, which are formed at the radical initiation stage (geminate pairs) and later on in free diffusional encounters (F-pairs).

The EPR-time profiles which are obtained after flash photolytic radical generation contain all information about the chemical and spin dynamics of the system. They can be analyzed on the basis of Bloch equations, modified with additional terms to allow for chemical kinetics, CIDEP, and Heisenberg spin exchange (see [12], p. 36). These modified Bloch equations are rather complex and contain a lot of unknown parameters. However, if the radical concentration is small and the initial polarization large (both being the case in our experiments), then, a good approximation (for the on-resonance condition) are the well-known equations

$$\frac{d}{dt}v^{\,i} = -\frac{v^{\,i}}{T_2} + \omega_1 M_z^i \tag{1a}$$

$$\frac{d}{dt}M_z^i = -\omega_1 v^{\,i} - \frac{M_z^i}{T_1} + x_i P^i P_{eq} \Phi_R k_Q [\mathrm{AC}][\mathrm{T}] \tag{1b}$$

where x_i is the statistical weight of the line under study, P^i its polarization measured in units of the Boltzmann polarization P_{eq} , Φ_R the quantum yield of radicals

per ^{3}AC, k_Q the rate constant for triplet quenching, [AC] the quencher concentration, and [T] the concentration of ^{3}(1-NN). [AC] can be considered as constant and [T] is given by the rate law

$$\frac{d}{dt}[\mathrm{T}] = -k_{TT}[\mathrm{T}]^2 - \left(\frac{1}{\tau_0} + k_Q[\mathrm{AC}]\right)[\mathrm{T}] \tag{2}$$

τ_0 is the residual life time of ^{3}(1-NN) in the absence of the quencher. Neglecting at small triplet concentrations the triplet-triplet annihilation term, one gets

$$[\mathrm{T}] = [\mathrm{T}]_0 \cdot e^{-\frac{t}{\tau}} \tag{3}$$

with $[\mathrm{T}]_0$ being the initial ^{3}(1-NN) concentration and $\frac{1}{\tau} = \frac{1}{\tau_0} + k_Q[\mathrm{AC}]$ its effective first order decay rate constant. Let the two lines marked in Fig. 3 be the resonances *i* and *j*. Because we are interested in the net and multiplet polarization we introduce: $v^{\pm} = v^i \pm v^j$, $M_z^{\pm} = M_z^i \pm M_z^j$, $x = x^i + x^j = 2x^i$, and $P^{\pm} = \frac{P^i \pm P^j}{2}$.

Then, insertion of (3) into (1b) and integration (with initial conditions: $v^{\pm}(t=0) = M_z^{\pm}(t=0) = 0$) yields

$$v^{\pm}(t) = \frac{xP^{\pm}P_{eq}\Phi_R k_Q[\mathrm{AC}]\cdot[\mathrm{T}]_0\,\omega_1}{\left[\left(\tau^{-1}\right)^2 + \omega_T{}^2 - 2\tau^{-1}\sigma\right]\cdot\omega_T}\left\{\omega_T\left(e^{-\frac{t}{\tau}} - e^{-\sigma t}\cos(\omega_T t)\right) + \left(\tau^{-1} - \sigma\right)e^{-\sigma t}\sin(\omega_T t)\right\} \tag{4}$$

where $\sigma = \frac{1}{2}\left(\frac{1}{T_1} + \frac{1}{T_2}\right)$ and $\omega_T = \sqrt{\omega_1^2 - \frac{1}{4}\left(\frac{1}{T_1} - \frac{1}{T_2}\right)^2}$. The oscillating terms in eq. (4) are the Torrey oscillations [18-19], somewhat modified for our reacting system.

The TREPR signal represents the v-component of the magnetization vector, integrated over the irradiated volume, convoluted with the response function, and multiplied with the sensitivity factor C of the spectrometer (choosing the dimension of *C* equal V/mole we put $P_{eq} = 1$) :

$$S(t) = C \cdot f(t) \otimes \int v(t)\, dV_{irrad} \tag{5}$$

Here, $f(t)$ is the response function determined by the expression:

$$\begin{cases} t \le 0: \ f(t) = 0 \\ t > 0: \ f(t) = \dfrac{1}{\tau_{exp}} e^{-\frac{t}{\tau_{exp}}} \end{cases} \tag{6}$$

The integration of the magnetization over the irradiated volume comes down to just a replacement of the parameter $[T]_0$ in expression (4) by its integrated value, which can be estimated from the known quantum yield Φ_T of ^{3}(1-NN) and the amount of light energy absorbed by the 1-NN molecules (LE_{NN}):

$$\int [T]_0 \, dV_{irrad} = \frac{LE_{NN} \Phi_T}{h\nu N_A} \tag{7}$$

Putting (4), (6), (7) into (5) yields for the TREPR signal amplitude the analytical expression:

$$S^{\pm}(t) = \frac{CxP^{\pm}\Phi_R k_Q [AC] LE_{NN} \Phi_T \omega_1}{h\nu N_A \left[\left(\tau^{-1}\right)^2 + {\omega_T}^2 - 2\tau^{-1}\sigma \right] \cdot \omega_T} \left\{ \frac{\omega_T \left(e^{-\frac{t}{\tau}} - e^{-\frac{t}{\tau_{exp}}} \right)}{1 - \frac{\tau_{exp}}{\tau}} + \right.$$

$$+ \frac{e^{-\sigma t} \sin(\omega_T t) \left[\left(\tau^{-1} - \sigma\right)\left(1 - \sigma\tau_{exp}\right) - {\omega_T}^2 \tau_R \right]}{\left[\left(1 - \tau_{exp}\sigma\right)^2 + \left(\omega_T \tau_{exp}\right)^2 \right]} -$$

$$\left. - e^{-\sigma t} \omega_T \cos(\omega_T t) \left(1 + \frac{\tau_{exp}}{\tau} - 2\sigma\tau_{exp} \right) + e^{-\frac{t}{\tau_{exp}}} \omega_T \left(1 + \frac{\tau_{exp}}{\tau} - 2\sigma\tau_{exp} \right) \right\} \tag{8}$$

Although expression (8) contains many parameters, only four of them are unknown: $P^{\pm}$, σ, ω_T, and ω_1. The quenching rate constants (k_Q), the residual life times of ^{3}(1-NN) (τ_0), as well as the radical quantum yields (Φ_R) for all solvents under study have been obtained in the optical absorption experiments [6, 12] and are collected in Table 1. $\Phi_T = 0.63$ for non-polar solvents was also known [19]. The amount of absorbed light energy was calculated according to

(Table 1 about here)

the equation: $\frac{LE \cdot OD_{355}^{NN}}{OD_{355}^{NN} + OD_{355}^{AC}} \left\{ 1 - 10^{-\left(OD_{355}^{NN} + OD_{355}^{AC}\right)} \right\}$ from the laser pulse energy per shot (*LE*) and the optical densities of 1-nitronaphthalene (OD_{355}^{NN}) and azocumene (OD_{355}^{AC}) in the solution. The statistical weight of the lines under study (i.e. the number of radicals in that particular hyperfine state, divided by the total number of radicals) is $x = 40/2048$ and the sensitivity factor $C = 1.2 \cdot 10^9$ V/mole was known from previous work [14].

In the fitting procedure, we compared the spectral power of the Fourier transforms of function (8) and the TREPR signal, because there, the effects of the fit parameters are optimally separated, and the influence of the high and low frequency noise, distorting the real signal, becomes minimal. Like in previous studies [20-21], this way of fitting was found to be the more reliable and accurate one. As an example, we describe the analysis of the results obtained in paraffin oil solution. Of the four free parameters $P^{\pm}$, σ, ω_T, and ω_1 in eq. (8), $P^{\pm}$ and ω_1 are not separable because only their product $P^{\pm}\omega_1$ appears in the amplitude factor of the signal. Thus additional information must be employed for the determination of $P^{\pm}$. The microwave amplitude ω_1 could be extracted from the slope of linear plots of ω_T^2 versus the microwave power (which is proportional to ω_1^2), because of the relation $\omega_T = \sqrt{\omega_1^2 - \frac{1}{4}\left(\frac{1}{T_1} - \frac{1}{T_2}\right)^2}$. Fig 4 shows, in a plot versus the microwave power, the values of ω_T^2 which were obtained by fitting relation (8) to the sum of the time-profiles of the two resonance lines under study. As expected, the dependence of ω_T^2 on the microwave power is linear with very good accuracy. The slope of the line is the magnitude of ω_1^2 at 1 mW microwave power incident at the EPR cavity. The intercept should be given by $\frac{1}{4}\left(\frac{1}{T_1} - \frac{1}{T_2}\right)^2$. As this parameter is even smaller than the tiny statistical error we set it to zero, i.e. $\omega_1 = \omega_T$. Thereby a direct determination of the polarization $P^{\pm}$ by fitting the signals with the function given in equation (8) could be achieved.

(Figure 4 about here)

Fig. 5a presents experimental and simulated time-profiles of $S^+(t)$ for two quencher concentrations: 4.6 mM and 47 mM. The curves were calculated with parameters, which were obtained by fitting the numerically calculated Fourier transforms of the experimental time-profiles, as is shown in Fig 5b. The fitting procedure was implemented only in the frequency range lying relatively near to the maximum peak in Fourier space, which corresponds to the Torrey oscillation frequency. This seems to be quite reasonable, because the ratio of useful information to noise is maximal in this frequency range.

(Figure 5 about here)

Fig. 6 presents the values of the parameters P^+ and σ, obtained as results of fitting equation (8) to the experimental time profiles $S^+(t)$ for a set of different microwave powers and AC concentrations in the range 2.5 - 82 mM. As one can see from the figure the average values of the parameters are -106 P_{eq} and $4.2 \cdot 10^5$ s^{-1} for P^+ and σ, respectively. Within the limits of their statistical scattering (about 10-15 %) they are independent of the quencher concentration. It is evident that the parameter σ must be independent of the quenching rate, because its value is determined only by the rates of spin relaxation in the cumyl radicals. That the net polarization P^+ is independent of the quencher concentration, proves that it must be generated within the ^{3}AC molecules and their decay. Any polarization created in the ^{3}(1-NN) ensemble and then being transferred to the ^{3}AC molecules would necessarily have to depend on the quencher concentration.

(Figure 6 about here)

Finally, the ratio $\frac{P^-}{P^+}$ between multiplet and net polarization may be used for an independent check, if our value $P^+ \approx -106 \cdot P_{eq}$ makes sense. This ratio is not affected by a variety of possible systematic errors, which might be contained in the determination of P^+ (inaccuracy of quantum yield , the value of absorbed light energy, etc). As visible in Fig. 7 the ratio $\frac{P^-}{P^+}$ decreases with increasing AC concentration and even changes sign at high AC concentrations. This behavior is caused by the direct photolysis of AC, which for higher quencher concentrations

becomes more and more prominent ($OD_{355}^{AC}(82\ \text{mM}) \approx 0.23$). A linear fit of the ratio $\frac{P^-}{P^+}$ versus the AC concentration yields an intercept at $\approx \frac{1}{4}$, i.e. the

(Figure 7 about here)

multiplet polarization amounts to $P^- \approx$ -26.5 P_{eq} . Assuming that the ratio between the multiplet polarizations stemming from radical pairs with singlet and triplet precursors should be about 3:1, it is easy to obtain an estimation of about -80 P_{eq} for the multiplet polarization in the case of direct singlet photolysis of AC. This value is not far away from the previously measured multiplet polarization (-111 ± 25) P_{eq} for the direct photolysis of AC in paraffin oil solution [22]. Thus, our data analysis seems to be consistent.

In a similar way we have determined the net polarization P^+ also in other non-polar solvents of different viscosities. The results are summarized in Table 2.

(Table 2 about here)

4. Theoretical analysis

The observation of a magnetic field effect on the formation of cumyl radicals from triplet azocumene as well as a net spin polarization of the radicals manifests the occurrence of a *d*-type triplet mechanism in ^{3}AC. For a quantitative analysis of our experimental data we follow the model used by Steiner to explain the MFE on the decay of certain exciplexes [9, 23]. We assume that ^{3}AC undergoes simultaneously spin state selective ISC to the ground state and spin state independent decay into radicals, according to Fig. 8. The spin selective ISC causes non-thermal populations of the zero-field sub-states T_x, T_y, and T_z, which are partially transferred to the radical products. The quantum yield of cleavage is determined by the ratio of the decay rate k_p to the rates

(Figure 8 about here)

k_x, k_y, and k_z of the ISC process. An external magnetic field mixes the zero-field sub-states and, combined with the rotational Brownian tumbling of the molecule, induces transitions between them. This affects the total depopulation rate via ISC and, hence, influences the quantum yield of radicals and their polarization. For simplicity we assume for ^{3}AC axial symmetry of the ZFS tensor ($D_{xx} = D_{yy}$) and the ISC rate constants ($k_x = k_y = k_\perp$). This should be a good approximation, because the triplet electrons are localized on the azo-group having a C_2 symmetry axis, which can be reasonably considered as axially symmetric. Even if D_{xx} and D_{yy} were somewhat different, the approximation would be good as long as $|E_{ZFS} / D_{ZFS}| << 1$ (see ref. [12], p. 65).

The interactions and processes determining the triplet spin dynamics are: Zeeman and dipole-dipole interaction, rotational diffusion, depopulation via ISC, and decay into radicals. The magnitudes of the Zeeman and dipole-dipole interaction are determined by the magnetic field $\boldsymbol{B}$ and the ZFS parameter D_{ZFS}, respectively, and the rates of the depopulation processes are described by the rate constants $k_\perp$, k_z and k_p. The diffusional tumbling is measured by the correlation time τ_c for reorientational motion. The influence of any of these processes on the spin dynamics is determined by the ratio of the parameter measuring the process to the rate of triplet state depopulation. The value of τ_c increases with increasing viscosity. If the condition $1/\tau_c << \max\{k_p, \min\{k_\perp, k_z\}\}$is met, the influence of the diffusional motion becomes negligibly small, because the molecule has simply no time to change noticeably its orientation during the life time of the triplet state. Then, the polarization and quantum yield of the radicals become independent of the viscosity of the solution. We believe that this situation is met for ^{3}AC in at least the two most viscous solvents, squalane and paraffin oil, because P^+ levels off there (Table 2), as do Φ_R and the maximum magnetic field effect MFE_{max} (see Fig. 7 in [6]). Thus, for these two solvents the experimental data can be analyzed with neglect of the rotational diffusion and assumption of a static triplet molecule, which is described in the following.

Let the molecular z-axis be along the C_2 axis of the molecule, and the magnetic field vector $\mathbf{B}$ oriented at a polar angle θ against the z-axis. In the general case, the statistical description of the quantum system requires the solution of the appropriate Liouville equation. However, if the influence of diffusion is negligible, the processes can be described in terms of the Schrödinger equation. For our case it reads

$$\frac{d}{dt}\Psi = -i\hat{\mathbf{H}}_{EFF}\Psi = -i\left(\hat{\mathbf{H}}_Z + \hat{\mathbf{H}}_{ZFS}\right)\Psi - \frac{1}{2}\hat{\mathbf{K}}\,\Psi \tag{9}$$

Here $\hat{\mathbf{H}}_{EFF}$ denotes the effective Hamiltonian including all interactions and processes. In the basis $\{T_+\} = \{-(T_x+iT_y)/\sqrt{2}\}$, $\{T_0\} = \{T_z\}$, and $\{T_-\} = \{(T_x-iT_y)/\sqrt{2}\}$, quantized along the z-direction in the molecular frame, the Hamiltonian of the Zeeman interaction, $\hat{\mathbf{H}}_Z = \omega_0\left(\hat{\mathbf{S}}_z\cos(\theta) + \hat{\mathbf{S}}_x\sin(\theta)\right)$, can be expressed in terms of the magnetic field ω_0 and the spin operators in the molecular frame

$$\hat{\mathrm{S}}_Z = \begin{pmatrix} 1 & 0 & 0 \\ 0 & 0 & 0 \\ 0 & 0 & -1 \end{pmatrix} \text{ and } \hat{\mathrm{S}}_X = \frac{1}{\sqrt{2}}\begin{pmatrix} 0 & 1 & 0 \\ 1 & 0 & 1 \\ 0 & 1 & 0 \end{pmatrix}. \tag{10}$$

The zero-field interaction as well as the operator describing the decay via ISC and cleavage are given by the matrices

$$\hat{\mathbf{H}}_{ZFS} = \frac{1}{3}\begin{pmatrix} D_{ZFS} & 0 & 0 \\ 0 & -2D_{ZFS} & 0 \\ 0 & 0 & D_{ZFS} \end{pmatrix} \text{ and } \hat{\mathbf{K}} = \begin{pmatrix} k_\perp + k_p & 0 & 0 \\ 0 & k_z + k_p & 0 \\ 0 & 0 & k_\perp + k_p \end{pmatrix}. \tag{11}$$

The solution of the first order linear differential equation (9) has the general form

$$\Psi(\theta,t) = C_1 \cdot l_1 \cdot e^{\lambda_1 t} + C_2 \cdot l_2 \cdot e^{\lambda_2 t} + C_3 \cdot l_3 \cdot e^{\lambda_3 t} \tag{12}$$

with $l_{1,2,3}$ and $\lambda_{1,2,3}$ being the eigenvectors and corresponding eigenvalues of the matrix $-i\hat{\mathbf{H}}_{\mathrm{EFF}}$, and $C_{1,2,3}$ the set of arbitrary constants, which are determined by the initial conditions. For comparison with the experimental data for the quantum yield and spin polarization, the integrations

$$\Phi_{\mathrm{C}} = \frac{1}{3}\sum_{k=+,0,-} k_{\mathrm{p}} \frac{1}{2}\int_0^{\pi} \sin(\theta)\, d\theta \int_0^{\infty} \left|\Psi^k(\theta,t)\right|^2 dt \qquad (13a)$$

$$P = \Phi_C^{-1} \frac{1}{3}\sum_{k=+,0,-} k_{\mathrm{p}} \frac{1}{2}\int_0^{\pi} \sin(\theta)\, d\theta \int_0^{\infty} \left\langle \Psi^k(\theta,t) \middle| \hat{\mathbf{S}}'_z(\theta) \middle| \Psi^k(\theta,t) \right\rangle dt \qquad (13b)$$

are required, because the measured quantum yield and polarization are statistical averages over all initial polarizations and orientation angles of the triplet molecule. The primed operator $\hat{\mathbf{S}}'_z$ refers to the laboratory frame z-axis which is defined along the direction of the external magnetic field. The functions $\Psi^k(\theta,t)$ (k = +,0,-) represent the Zeeman states with M_S' = 1, 0 , -1 at t = 0. Note, that Φ_{C} in equation (13) now is the quantum yield for cleavage, i.e. $\Phi_{\mathrm{C}} = \Phi_{\mathrm{R}}/2$. The theoretical d-type TM polarization P in equation (13b) corresponds to the experimentally determined polarization P^+, i.e. $P \equiv P^+$.

In the two limiting cases of zero and infinite large field, the relations (11) can be given analytically (in both cases P is simply zero). In [6] we analyzed the MFEs for these two limiting cases and found, that there are two sets of parameters which describe the MFEs observed at low and high fields with equal accuracy:

$$\text{a)} \begin{cases} \alpha = 20.36 \\ \beta = 147.75 \\ k_{\perp} = 19.36 k_p \\ k_{\mathrm{z}} = 146.75 k_p \end{cases} \quad \text{and} \quad \text{b)} \begin{cases} \alpha = 75.5 \\ \beta = 12.72 \\ k_{\perp} = 74.5 k_{\mathrm{p}} \\ k_{\mathrm{z}} = 11.72 k_{\mathrm{p}} \end{cases} \qquad (14)$$

where the parameters α and β are defined by $k_{\perp} + k_p = \alpha k_p$ and $k_z + k_p = \beta k_p$. In order to get not only relative rate constants but absolute ones, we here now consider the case of an intermediate magnetic field which requires a numerical integration of (13).

To avoid an additional numerical integration over the time, we substitute (12) into (13) and, after having analytically integrated the exponential terms, we obtain:

$$\Phi_{\mathrm{C}} = k_p \frac{1}{2}\int_0^{\pi}\left\{\frac{1}{3}\sum_{k=+,0,-}\left(\sum_{i,j=1}^{3}\frac{1}{\lambda_j^{*}(\theta)+\lambda_i(\theta)}\mathbf{C}_j^{k*}(\theta)\mathbf{C}_i^{k}(\theta)\left\langle l_j(\theta)\middle| l_i(\theta)\right\rangle\right)\right\}\sin(\theta)\,d\theta \tag{15a}$$

$$P = \Phi_C^{-1} k_p \frac{1}{2}\int_0^{\pi}\left\{\frac{1}{3}\sum_{k=+,0,-}\left(\sum_{i,j=1}^{3}\frac{1}{\lambda_j^{*}(\theta)+\lambda_i(\theta)}\mathbf{C}_j^{k*}(\theta)\mathbf{C}_i^{k}(\theta)\left\langle l_j(\theta)\middle|\hat{\mathbf{S}}_Z(\theta)\middle| l_i(\theta)\right\rangle\right)\right\}\sin(\theta)\,d\theta \tag{15b}$$

Here, $\mathbf{C}^k(\theta)(k=+,0,-)$ are now no arbitrary constants but vectors, each of which is determined by the condition when the triplet has one of the three possible initial polarizations:

$$\left\{C^{+}(\theta), C^{0}(\theta), C^{-}(\theta)\right\} = \left[l_1(\theta) \quad l_2(\theta) \quad l_3(\theta)\right]^{-1} \cdot \left\{\begin{pmatrix}1\\0\\0\end{pmatrix}, \begin{pmatrix}0\\1\\0\end{pmatrix}, \begin{pmatrix}0\\0\\1\end{pmatrix}\right\} \tag{16}$$

where $\left[l_1(\theta) \quad l_2(\theta) \quad l_3(\theta)\right]$ is a matrix composed of the eigenvectors $l_i(\theta)(i=1,2,3)$.

Note that, since $\mathbf{H}_{EFF}$ is no hermitian matrix (because of the reaction operator) the condition of orthogonality of the l_i may not be fulfilled, i.e. $\left\langle l_j(\theta)\middle| l_i(\theta)\right\rangle \neq \delta_{ij}$.

From equation (15b) we calculated the polarizations in dependence on the parameter D_{ZFS} for different values of k_p, the rate of cleavage into two cumyl radicals. In these calculations the ISC rates were introduced as multiples of k_p according to

$\alpha - 1 = \frac{k_p}{k_\perp} = 19.36$ and $\beta - 1 = \frac{k_p}{k_z} = 146.75$ for solution 1) in (14), as well as

$\alpha - 1 = \frac{k_p}{k_\perp} = 74.5$ and $\beta - 1 = \frac{k_p}{k_z} = 11.72$ for the second possible solution in (14).

The results for the parameter sets *a* and *b* are given in Fig. 9a and 9b, respectively. Comparison of the numerically calculated polarizations P with the experimentally measured value P^{+} = -106 P_{eq} = -0.082 allows to find a correlation between the

two unknown parameters D_{ZFS} and k_p for each of the two possible sets $\{\alpha, \beta\}$ in (14). Fig. 9 illustrates the procedure of determining D_{ZFS} for each given value of k_p . In fact, there are two values of D_{ZFS}, at which the

(Figure 9 about here)

curve $P(D_{ZFS})$ crosses the horizontal line determined by the condition P = -0.082, because $P(D_{ZFS})$ must vanish when D_{ZFS} approaches either zero or infinity and reaches the maximum of its absolute value when D_{ZFS} becomes comparable with the external magnetic field. However, the D_{ZFS} values corresponding to the second crossing turned out to be well above 1 T and were simply rejected as physically unrealistic.

The parameter k_p was varied in sufficiently small steps (we took 5×10^7 s^{-1}) over the range from 10^8 s^{-1} to 10^{10} s^{-1}, and for each k_p the matching zero-field splitting D_{ZFS} was determined as described above. Doing so for both parameter pairs $\{\alpha, \beta\}$ in (14) resulted in two vectors, each of them containing as elements 200 number pairs $\{k_p, D_{ZFS}\}$, for which the set of all four values $\{\alpha, \beta, k_p, D_{ZFS}\}$ satisfied the requirement: $\{\Phi_C = 0.035,\ MFE_{\max} = -0.43,\ P = -0.082\}$. Equation (15a) was then used to calculate the magnetic field effect $MFE(B)$ for all 2×200 number pairs $\{k_p, D_{ZFS}\}$. Using a least squares procedure the results were compared with the experimentally obtained $MFE(B)$ in paraffin oil solution (see Fig. 6 in [6]). Best fits were found for the two parameter sets:

$$a)\begin{cases} \alpha = 20.36 \\ \beta = 147.75 \\ k_p = 8\cdot10^8\, s^{-1} \\ k_\perp = 19.36 k_p \approx 15.5\cdot10^9\, s^{-1} \\ k_z = 146.75 k_p \approx 11.7\cdot10^{10}\, s^{-1} \\ D_{ZFS} = 30.7\cdot10^9\, s^{-1} \approx 174 mT \end{cases} \qquad (17a)$$

$$b)\begin{cases} \alpha = 75.5 \\ \beta = 12.72 \\ k_p = 1.65 \cdot 10^9\, s^{-1} \\ k_\perp = 74.5 k_p \approx 12.3 \cdot 10^{10}\, s^{-1} \\ k_z = 11.72 k_p \approx 19.34 \cdot 10^9\, s^{-1} \\ D_{ZFS} = -34.2 \cdot 10^9\, s^{-1} \approx -194 mT \end{cases} \qquad (17b)$$

Fig.10 illustrates the quality of the agreement between the experimental and calculated curves as well as the sensitivity of the calculated *MFE* (*B*) to changes of the parameter pairs $\{k_p, D_{ZFS}\}$. In fact *MFE*(*B*) is rather sensitive to the parameters, because the dependence of the radical yield on the magnetic field is mainly determined by the ratio between on one hand k_p and on the other hand the ISC rates and, therefore, the size of D_{ZFS}. The larger the values are for D_{ZFS} and k_p the stronger the magnetic field must be to produce a similar magnetic effect. In view of the good sensitivity to the parameters we estimate the accuracy of the determination of k_p and D_{ZFS} from *MFE*(*B*) to be not worse than 20%.

(Figure 10 about here)

So far, both parameter sets given in (17) seem to describe with about equal accuracy the observed initial spin polarization of the cumyl radicals as well as the magnetic field effect on their yield. To find arguments in favor of one of the parameter sets, we considered the symmetry properties of ^{3}AC and the selection rules for ISC (see [12], p. 61ff). They suggest that there is one slow ISC rate and two fast ones, i.e. they favor set *b*. The symmetry arguments suggest that the C_2 symmetry axis as shown in Fig. 11 represents the principal axis of the reaction tensor characterized by the components k_z and $k_\perp$. In our approach (cf. equation 11) identical principal axes were assumed for the ZFS and the reaction tensors. Within a point dipole approximation, i.e. spins localized at the nitrogen nuclei, the principal axis of the ZFS tensor would be expected to coincide with the N-N bond. However, in this triplet, spin-orbit coupling will also strongly contribute to the ZFS. Without a detailed quantum chemical calculation we cannot be sure about the principal axis of the ZFS tensor and the sign of D_{ZFS}.

(Figure 11 about here)

The parameters given in (17) have been obtained by analysis of the spin polarizations and MFEs in high viscous solutions, where the reorientational diffusion is slow enough to model the 3AC molecules as static triplets. The question remains whether these parameter sets are also suitable for low viscous solvents, when the reorientational diffusion influences the spin dynamics in ^{3}AC. In fact, the stochastic tumbling of the triplet molecule induces transitions between different triplet states, thus equalizing their populations, and, therefore, reduces any magnetic field dependent effect. To account for such situations with significant rotational relaxation, we resorted to full solutions of the stochastic Liouville equation (SLE) for a triplet ensemble subject to isotropic reorientational diffusion with coefficient $6D_r \approx \frac{3kT}{4\pi\eta a^3}$ (a being the hydrodynamic radius of ^{3}AC) and decay with rates as given in (17). The SLE was solved numerically by a series expansion of the orientational dependence of the spin density matrix in terms of the Wigner rotation matrices [7, 24], as well as by a Monte Carlo path integration method (see ref. [12], p.66 ff).

The results are given in Fig. 12. Calculations were performed for both parameter sets $\{\alpha, \beta, k_p, D_{ZFS}\}$ of (14) and three different hydrodynamic radii ($a \cong 2.27$ Å, 2.74 Å, and 3.45 Å). For comparison, the experimental results are also shown. The calculated and experimental curves show good qualitative agreement, although some quantitative discrepancies are quite noticeable.

(Figure 12 about here)

These discrepancies can have many different reasons, such as a more complicated nature of the diffusion process than considered in the SLE, or also some possible systematic errors, either in the experimental determination of the quantum yields and polarizations and/or in the theoretical models, which were used for the analysis of the experimental data. For example, in our analysis of the experimental data we did not include the possible influence of the cage effect on the radical quantum yield (we just assumed $\Phi_R=2\Phi_C$). The cage effect should be rather small as the radicals originate from a triplet precursor and, therefore, any primary cage effect should be absent. However, the secondary cage effect in the very viscous paraffin

oil solvent might well reach a value of about 5% and might be one of the reasons for the discrepancy in the experimental and calculated results for Φ_C. Therefore, our quantitative results regarding the triplet state of AC can not be considered as extremely precise, but they are expected to be good estimations, and they provide a good semi-quantitative description of the intramolecular processes affecting the spin dynamics in the first excited triplet state of AC. It remains to be noted, that the obtained diffusional radius (≈ 3 Å) is absolutely reasonable, because a sphere with this radius has roughly the volume of an AC molecule.

In summary, even if there remain some ambiguities in the assignment of the ZFS tensor axes, in this work it has been corroborated that the decay of triplet sensitized *trans*-azocumene is governed by a depopulation-type triplet mechanism, causing the cumyl radicals to originate with initial spin polarization and their yield to depend on external magnetic fields. Both, spin polarization and magnetic field effect can be satisfactorily described with one and the same set of microscopic parameters. To the best of our knowledge this is the first observation and determination of zero-field splitting and substate selective decay kinetics of a triplet state for a non-cyclic azoalkane.

Electronic Supplementary Material

Large parts of ref. [12] are available as a PDF file.

Acknowledgement

S. M. and H. P. gratefully acknowledge financial support by the Swiss National Foundation for Scientific Research.

References

[1] W. Adam, G. Fragale, D. Klapstein, W. M. Nau, J. Wirz, J. Am. Chem. Soc. 117, 12578 (1995)

[2] W. M. Nau, P. U., in *Organic Photochemistry and Photophysics* (Eds.: V. Ramamurthy, K. S. Schanze), CRC Press, Boca Raton, 2006, p. 75.

[3] P. S. Engel, Chem. Rev. 80, 99 (1980)

[4] M. Klessinger, J. Michl, *Excited States and Photochemistry of Organic Molecules*, VCH, New York, 1995.

[5] A. N. Savitsky, H. Paul, Chem. Phys. Lett. 319, 403 (2000)

[6] S. Milikisyants, A. Katsuki, U. E. Steiner, H. Paul, Mol. Phys. 100, 1215 (2002)

[7] A. Katsuki, Y. Kobori, S. Tero-Kubota, S. Milikisyants, H. Paul, U. E. Steiner, Mol. Phys. 100, 1245 (2002)

[8] U. E. Steiner, Chem. Phys. Lett. 74, 108 (1980)

[9] U. E. Steiner, Ber. Bunsenges. 85, 228 (1981)

[10] H. Hayashi, Y. Sakaguchi, J. Photochem. Photobiol. C: Photochemistry Reviews 6 (2005)

[11] S. Sasaki, Y. Kobori, K. Akiyama, S. Tero-Kubota, J. Phys. Chem. A 102, 8078 (1998)

[12] S. Milikisyants, PhD thesis, University of Zurich, (2002)

[13] F. Jent, H. Paul, Chem. Phys. Lett. 160, 632 (1989)

[14] A. N. Savitsky, PhD thesis, University of Zurich, (1998)

[15] R. W. J. Anderson, R. M. Hochstrasser, M. Lutz, A. M. Scott, J. Chem. Phys. 61, 2500 (1974)

[16] K. M. Salikhov, Y. N. Molin, R. Z. Sagdeev, A. L. Buchachenko, *Spin polarization and magnetic effects in radical reactions*, Elsevier, Amsterdam, 1984.

[17] F. J. Adrian, Res. Chem. Intermed. 16, 99 (1991)

[18] H. C. Torrey, Phys. Rev. 76, 1059 (1949)

[19] P. J. Hore, C. G. Joslin, K. A. McLauchlan, Specialist Period. Report 5 ("Electron Spin Resonance"), 1 (1979)

[20] A. N. Savitsky, H. Paul, Appl. Magn. Reson. 12, 449 (1997)

[21] A. N. Savitsky, H. Paul, A. I. Shushin, J. Phys. Chem. A 104, 9091 (2000)

[22] R. Hurley, A. C. Testa, J. Am. Chem. Soc. 90, 1949 (1969)

[23] U. E. Steiner, T. Ulrich, Chem. Rev. 89, 51 (1989)

[24] J. B. Pedersen, J. H. Freed, J. Chem. Phys. 62, 1706 (1974)

Figure

Click here to download Figure: Fig 1.doc

Milikisyants et al. **Figure 1**

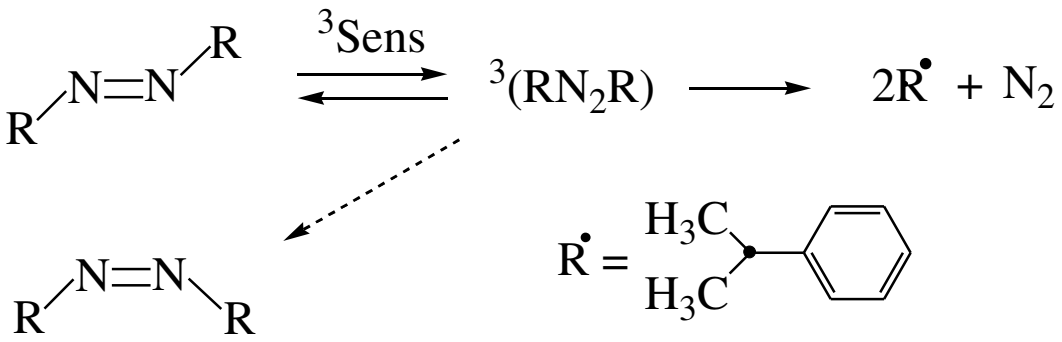

Figure

Click here to download Figure: Fig 2.doc

Milikisyants et al. **Figure 2**

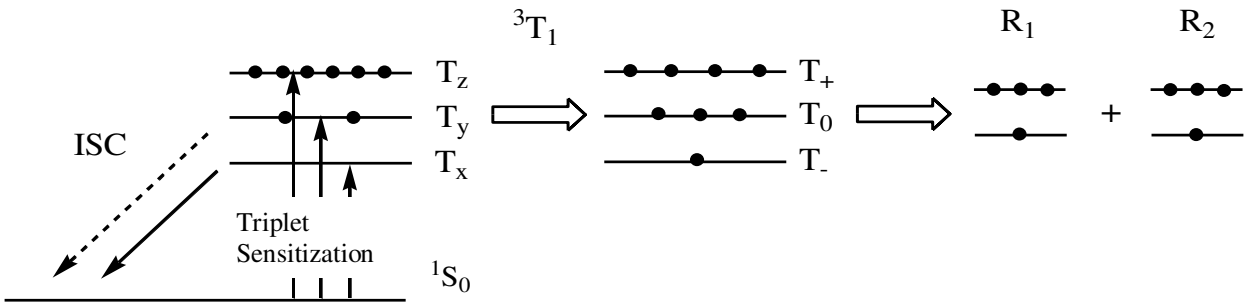

Figure

Click here to download Figure: Fig 3.doc

Milikisyants et al. **Figure 3**

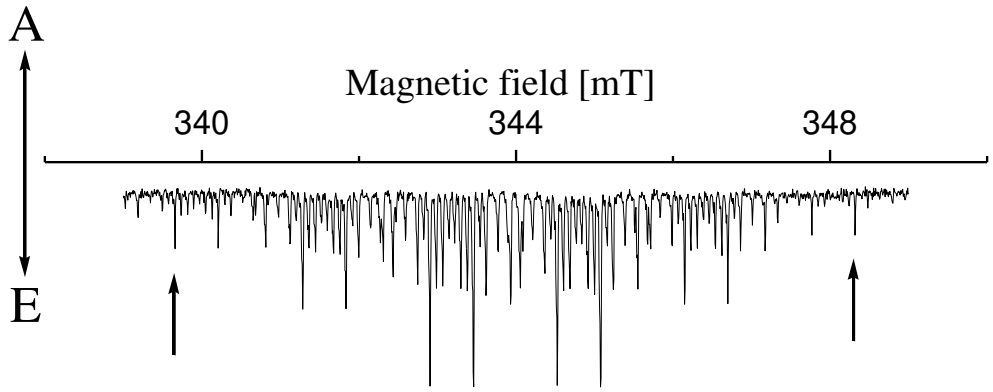

Figure

Click here to download Figure: Fig 4.doc

Milikisyants et al. **Figure 4**

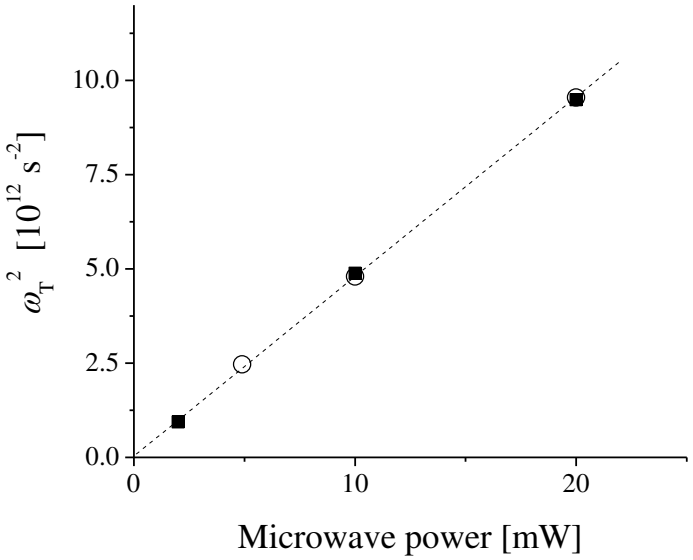

Figure

Click here to download Figure: Fig 5.doc

Milikisyants et al. **Figure 5**

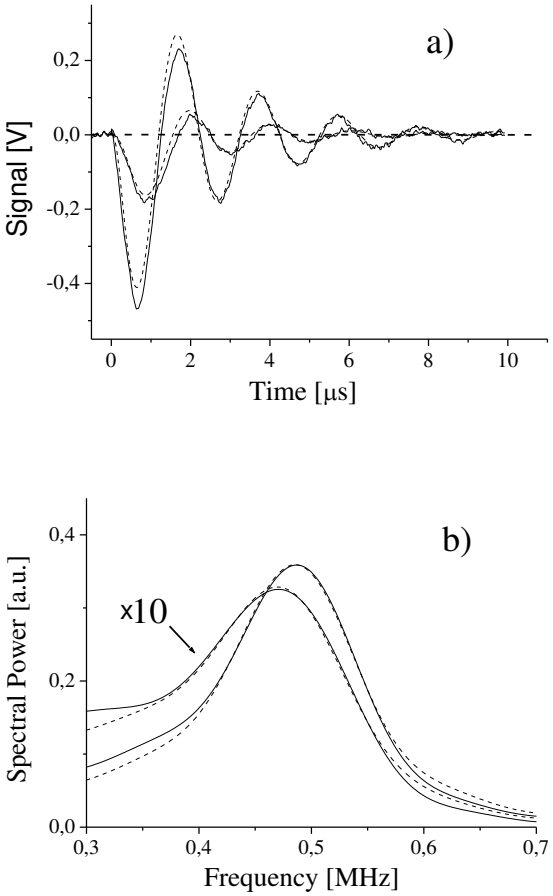

Figure
Click here to download Figure: Fig 6.doc

Milikisyants et al. **Figure 6**

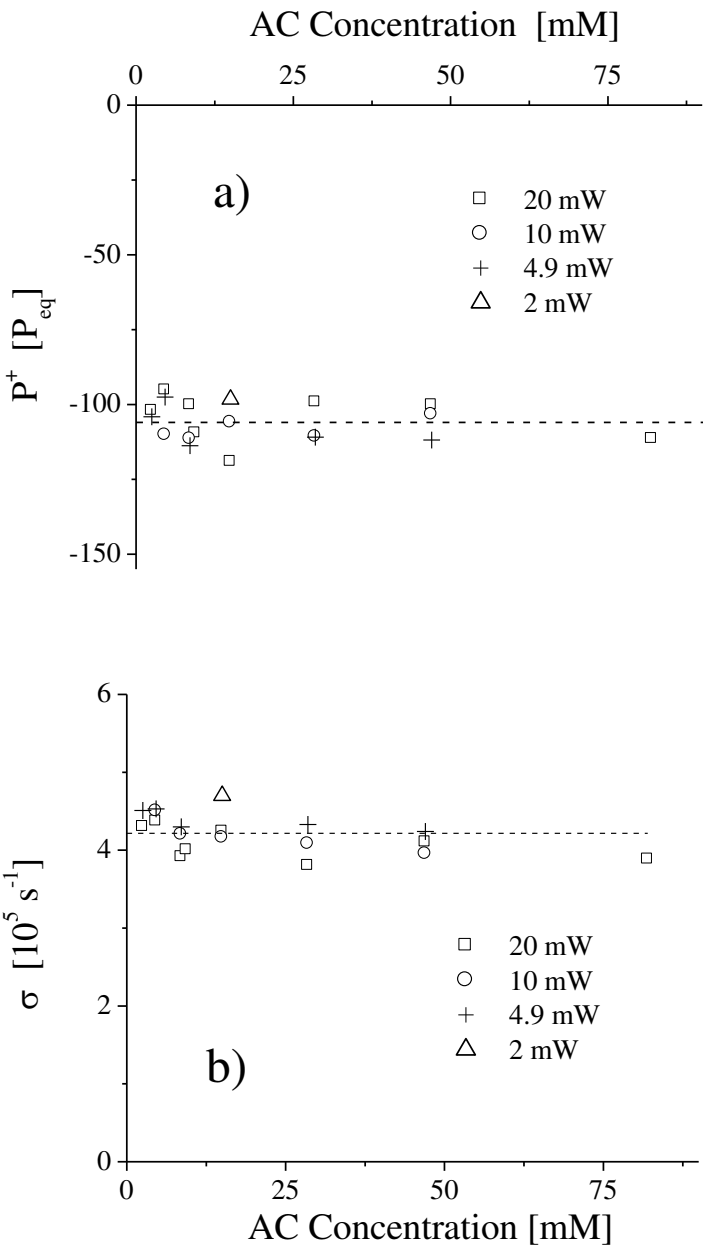

Figure
Click here to download Figure: Fig 7.doc

Milikisyants et al. **Figure 7**

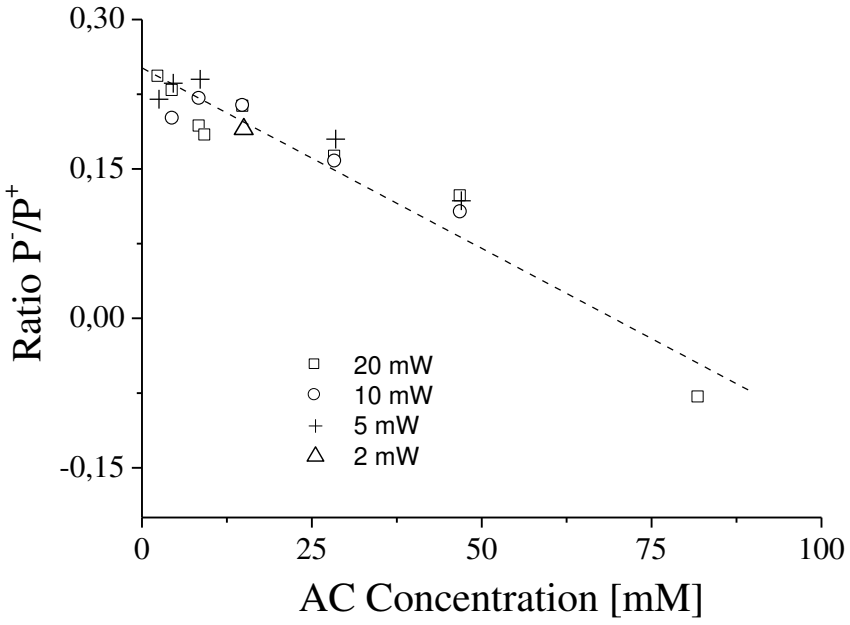

Figure
Click here to download Figure: Fig 8.doc

Milikisyants et al. **Figure 8**

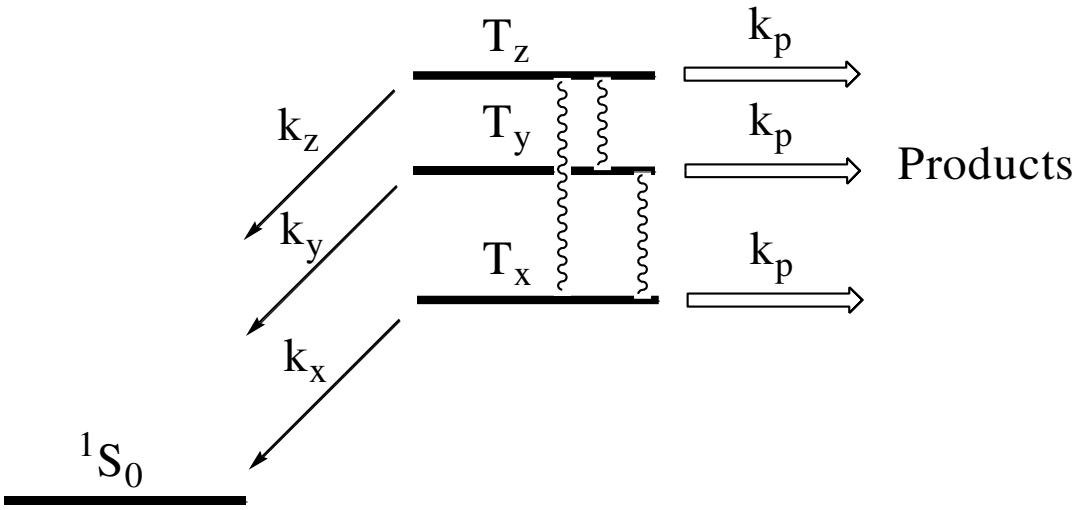

Figure
Click here to download Figure: Fig 9.doc

Milikisyants et al. **Figure 9**

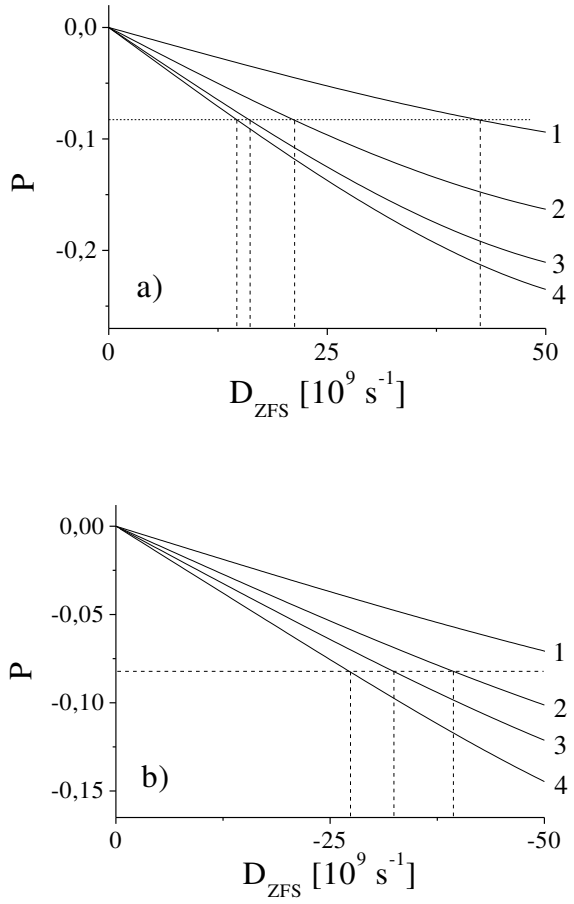

Figure
Click here to download Figure: Fig 10.doc

Milikisyants et al. **Figure 10**

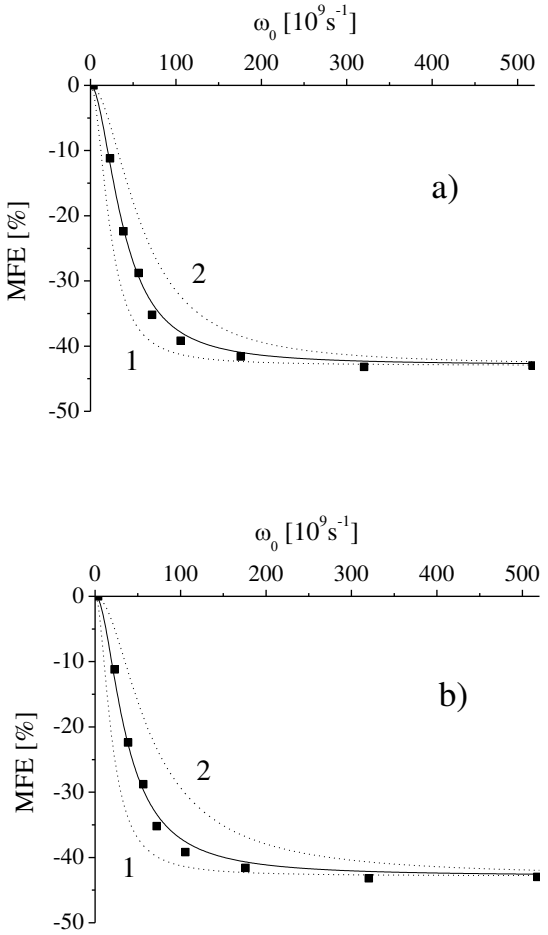

Figure
Click here to download Figure: Fig 11.doc

Milikisyants et al. **Figure 11**

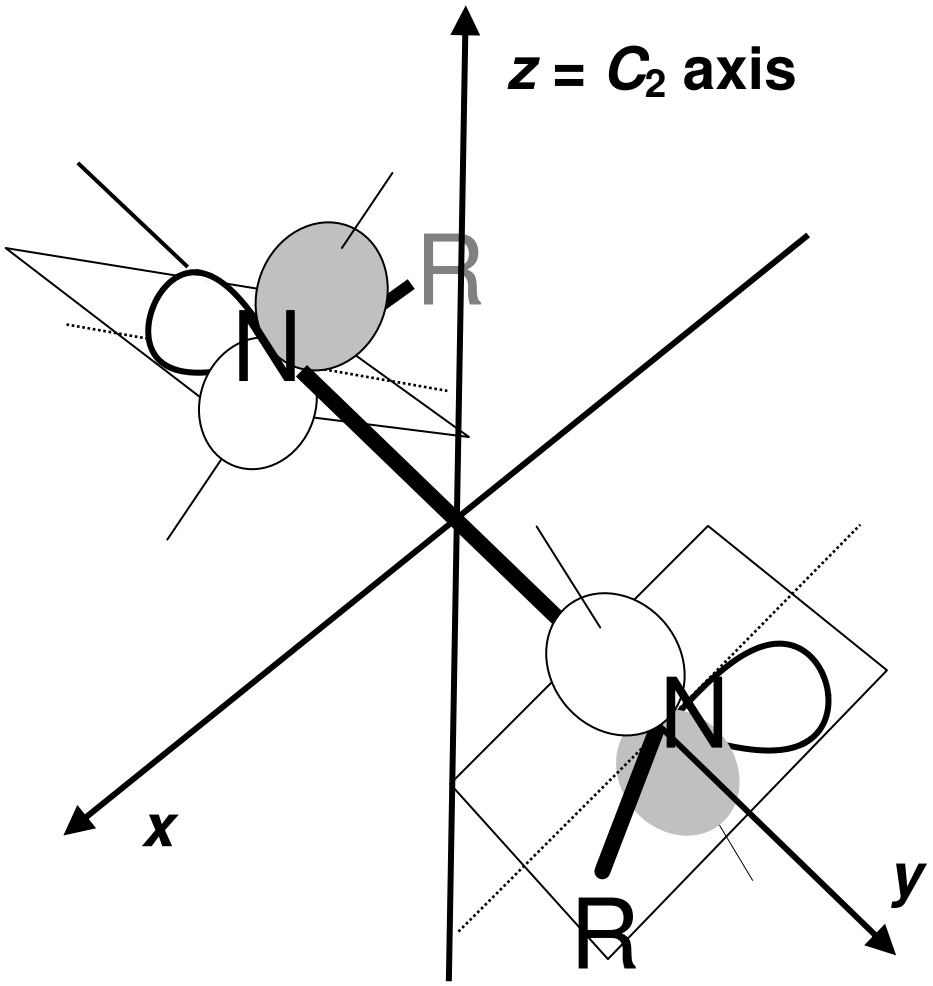

Figure
Click here to download Figure: Fig 12.doc

Milikisyants et al. **Figure 12**

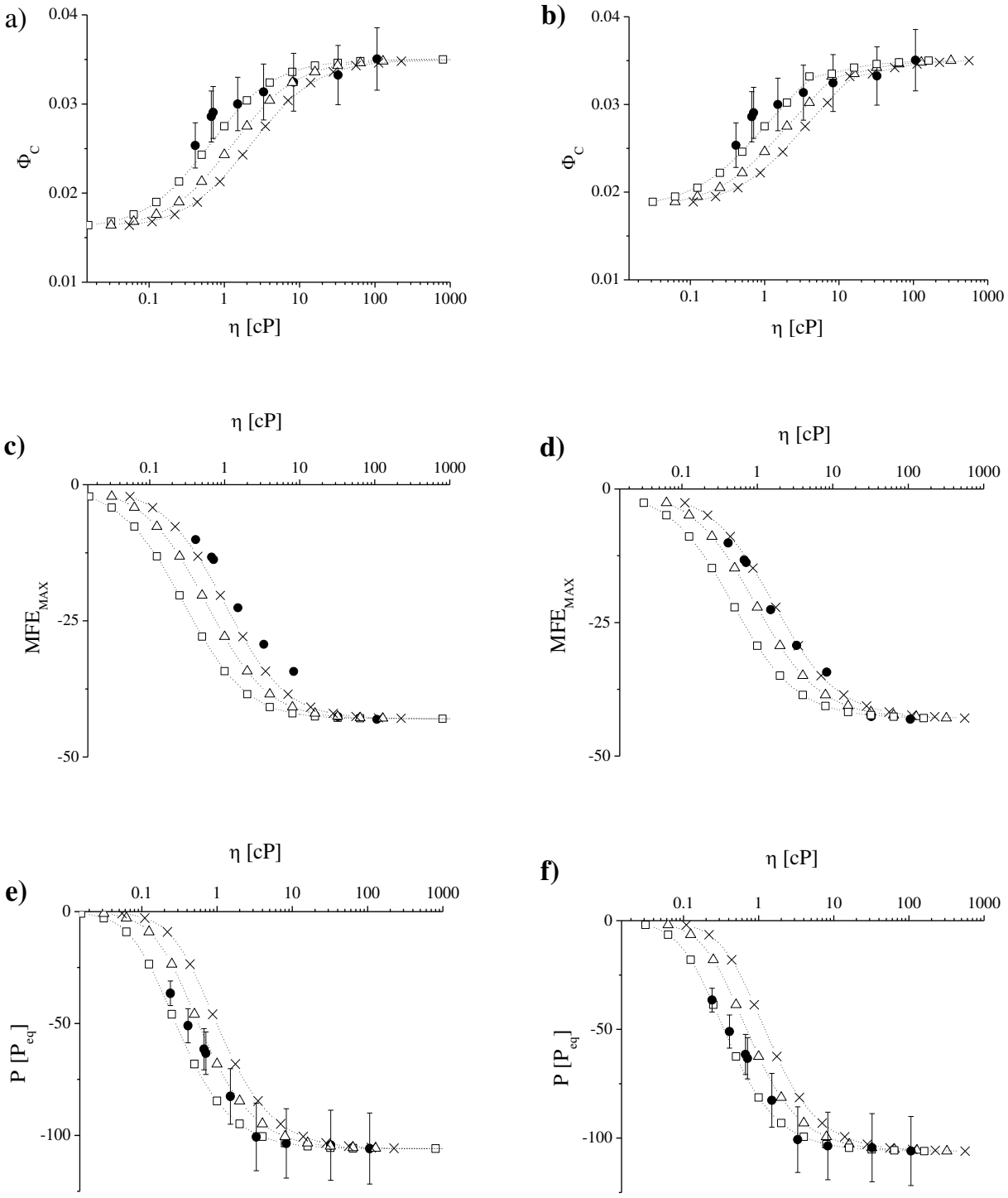

Table 1: Kinetic parameters for the quenching of ^{3}(1-NN) by AC, obtained in LFP experiments

	$k_Q[10^9\ M^{-1}s^{-1}]$	$\tau_0[\mu s]$	Φ_R [1)]
Paraffin Oil	2.0	1.4	0.050
Squalane	3.6	1.2	0.047
Squalane:Heptane	6.1	1.1	0.052
Hexadecane	7.4	1.0	0.053
Dodecane	8.3	0.6	0.052
Nonane	9.7	0.5	0.054
Benzene	3.1	1.0	0.055
Heptane	10.5	0.8	0.049

[1)] Obtained for an external magnetic field of 320 mT

Table 2: Dependence of the *d*-type TM polarization induced in ^{3}AC on solvent viscosity

	η [cP] [1)]	P^+ [P_{eq}]
Paraffin Oil	106.7	-106
Squalane	32.4	-104
Squalane:Heptane (4:1 vol.)	8.32	-104
Hexadecane	3.32	-100
Dodecane	1.50	-82
Nonane	0.71	-63
Benzene	0.67	-61
Heptane	0.41	-51
Pentane	0.24	-36 [2)]

[1)] at room temperature

[2)] obtained under assumption that the radical quantum yield at 3 T equals 0.05